

PETROGRAPHIC AND PETROPHYSICAL
CHARACTERIZATION OF THE WOODFORD SHALE
NORTHERN SHELF, ANADARKO BASIN,
OKLAHOMA

By

KATHRYNE ELIZABETH FOLTZ

Bachelor of Science in Geology

Wheaton College

Wheaton, IL

2013

Submitted to the Faculty of the
Graduate College of the
Oklahoma State University
in partial fulfillment of
the requirements for
the Degree of
MASTER OF SCIENCE
July, 2015

PETROGRAPHIC AND PETROPHYSICAL
CHARACTERIZATION OF THE WOODFORD SHALE
NORTHERN SHELF, ANADARKO BASIN,
OKLAHOMA

Thesis Approved:

Dr. Jim Puckette

Thesis Adviser

Dr. Jack Pashin

Dr. Mary Hileman

ACKNOWLEDGEMENTS

I am very grateful that I was able to work on this project and I'd like to thank Dr. Jim Puckette for being my thesis adviser. You are an amazing role model and I've learned so much from you. Thank you to my committee, Dr. Jack Pashin and Dr. Mary Hileman, and the rest of the Oklahoma State University geology professors and students for making my time here productive and enjoyable. I'd like to thank my parents, Jeffrey and MaryAnn, for being the best parents I could have ever dreamed of, my very first teachers, my cheerleaders, and my heroes. I love you so much and I can't express how blessed I am to have you in my life, supporting me and loving me, even when it's a few states away. To my siblings, Tori, Gracie, Logan, family, and friends who have supported me and loved me from the very beginning, thank you for helping me accomplish what I've set out to do. Thank you Wheaton College geology department for 'converting' me to this amazing world of geology (Dr. Jeff Greenberg, Dr. Stephan Moshier, Dr. James Clark, Jamie Selander, Mrs. Heidlauf). I would not be here without your passion for teaching and encouragement. Most of all, I praise God for leading down this path of so many blessings and I look forward to the next step in my life.

Name: KATHRYNE ELIZABETH FOLTZ

Date of Degree: JULY, 2015

Title of Study: PETROGRAPHIC AND PETROPHYSICAL CHARACTERIZATION
OF THE WOODFORD SHALE, NORTHERN SHELF, ANADARKO
BASIN, OKLAHOMA

Major Field: GEOLOGY

Abstract: This investigation of the Woodford Shale was prompted by observed variations in depositional and diagenetic content across the northern shelf of the Anadarko Basin in Oklahoma. Three cores, two from north-central Oklahoma and one from southern Kansas, were subdivided based on lithologic and geochemical properties. The two cores from Oklahoma contain three generalized, but distinct units: lower pyrite-rich, middle silica-rich, and upper carbonate-rich. Trace metal analyses including x-ray fluorescence and inductively coupled plasma mass spectrometry support the interpretation that the lowermost pyrite-rich interval was deposited in mainly anoxic to euxinic conditions. The middle silica-rich interval is composed of high frequency centimeter-scale silica-rich bands that represent the cyclical accumulation of radiolarians. The uppermost carbonate-rich interval contains increased deformation and features such as calcite-filled fractures and pyrite. Along with fluctuation in trace metal analysis, paleoredox conditions for this interval are interpreted as suboxic to anoxic. Centimeter-scale elemental analyses did not identify high-frequency deviations in concentrations of redox elements indicative of frequent disruption of water stratification. Instead, high-frequency measurement suggest relatively continuous stratification and the presence of an upper oxygenated layer that hosted radiolarian and algal populations that bloomed and collapsed, providing silica and organic matter that accumulated in the anoxic layer below. The silica-rich interval is recognized on gamma-ray logs by a decrease in API units and on porosity logs as suppression of neutron porosity, which represents decreased clay content compared to the surrounding subunits. The silica-rich interval may provide brittleness necessary for fracture propagation, but pore size and volume are greater in the pyrite-rich interval. The Woodford Shale from southern Kansas lacks the silica-rich interval and carbonate interval, and instead has two pyritic shale zones. The lack of the silica bands is attributed to the position of the Woodford distal to upwelling on the margin of the Ouachita Trough/Oklahoma Basin and the associated radiolarian blooms.

TABLE OF CONTENTS

Chapter	Page
I. INTRODUCTION	1
II. BACKGROUND INFORMATION.....	5
Black Shale	5
Anoxia.....	6
Geochemistry	6
Woodford Geologic Setting	7
III. METHODS	12
IV. RESULTS	15
Rother 1H-5X Core Description	15
Rother 1H-5X Gamma-ray Characteristics.....	26
Rother 1H-5X Chemostratigraphy	28
Yost 1H-18X Core Description	32
Yost 1H-18X Gamma-ray Characteristics	39
Yost 1H-18X Chemostratigraphy	40
Matthews 2-8H Core Description	44
Matthews 2-8H Gamma-ray Characteristics.....	52
Matthews 2-8H Chemostratigraphy	55
Wireline Log Analysis	56
Scanning electron microscope (SEM)	62

Chapter	Page
V. DISCUSSION	65
Anderson 12 no.1 Core	65
Inferences from redox indices (U, V, Mo) and organic productivity proxies (Zn, Cu)	66
Comparison of wireline logs for mechanical rock properties	73
SEM interpretations	77
VI. SUMMARY AND CONCLUSIONS	78
REFERENCES	83
APPENDICES	89

LIST OF FIGURES

Figure	Page
1 Oil and gas completions in Woodford Shale and core locations	4
2 Late Devonian paleogeography	8
3 Informal stratigraphic nomenclature for Anadarko Basin	10
4 Schematic descriptions of Rother 1H-5X core	17
5 Contact between Hunton Group and Woodford Shale, Rother 1H-5X	18
6 Representative section pyrite-rich zone, Rother 1H-5X	19
7 Photomicrograph of pyrite band, Rother 1H-5X	20
8 Core photograph of contact between pyrite and silica-rich intervals	21
9 Photomicrograph of silica-rich band.....	23
10 Photomicrograph of radiolarians cemented with quartz and pyrite	23
11 Core photograph of pyritized burrows	24
12 Core photograph of phosphate nodule, clay clasts, and burrows.....	25
13 Photomicrograph of conodont and radiolarian	26
14 Gamma-ray profile with concentrations of select elements.....	27
15 Gamma-ray profile with concentrations of silica and calcium	30
16 Profile comparing concentrations of V and U from XRF and ICP analyses	31
17 Schematic diagram of the Yost 1H-18X core	33
18 Core photograph of representative pyrite-rich interval, Yost 1H-18X	34
19 Photomicrograph of silty pyrite-rich interval, Yost 1H-18X.....	35
20 Photomicrograph of silica cementation in pyrite-rich interval, Yost 1H-18X....	35
21 Core photograph of silica bands in silica-rich interval, Yost 1H-18X	38
22 Photomicrograph of pyrite band, Yost 1H-18X.....	39
23 Gamma-ray profile and select trace metal concentrations, Yost 1H-18X	41
24 Gamma-ray profile and silica and calcium concentrations, Yost 1H-18X	43
25 Schematic description of the Matthews 2-8H core	45
26 Core photograph of representative lower pyrite-rich interval, Matthews 2-8H..	46
27 Photomicrograph of quartz and pyrite-rich interval, Matthews 2-8H.....	47
28 Photomicrographs of pyrite and skeletal material, Matthews 2-8H	47
29 Photomicrograph of pyrite and silt lenses, Matthews 2-8H.....	49
30 Core photograph of representative upper pyrite-rich zone, Matthews 2-8H	50
31 Core photograph of calcite band and pyritized features, Matthews 2-8H	51
32 Photomicrograph of “Kinderhook Shale”, Matthews 2-8H.....	52
33 Gamma-ray profile and concentration of selected elements, Matthews 2-8H....	53
34 Gamma-ray profile and silica and calcium concentrations, Matthews 2-8H.....	54
35 Gamma-ray, PE, and porosity logs, Rother 1H-5X	59
36 Gamma-ray, porosity, and PE logs, Yost 1H-18X	60

Figure	Page
37 Gamma-ray, PE, and porosity logs, Matthews 2-8H	61
38 SEM images of pore types, silica-rich interval, Rother 1H-5X.....	63
39 SEM images of pore types, pyrite-rich interval, Rother 1H-5X.....	64
40 Molybdenum concentrations in redox environments.....	67
41 Trace element behavior in modern environments.....	68
42 Gamma-ray and Mo, V, and U concentrations, Rother 1H-5X	72
43 Trace element concentrations, high resolution sampling.....	74
44 Gamma-ray, TOC, and elemental concentrations, Rother 1H-5X.....	75
45 Gamma-ray, TOC, and elemental concentrations, Yost 1H-18X	76
46 Schematic diagram of the two-part paleo redox conditions.....	82

CHAPTER I

INTRODUCTION

The Woodford Shale of Oklahoma is a significant petroleum source and is recognized as the primary source rock in the southern Midcontinent of North America (Kirkland et al., 1992). The Woodford Shale and time-equivalent formations, such as the Marcellus (Pennsylvania, West Virginia), Chattanooga (Tennessee, Kentucky), and Bakken (North Dakota) shales, are believed to have sourced nearly 8% of the world's oil and gas reserves (Ulmishek and Klemme, 1990). Historically, the superjacent Mississippian limestone and subjacent carbonates of the Hunton Group, as well as the Misener sandstone that lies unconformably on the Hunton Group, have been primary target reservoirs for Woodford Shale-sourced oil and gas production in Oklahoma. The innovation that hydraulic fracturing and horizontal drilling bring to the energy industry allow the Woodford Shale to be exploited as a direct, self-sourcing exploration target.

The Woodford Shale in southern Oklahoma is well studied for its source rock potential (Kirkland et al., 1992) and drilled for oil and gas production for more than a decade (Figure 1A; Cardott, 2012). In contrast, while the Woodford Shale in northern Oklahoma is the focus of exploration, much about the Woodford Shale in the study area is still rather unknown. A number of differences are evident between the Woodford Shale

exposed in outcrops and examined in core from southern Oklahoma in comparison with the Woodford Shale in cores taken in northern Oklahoma and outcrops on the flanks of the Ozark Uplift. These differences are the result of changes in the depositional processes operating in these respective areas and the resultant diagenetic overprints. As an example, in the south, the Woodford Shale contains a higher percentage of chert in the form of silica cement that generated brittle bands that were naturally fractured and are more easily accessed by hydraulic fracturing. Cores and outcrops of the Woodford Shale in northern Oklahoma lack chert, however, high-volume oil and gas production is reported for wells completed in the Woodford Shale in Payne County and other areas in northern Oklahoma (IHS, 2014). Based on this evidence, there is a need to understand the reservoir properties of the Woodford Shale outside the southern chert-rich area and identify the brittle intervals in the north to drill and fracture stimulate. Identifying the better reservoir intervals will enhance exploration and production strategies, and thereby save the industry both time and money.

This study will investigate the lithologic and petrophysical properties of the Woodford Shale on the northern shelf of the Anadarko Basin in northern Oklahoma and southern Kansas (Figure 1). The primary objective is to better comprehend the depositional processes responsible for the rock fabric evident in northern Oklahoma and foremost the identification of cemented zones. The recognition of cemented brittle zones will contribute to a greater understanding of the internal stratigraphy of the Woodford Shale and improve reservoir assessment by identifying the more economic intervals for hydraulic fracturing (Snider, 2014). The petrographic characterization will be augmented with analytical techniques including thin section analysis and x-ray fluorescence to

establish bulk rock mineralogy and identify trace metal concentrations. These metals are proxies for bottom and pore water paleogeochemistry and will be used to help construct a preliminary depositional model for the Woodford Shale and expand our understanding of depositional processes during the Late Devonian and Lower Mississippian. Secondary objectives include:

1. Establish frequency of bottom water cyclicity during Woodford Shale deposition,
2. Place depositional cycles in the context of larger scale processes to develop a depositional model for the Woodford Shale,
3. Relate rock properties resulting from depositional fabric and subsequent diagenesis to mechanical properties, and
4. Determine the types and frequency of pores in specific facies and fabrics through scanning electron microscope (SEM) imaging.

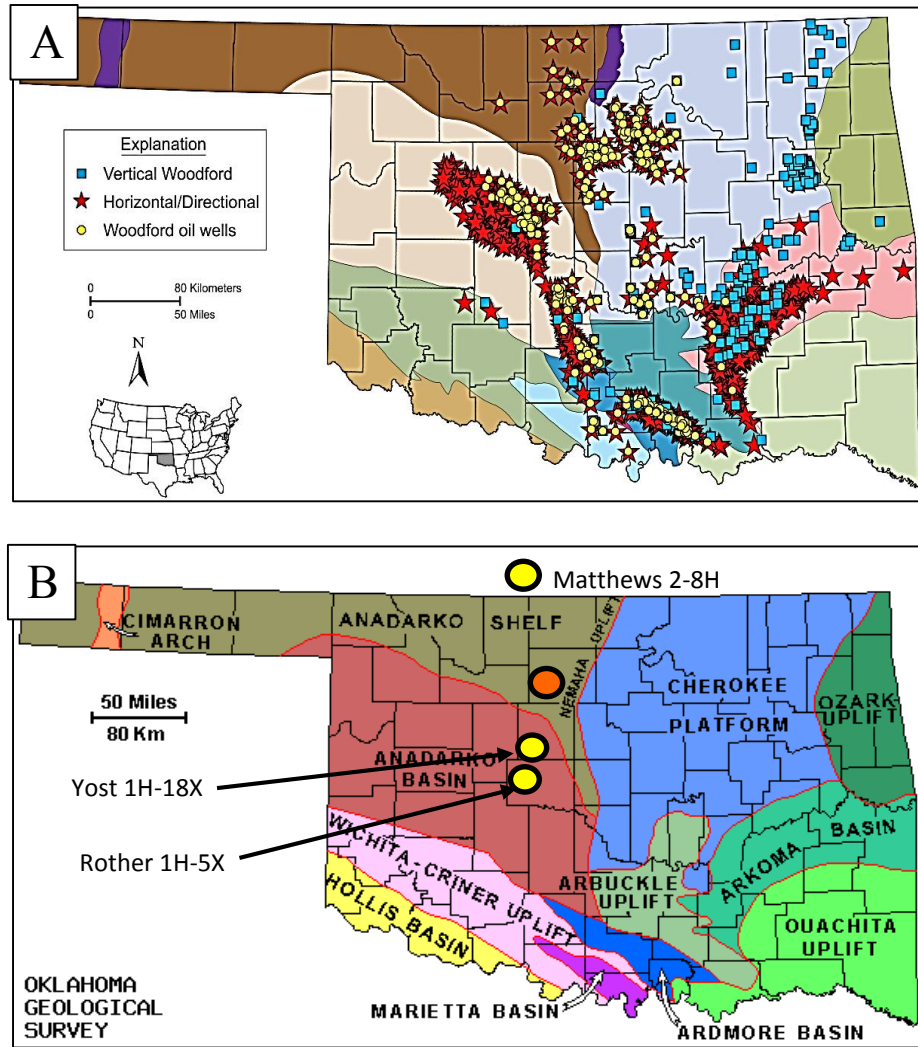


Figure 1. (A) Map of Oklahoma showing Woodford Shale oil and gas completions 2004-2014 (Modified from Cardott, 2012). (B) Map of geologic provinces of Oklahoma. The three core locations for this study are shown as yellow circles while the core given in the analysis by Callner, 2014 is shown in orange (Modified from Northcutt and Campbell, 1998).

CHAPTER II

BACKGROUND INFORMATION

Black Shale

The Woodford Shale is best classified as a mudrock, a sedimentary rock of clay- or silt-sized constituents that include differing amounts of clay, silica, carbonate, and metals (Arthur and Sageman, 1994). “Black Shale” is a dark grey to black colored mudrock, with 2-10% organic matter, usually marine in origin, and metal enriched (Tourtelot, 1979). Black shale is interpreted as stratified shallow water or deep water basinal facies and the subsequent preservation of organic material is dependent on the redox conditions of the water column (Ettensohn et al, 1988). Early depositional models of black shales almost uniformly placed deposition in anoxic deeper water basins in epicontinental seas, using the modern Black Sea as a modern analog (Tyson and Pearson, 1991; Lambert, 1993). However, observations made in the Chattanooga Shale conclude that dark shales may not necessarily represent deep basinal deposition (Schieber, 1998; Schieber, 2001). Instead, the Chattanooga Shale shows evidence of storm reworking and other observed structures such as pyritized ooid beds, suggesting that deposition of these clastic mudrocks may have occurred along a shelf edge, in water depths of 10-15 m that are easily affected by higher order sea level change (Schieber, 1998; Schieber and Riciputi, 2004). These more recent interpretations of depositional environments allow for

a wider range of explanations for other observed sedimentary structures and depositional processes in shale.

Anoxia

The redox state is a function of the amount of oxygen dissolved in the water column and is primarily controlled by the degradation of organic material which bonds with any free oxygen at the sediment-water interface (Musa, 2013). Based on the terminology clarified by Tyson and Pearson (1991), ‘oxic’ indicates that dissolved oxygen is present, ‘anoxic’ defines an environment in which there is no dissolved oxygen, and ‘euxinic’ implies that not only is there no dissolved oxygen, but also that free hydrogen sulfide (H₂S) is present within the water column (Tribovillard et al., 2006; Berryman, 2008; Jenkyns, 2010; Musa, 2013). Occasionally, the term ‘suboxic’ is used, which is characterized by the presence of very low oxygen and limited H₂S below the sediment water interface (Tyson and Pearson, 1991; Tribovillard et al., 2006). Sediment accumulation and the episodic bottom water anoxia that results from stratification of the water column facilitate preservation of deposited organic material and the concentration of trace metals.

Geochemistry

Trace-metal accumulation rates are controlled by redox conditions and can be used as proxies to estimate if a paleomarine environment was oxic, suboxic, or anoxic (Calvert and Pederson, 1993; Tribovillard et al., 2006; Algeo and Rowe, 2012; Rowe et al., 2012). Hydrographic factors tend to be the controlling element for anoxic conditions

and when trace metal accumulations and redox proxies such as molybdenum (Mo), uranium (U), and vanadium (V) are compared against total organic carbon (TOC) concentration, these ratios can help determine the degree of basin restriction (Algeo and Maynard, 2004; Algeo and Rowe, 2012). The presence of metals such as zinc (Zn), copper (Cu), and nickel (Ni), which are dominantly delivered and released into sediment by organic material and its decay, can indicate the original input of detrital organic matter (Tribovillard et al., 2006). To remove the effects of detrital/aluminosilicate influence, Al and Ti are common proxies used for normalization of metal concentrations (Calvert and Pederson, 1993; Thomson et al., 2006; Löwemark et al., 2011).

Woodford Geologic Setting

The Woodford Shale is Late Devonian to Lower Mississippian (Frasnian – Tournaisian/Kinderhookian) in age, lacks normal marine invertebrate fauna, and is silty to clay-rich with high organic content, phosphate and pyrite (Over, 1992; Kirkland et al, 1992; Over, 2002). First described in outcrop as the Woodford Chert in the Arbuckle Mountains of southern Oklahoma, the Woodford Shale is partially time equivalent to the Chattanooga (Tennessee), Ohio/New Albany (Kentucky, Ohio), Marcellus (Ohio, Pennsylvania, West Virginia) and Bakken (North Dakota, Canada) shales (Taft, 1902; Lambert, 1993). These black shales are widely distributed across the North American continent (Figure 2; Ettensohn, 1992).

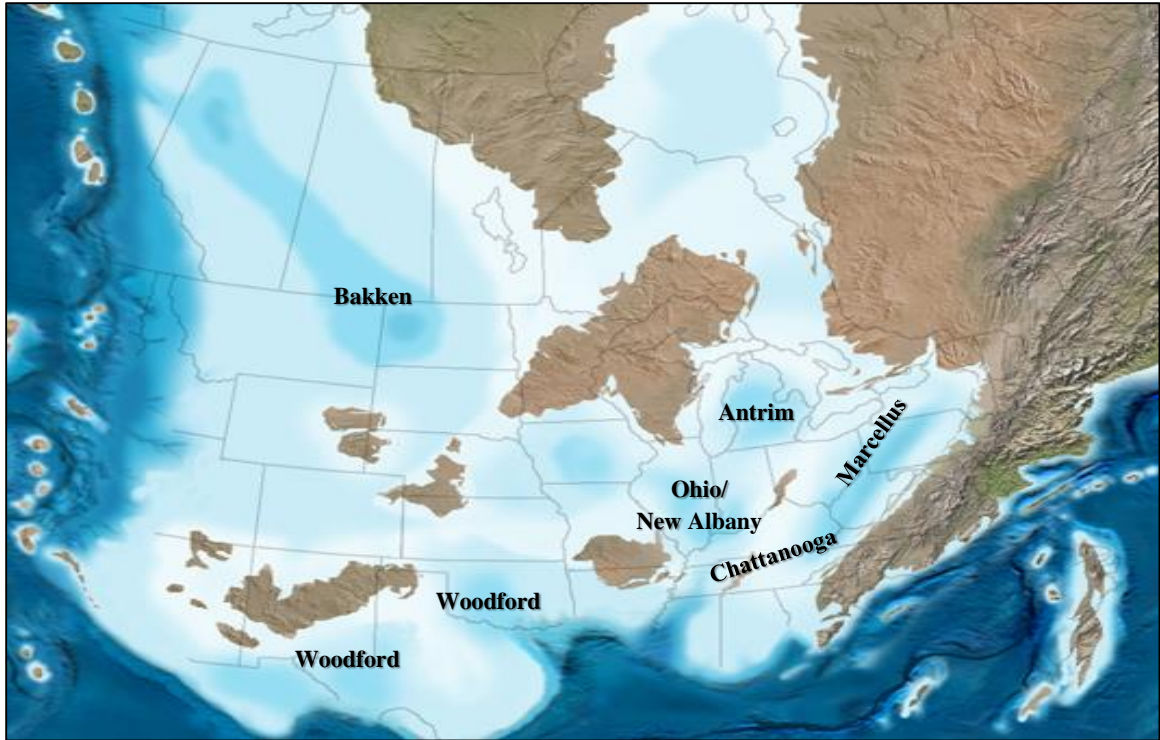


Figure 2. Paleogeographic map of the North American continent from the Late Devonian (360 mya) showing depocenters of Devonian black shales. Modified from Blakey (2015).

The Anadarko Basin is the deepest sedimentary basin in North America (Gilbert, 1992). The tectonic history of the basin begins in the Cambrian with the cratonic rifting that formed the Southern Oklahoma Aulacogen (SOA) (Johnson, 1989; Gilbert, 1992; Kirkland et al., 1992). Igneous rocks in the area of the present Wichita Uplift, which is now the southern margin of the Anadarko Basin, filled the aulacogen around 520 mya (Gilbert, 1992). Igneous activity was followed by slow subsidence of the successive Oklahoma Basin from the late Cambrian up through the Mississippian. The widespread epicontinental sea that covered most of the present day North American continent deposited the shallow-marine carbonate-rich Cambro-Ordovician Arbuckle Group, the sand-rich Ordovician Simpson Group, and the carbonate-dominated Ordovician-Devonian Hunton

Group. The widespread restriction of marine circulation in the Late Devonian resulted in the deposition of Woodford sediments. Today, the Woodford Shale extends from Texas to Kansas and thickens toward the axis of the Anadarko Basin and over the ancient Southern Oklahoma Aulacogen. The Woodford is bounded by unconformities: the widespread Pre-Woodford unconformity and the Post-Woodford unconformity (Figure 3). Following Woodford deposition, there was a shift to a shallow marine carbonate-dominated shelf (shallow ramp) system (Johnson, 1989). Orogenic events of the Pennsylvanian reactivated the faults of the SOA, uplifting the igneous basement while initiating the subsidence that resulted in the foreland Anadarko Basin. From the Pennsylvanian to the Permian, subsidence of the Anadarko Basin continued as the Wichita Mountains were uplifted. During the Mesozoic and Cenozoic, there was no tectonic activity of note in the Midcontinent. However, since the Laramide orogeny in the late Cretaceous, the North American continent has continued to rise, exposing the section to erosion that forms the present outcrop pattern evidenced in the southern Mid-Continent.

The Woodford Shale contains pyritized burrows that, based on Lobza and Schieber (1999), supports the premise that life was able to exist at least episodically within this normally anoxic environment. Horizontal pyrite laminations also occur, which could indicate shallow erosion surfaces, change in organic material, or an interruption of primary sedimentary fabric due to bioturbation (Doser and Bottjer, 1986; Schieber, 1998). However, there is an exclusion of any other evidence of normal marine benthic organisms, heavy bioturbation, mottled facies, and large trace fossils such as marine ichnofacies (Barron and Eddensohn, 1981). This exclusion of continuous benthic activity

indicated a sufficient depletion of O₂ when the Woodford sediments were deposited and is interpreted that when the seafloor was colonized, it was episodic (Kirkland et al, 1992; Schieber and Riciputi, 2004; Algeo and Maynard, 2004). Phytoplankton such as *tasmanites* and radiolarians are observed in the Woodford Shale and play a significant role as source of organic matter and silica respectively (Barron and Ettensohn, 1981; Comer and Hinch, 1987; Schieber et al., 2000).


<i>System/Series</i>		<i>Anadarko Basin Stratigraphy</i>	
Mississippian	Meramecian	"Miss Lime"	"Meramac Lime"
	Osagean		"Osage Lime"
	Kinderhookian		
Devonian	Upper	Woodford Shale Misener Sandstone	
	Middle		
	Lower		
Silurian	Upper	Hunton Group	Haragan Fm. Henryhouse Fm.
	Lower		Chimney Hill Subgroup
Ordovician	Upper		Sylvan Shale
			Viola Group

Figure 3. Informal stratigraphic nomenclature of the upper Ordovician to Mississippian section, Anadarko Basin, Oklahoma. Modified from Johnson and Cardott (1992).

Pyrite is common in the Woodford Shale and can form syndepositionally under conditions of correct water column chemistry (Kirkland et al, 1992; Cruse and Lyons, 2004; Tribovillard et al., 2006). In the Woodford Shale, it appears that much of the pyrite is post-depositional in origin due to the crystal size and morphology and its occurrence as cementing burrows and grains that form laminae. Marcacite, a polymorph of pyrite, is

also found in the Woodford but due to its similarity to pyrite, it is hard to distinguish outside of its instability at the surface.

There is also abundant silica in the Woodford Shale in the form of silica-cementation as well as silt-sized grains, interpreted as detrital quartz or radiolarians (Kirkland et al., 1992). While massive beds of microcrystalline quartz (chert) are found in southern Oklahoma, silica in Woodford Shale in northern Oklahoma seems to concentrate in cemented bands. Silica can come from two petrographically recognized sources: detrital material, principally quartz silt, or the dissolution of silicified radiolarians that were opaline-chert (Roberts and Mitterer, 1992; Schieber et al., 2000). If early diagenesis was the primary producer of silica, these radiolarian beds could be important proxies for productivity levels as well as reflecting shoreline proximity (Schieber et al., 2000). Non-skeletal phosphate, which is scarce to absent in cores from northern Oklahoma and outcrops in the Ozark Mountains, yet common in outcrops in southern Oklahoma, likely formed in zones of upwelling along the northern margin of the Ouachita Trough.

The Woodford Shale has a distinct signature on conventional petroleum industry wireline logs because it is radiogenic and recognized as a “hot shale”. This radioactivity is the result of higher than normal concentrations of uranium (U) that causes a significant increase in the values measured by the gamma-ray curve to exceed 150 API units (Paxton et al., 2006). In general, the environmental and depositional conditions that facilitate concentrating U in sediments, slow diffusion rates of U out of seawater under anoxic conditions, also favor the preservation of organic matter, confirming the conditions during deposition (Lüning and Kolonic, 2003).

CHAPTER III

METHODS

Three cores were examined, described, and sampled to provide the primary data for this project: Newfield Exploration Company Rother 1H-5X, Newfield Exploration Company Yost 1H-18X, and the Tug Hill Operating, Matthews 2-8H (Figure 1B). Analyses of specific intervals, including total organic carbon (TOC), x-ray diffraction (XRD), x-ray fluorescence (XRF), and spectral gamma-ray were provided by Newfield for the Rother 1H-5X and Yost 1H-18X cores. These measurements were taken at approximately 5 foot intervals. This information formed the foundation for the project and was augmented in this study by core descriptions, which include 1 inch (2.45 cm) scale descriptions of rock type, color, texture and fabric, and physical phenomena such as diagenetic alteration and sedimentary and biogenic structures, such as pyritized burrows and phosphate nodules. Core photographs were provided for the Newfield wells and additional photographs were taken to highlight specific textures that were sampled for thin section. Thin sections were provided by Newfield (26 for Rother 1H-5X, 7 for Yost 1H-18X) along with accompanying photomicrographs. Ten additional thin sections were made for the Matthews 2-8H to petrologically characterize the Woodford Shale.

All cores were analyzed for elemental concentrations by x-ray fluorescence using a Niton TM XL 3t GOLDD hand-held device and test stand. Samples collected at 6 inch

(15.24 cm) intervals were surveyed for 180 seconds using the XRF instrument. Samples were collected at smaller intervals where depositional textures or diagenetic overprints warranted more detail. The instrument was calibrated approximately every 10 measurements using the United States Geological Survey (USGS) Cody Shale (SCo-1) standard. A correction factor was applied to the recorded values to reduce the effects of instrument drift. A unique correction value was applied to each measured trace element concentration, based on the deviation of the instrument recorded value from the known concentration of that element in the standard. This correction factor was determined using the equation:

$$\text{Correction Factor} = \frac{\text{USGS Reported Value for standard}}{\text{XRF Measured Average Value for standard}}$$

The XRF instrument is capable of measuring up to 35 different elements and trace metals. More information concerning the Niton TM device can be found on the Thermo Scientific website: www.us-tech.co.za. The primary elements considered for this project are those reported in the literature as acceptable proxies for interpreting paleo- bottom water chemistry, authigenic and detrital composition, and overall depositional environment: U, V, Mo, Zn, Cu, Titanium (Ti), Aluminium (Al), potassium (K), iron (Fe), sulfur (S), silica (Si), calcium (Ca), Ni, and cobalt (Co) (Tribovillard, 2006; Rowe et al, 2012; Musa, 2013; Callner, 2014). The concentrations of Cu, Zn, and Ti are proxies for assessing the relative contribution of detrital sediment input to the sediment column. The proxies for evaluating paleoceanic redox are Mo, U, and V. The USGS Cody Shale standard contains ten (10) elements that measure below the Level of Detection (<LOD): Pd, Ag, Mo, Nb, U, Ir, Au, Br, Ni, Co. A second standard (NIST 2780, from the National

Institute of Standards and Technology) was scanned to establish a correction factor for U. There was no XRF-provided correction factor available for Al, Si, Ca, and Mo so any use of these elements is strictly qualitative. The element/Ti ratio is used in this study for normalization instead of Al due to the lack of a correction factor for Al.

A scanning electron microscope (SEM) was used to contrast the pore fabric of silica-rich and clay-rich beds in the Woodford Shale. Two samples from the Rother 1H-5X core were taken at 10465 and 10485 ft. Samples were polished using a JEOL 13-19500 CP Cross-Section Polisher. This argon-gas ion mill creates an accurate 2D surface for viewing. Once milled, the samples were coated in gold palladium and viewed in a FEI Quanta 600F Environmental Scanning Electron Microscope. Images were taken at several levels of magnification on both the milled 2D surface as well as the unmilled, 3D surface as an overview of the structural and compositional components.

CHAPTER IV

RESULTS

Rother 1H-5X Core Description

The Rother 1H-5X core was recovered from a well drilled in Sec.8 T14N R8W, Canadian County, Oklahoma, within the Anadarko Basin (Figure 1B). The examined cored interval is continuous and contains 113 ft. of Woodford Shale, 3 ft. of the superjacent Mississippian carbonate, and about 3 ft. of the subjacent Hunton Group (Figure 4). The measured depth of the cored interval is 10312 ft. to 10431 ft.; the core depths are about 15 ft. deeper than the depth recorded by open-hole wireline logs. The Woodford Shale is greyish black to black, N2–N1 on the GSA Rock-Color Chart.

The Woodford core was divided into three units based on lithologic and petrographic similarity. The lowermost section extends from 10427 to 10371.7 ft. and includes the contact with the underlying Hunton Group. This contact is recognized by phosphate and clay clasts, calcite-filled fractures, sand-sized calcite and quartz grains, and color change to medium dark grey/olive black (N4–5 Y 2/1; Figure 5). Pyrite is common in this interval and occurs as bands, nodules, and laminae (Figure 6). Silica-cemented bands occur near the middle and base of the section, around depths of 10410 and 10390 ft., respectively. Pyrite occurs within these bands and appears to be

diagenetically linked with the silicified radiolarians. Phosphate nodules and clay clasts occur close to the base of the core at 10426–27 ft. Pyrite-rich bands, ranging from 0.1 to 3 cm thick, contain concentrations of silt to fine sand-sized pyrite (Figure 7). Some bands are normally graded and fine upwards. In contrast, pyrite laminae, which are characteristic of this lowermost zone, are typically less than 0.1 cm thick. The laminae are more apparent when the core is dampened to highlight the contrast between the adjacent dark shale and the yellow pyrite. Some well-defined pyritized laminae are evident (Figure 8), whereas other laminae are less distinct. Scattered pyrite in matrix outside these bands and laminae occurs as nodules and grains. Pyrite nodules are larger (1 cm) than the scattered grains (< 0.1 cm). Larger masses of pyrite are of uncertain origin, whereas scattered pyrite grains are often pyritized *tasmanites* or radiolarians. In thin section, this interval contains abundant clay to silt-sized calcite. The contact between the lowermost zone and the next interval is placed along a pyrite band at a depth of 10371.7 feet. This band appears graded and contains conodonts, radiolarians, *tasmanites* and other silt to sand-sized pyrite sediment. This lowermost zone from 10427 ft. to 10371.7 ft. is called the lower pyrite-rich zone (PR).

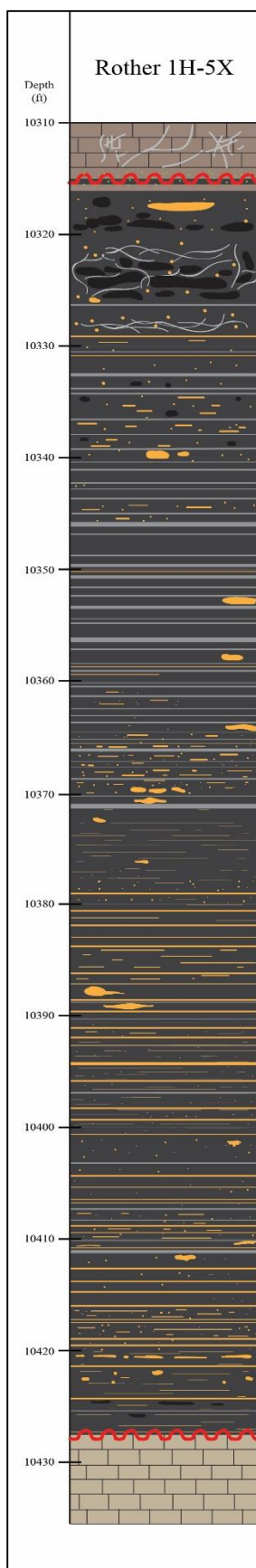





Figure 4. Schematic description of lithology and, depositional and authigenic features in the Newfield Rother 1H-5X core, depth 10310 to 10430 ft.

Stratigraphy

	Mississippian		Hunton Group
	Woodford Shale		

Sedimentary Features









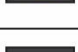

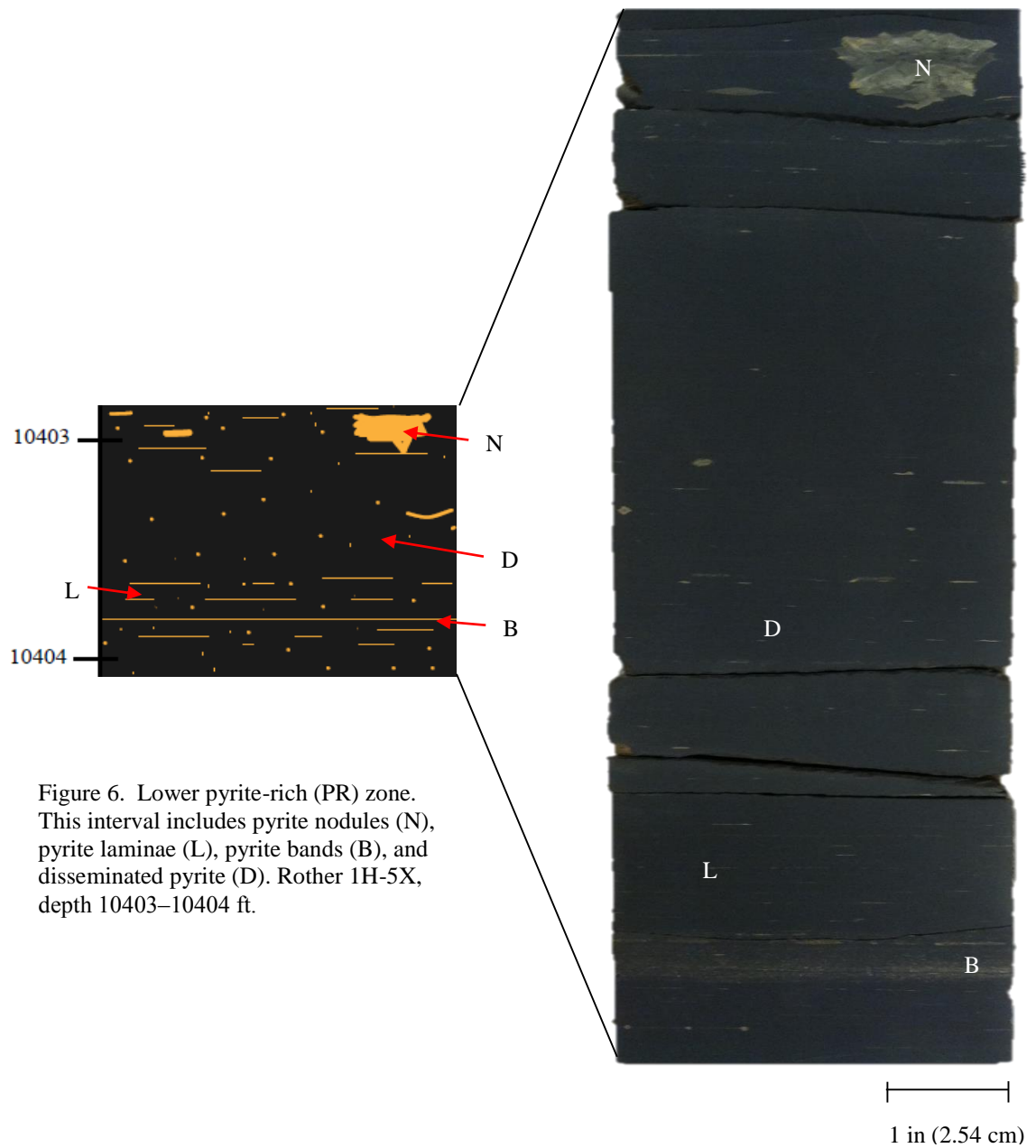
	Scattered pyrite		Carbonate-filled Fractures
	Pyrite bands		Glauconite zone
	Pyrite laminae		Phosphate/clay clasts
	Pyrite nodules		Soft-sediment deformation
	Silica-cemented bands		Unconformity



Figure 5. Contact between the underlying Hunton Group and the lower pyrite-rich (PR) zone of the Woodford Shale, Rother 1H-5X, depth 10404 ft.



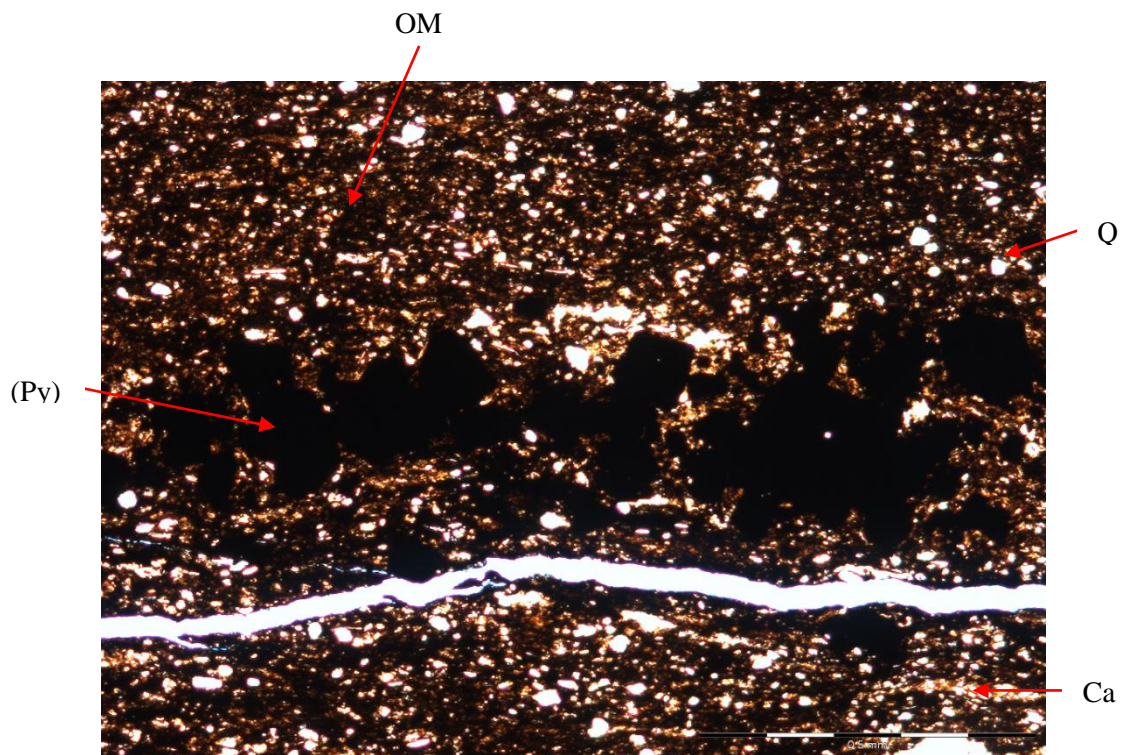


Figure 7. Photomicrograph of a pyrite band (Py) in plane polarized light. The fracture beneath the band probably formed during thin sectioning. The surrounding matrix contains silt-sized quartz (Q) and calcite (Ca) grains, and organic material (brown to black; OM). Rother 1H-5X, depth 10417 ft.

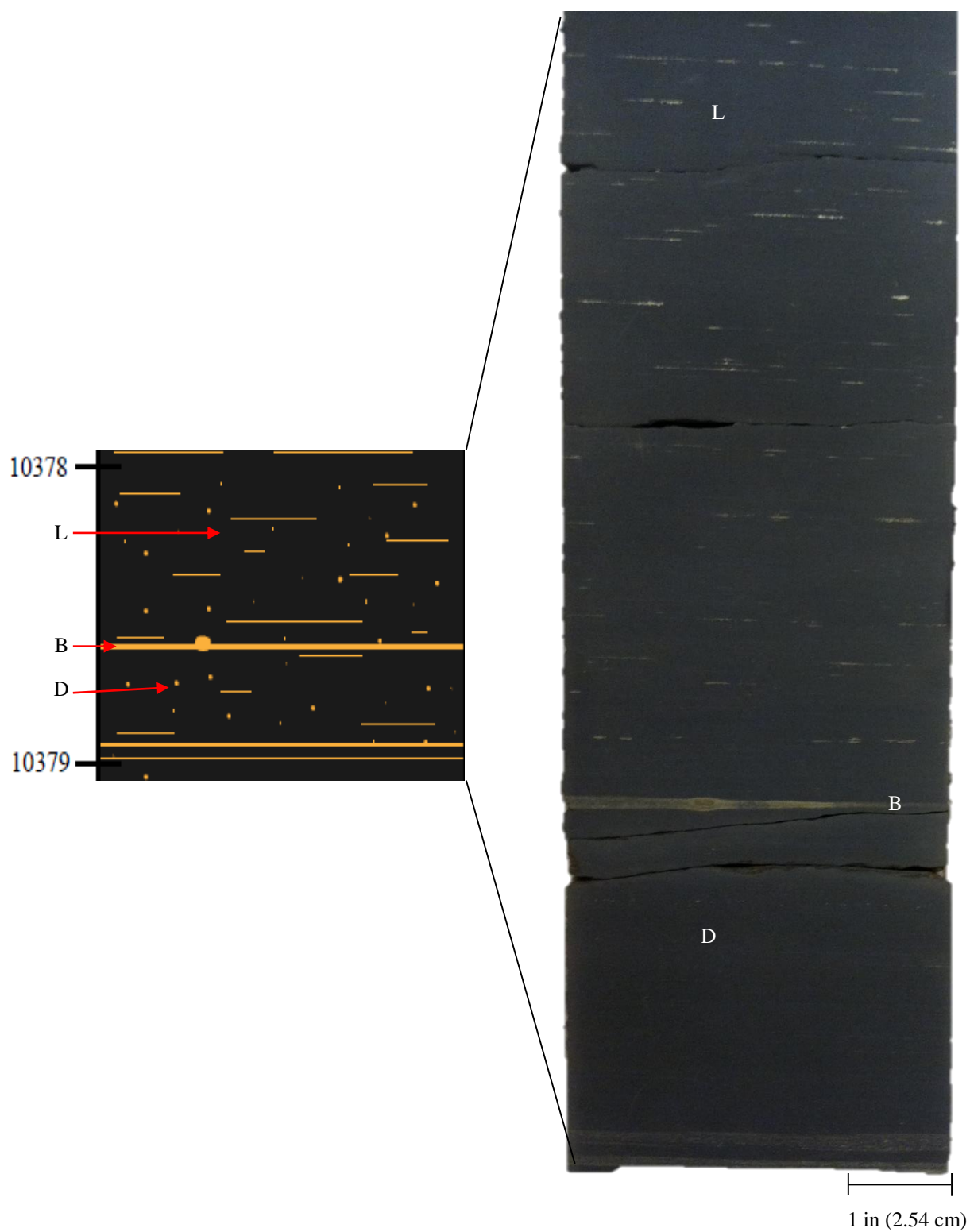


Figure 8. Pyritized horizontal laminae (L), pyrite band (B), and disseminated pyrite (D). Pyrite laminations are well defined at the top of this foot, greater than 0.1cm thick. Rother 1H-5X, depth 10378–10379 ft.

The next interval (10371.7–10340 ft.) is characterized by an abundance of silica-cemented bands and a scarcity of pyrite laminae. The silica-cemented bands range from 0.1 to 7 cm in thickness, average 1.4 cm thick, and are identified by their increased reflectivity compared to adjacent non silica-cemented intervals. These bands contain increased concentrations of silt to sand-sized pyrite. In thin section, the cement is microcrystalline quartz along with silicified radiolarians (Figure 9). Occasionally, cubic pyrite replaces silica in the interior of the radiolarians (Figure 10). Larger pyrite nodules also occur in this interval (Figure 11) and are occasionally contained within the silica bands. Larger bands are generally followed by one or two smaller ones. A few smaller pyrite bands (<0.5 cm) without silica-cementation and pyrite laminae occur in this section, and are concentrated near the base. The upper contact of the silica-rich interval was chosen based on the relative higher frequency of silica bands and lower pyrite content below the contact. This interval was labeled silica-rich (SR) due to the abundant silica bands it contains.

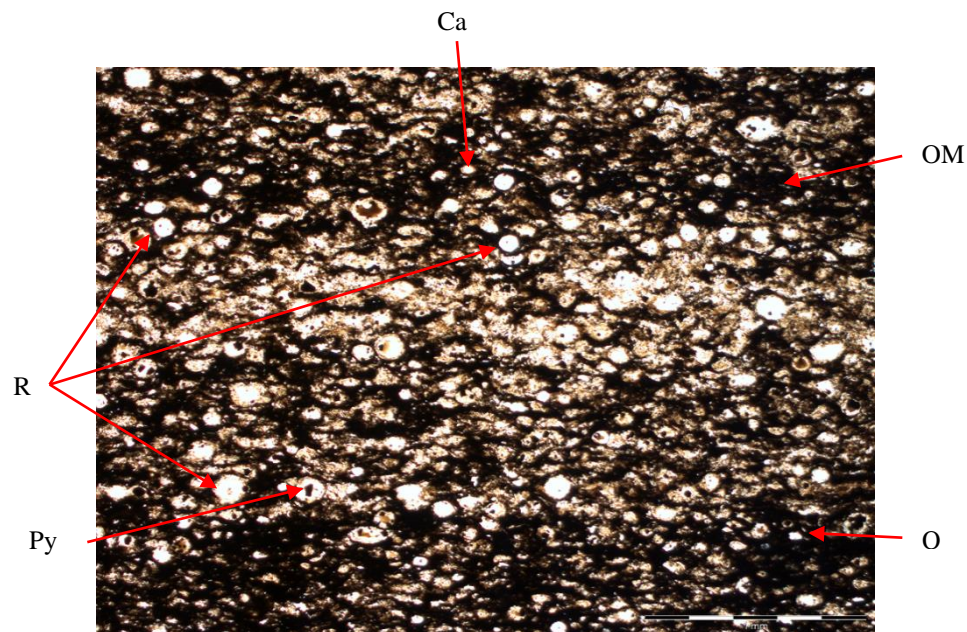


Figure 9. Thin section photomicrograph of a silica-cemented band. The circular objects are silicified radiolarians (R); the surrounding dark matrix is organic material (OM), pyrite (Py), and silt-sized calcite (Ca) and quartz (Q) grains. Rother 1H-5X, depth 10362 ft.

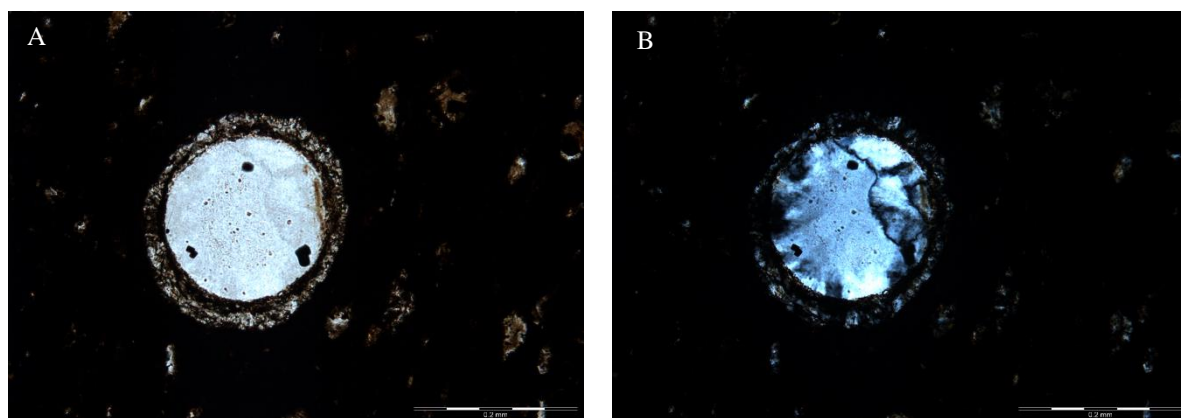


Figure 10. Thin section photomicrographs of a silica and pyrite-cemented radiolarian, Rother 1H-5X, depth 10352 ft. (A) Plane-polarized light of a radiolarian with pyrite beginning to replace the quartz. (B) Cross-polarized view of the same grain.



Figure 11. Core photograph of a larger pyrite nodule (N) in the SR interval. This feature appears to be two platey pyrite nodules, one cutting through the other. Rother 1H-5X, depth 10370 ft.

The uppermost interval (10340–10312 ft.) includes a sharp contact with the overlying Mississippian limestone, which hosts a distinct basal glauconitic zone that occurs immediately above the Woodford Shale. The Woodford Shale in this interval is medium dark grey to olive black in color (N3, N1, 5 Y 2/1). The upper zone is characterized by having increased soft-sediment deformation, scattered clay and peloidal phosphate clasts near the top of the core, carbonate-filled fractures, and scattered pyritized bands and nodules (Figure 12). In thin section, organic material and skeletal fragments such as sponge spicules are common, as well as silt to fine sand-sized calcite grains, disseminated pyrite, and both flattened and whole silicified radiolarians, and

conodonts (Figure 13). This upper section is called the upper carbonate-rich (CR) zone due to the carbonate-filled fractures and the abundant calcite evident in thin section.

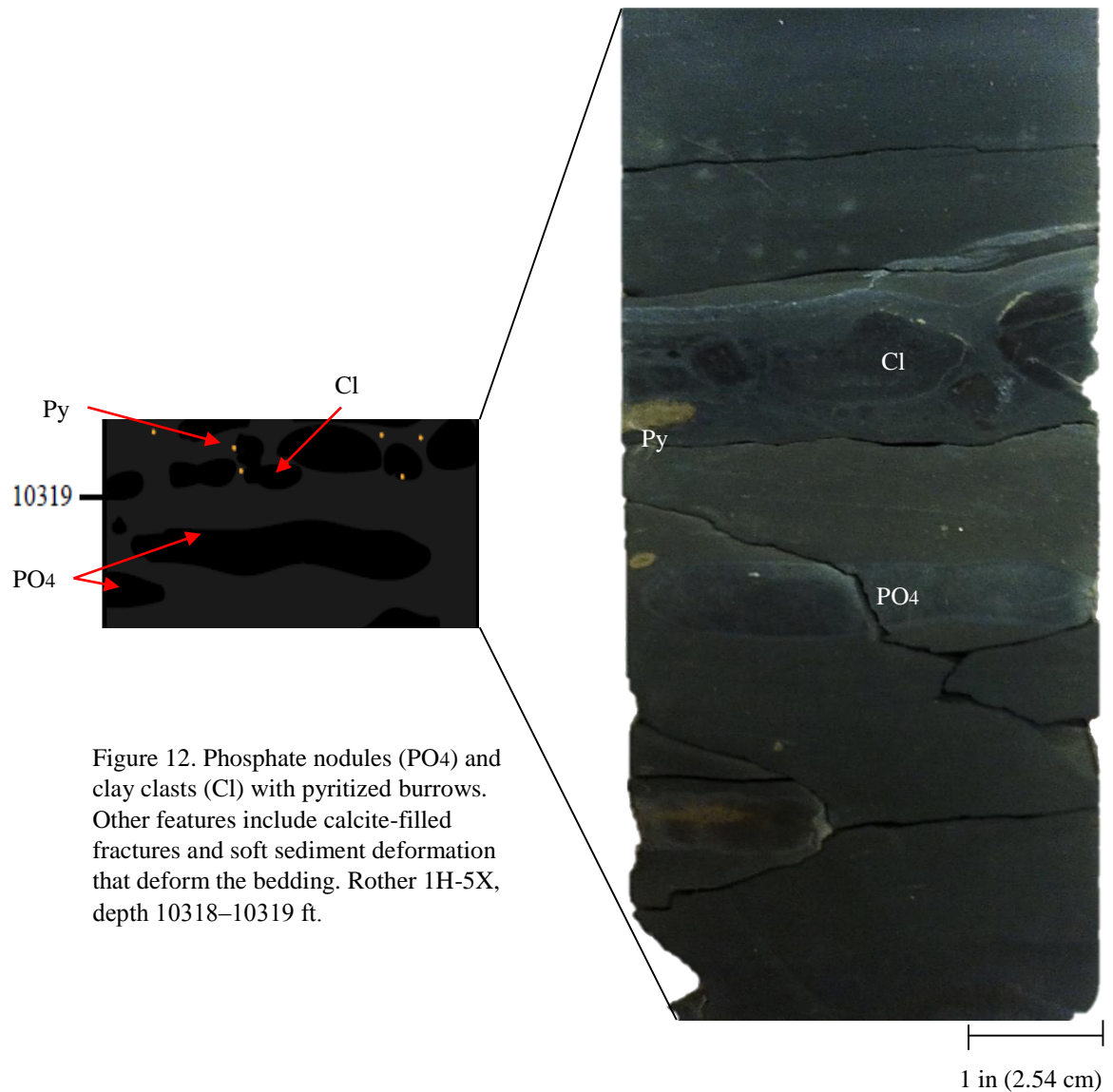


Figure 12. Phosphate nodules (PO₄) and clay clasts (Cl) with pyritized burrows. Other features include calcite-filled fractures and soft sediment deformation that deform the bedding. Rother 1H-5X, depth 10318–10319 ft.

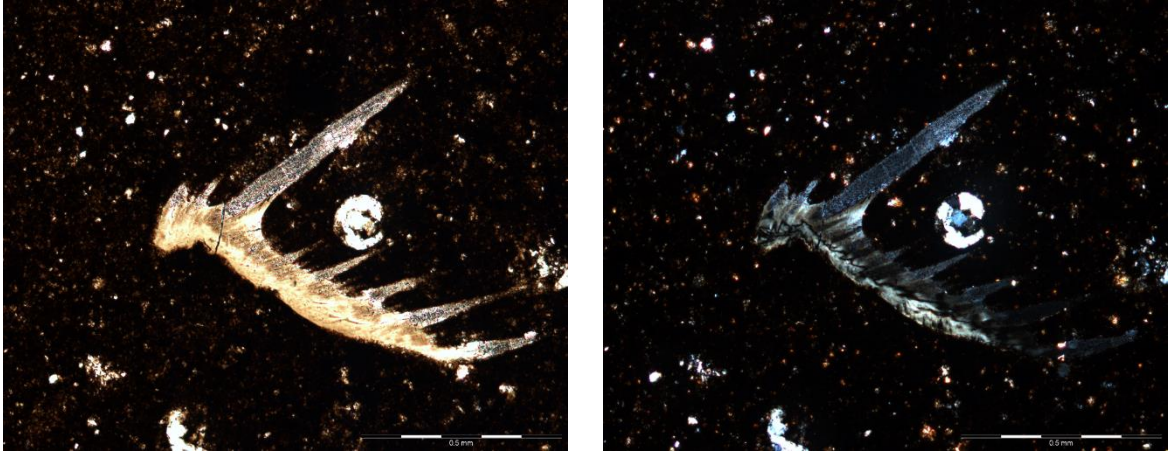


Figure 13. Thin section photomicrograph of a conodont fragment next to a silicified radiolarian. (A) Plane-polarized light. (B) Cross-polarized light. Rother 1H-5X, depth 10337 ft.

Rother 1H-5X Gamma-ray Characteristics

The gamma-ray signature for the Rother 1X-5H exhibits distinct patterns that are apparent in the profile (Figure 14). The lowermost pyrite-rich zone from 10431 to 10372 ft. has consistent gamma-ray values exceeding 400 API units. The high gamma-ray peak at 10427 ft. correlates to increases in trace element concentrations. The signature for the silica-rich interval from 10372 to 10340 ft. has a curved appearance, peaking at the base to about 800 API, decreasing to values around 350–400 API, and increasing to approximately 550 API. The carbonate-rich interval (10340–10315 ft.) has a fluctuating gamma-ray profile with values ranging from 150 to 700 API units. Values are higher toward the base and decrease upward until the peak at 10319 ft.

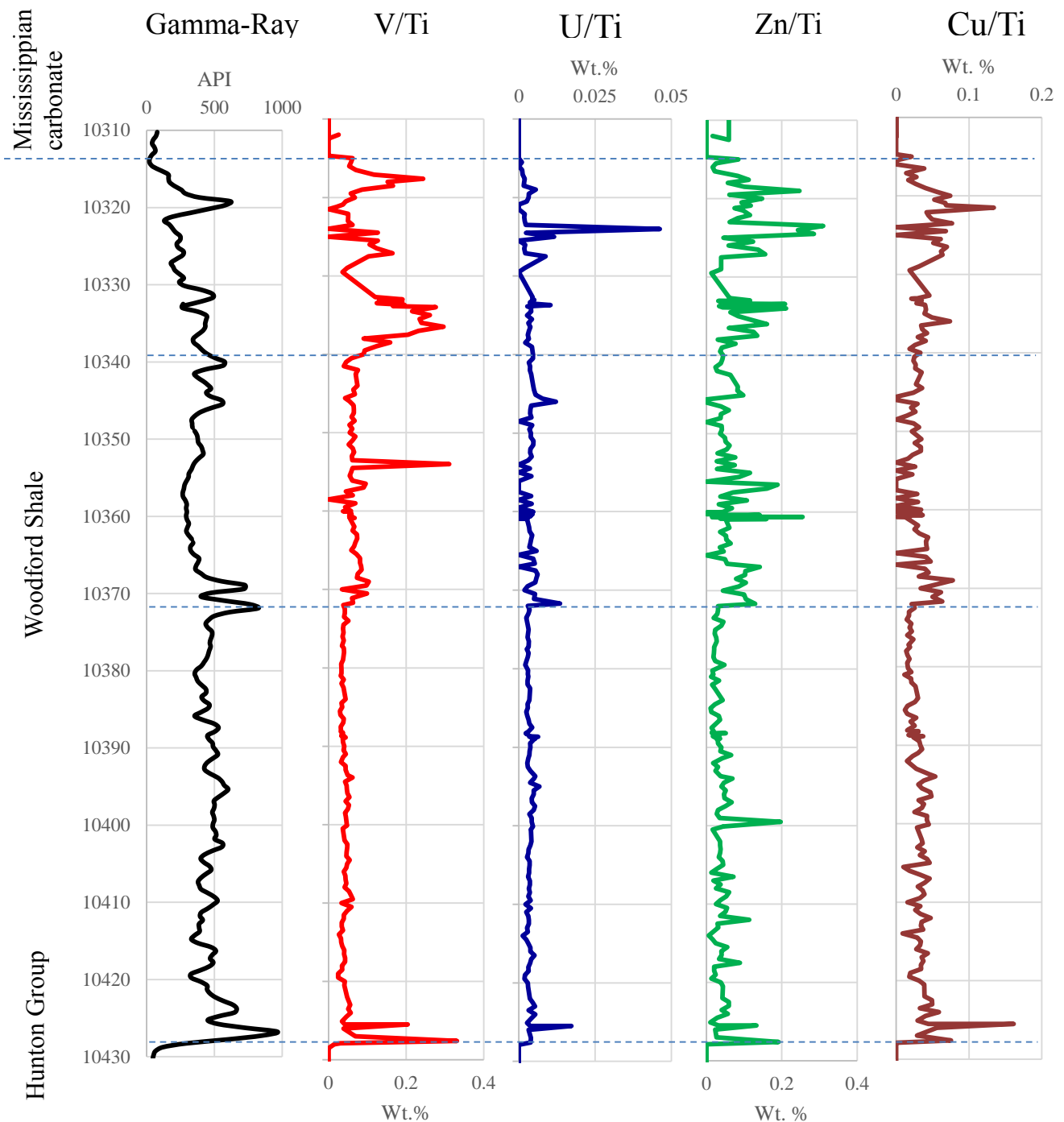


Figure 14. Gamma-ray profile and normalized concentration in weight percent (wt.%) of key trace elements (V, U, Zn, Cu) for Rother 1H-5X. Distinct patterns are apparent in the profile. Interval 1 from 10,431 to 10,372 ft has consistent gamma-ray values exceeding 400 API units and corresponding consistent V/Ti and U/Ti concentrations between 10,426 and 10,372. Interval 2 from 10,372 to 10,340 ft. has a lower gamma-ray value of approximately 350–400 API units from 10,368–10,340 ft. that corresponds to consistently higher normalized V, U, Zn, and Cu concentrations (0.07, 0.01, 0.15, and 0.025 wt.% respectively). Interval 3 (10,340–10,315 ft.) has a fluctuating gamma-ray profile with values ranging from 150 to 600 API units. Vanadium responds similarly with peaks at 10,336, 10,327, and 10,317 ft. Uranium peaks at 10,324 ft. but remains low otherwise. Zinc peaks at 10,333, and is higher from 10324 to 10,316 ft. Cu/Ti peak value is 0.14 wt.% at 10322 ft. but otherwise its concentration is similar to zinc.

Rother 1H-5X Chemostratigraphy

The x-ray fluorescence (XRF) scan of the Rother core showed that the primary trace metals detected were Si, Al, Ca, S, Fe, and K which all have weight percent (wt.%) concentrations greater than 1%. Because V, U, Cu, and Zn are redox and organic productivity indicators, these elements were plotted against the gamma-ray profile to generate a chemostratigraphy profile (Figure 14). There is relative stability of V/Ti ratios in the lowermost pyrite-rich (PR) zone, with a slight increase in values in the silica-rich (SR) zone from 10372 to 10340 ft. In the uppermost carbonate-rich (CR) section, V/Ti values are enriched and there is considerable variation between 10314 and 10338 ft. The U/Ti remains relatively constant throughout the core, except for a sharp increase up to 0.045 wt.% at 10324 ft. This increase corresponds to an increase in the Zn/Ti, but a decrease in the V/Ti and Cu/Ti ratios. Zn/Ti and Cu/Ti have similar patterns that indicate enrichment in zones SR and CR, while mostly consistent values in zone PR. There is a tendency towards brittle behavior when the Woodford Shale is highly carbonate or silica-cemented (Sierra et al., 2010). Figure 15 shows uncorrected values for Si and Ca across the Woodford interval. Si values are higher in the middle SR and upper CR sections (averaging 40 wt.% and 30 wt.%, respectively), and decrease accordingly in the lower PR section, which correlates with the core description. Ca concentrations in the PR interval remain constant at less than 5 wt. %, and decrease to less than 1% in the middle SR interval. In the upper CR interval, Si and Ca seem to have an inverse relationship, where the sharp decrease in Si concentrations correlates with increases in Ca concentrations.

Newfield Exploration Company provided results of chemical analysis of Woodford samples from the Rother 1H-5X core performed by a commercial laboratory. These analyses included TOC, XRF, and inductively coupled plasma mass spectrometry (ICP-MS). New XRF data were acquired using the OSU handheld instrument and compared to the provided commercial data (Figure 16). V concentrations share the same curve shape, peaking twice within the CR interval and decreasing to approximately 0.2 wt. % in the SR and PR intervals. Graphs of Zn and Cu concentrations (not shown) are also similar for both data sets. Larger concentrations of 0.1–0.3 wt. % occur in the CR and SR intervals and decrease to average 0.05 wt. % in the PR interval for both graphs. U is also somewhat similar to Zn and Cu, but the lack of specificity oversimplifies the original pattern. The commercial concentrations were within one standard deviation of the XRF values for all profiles.

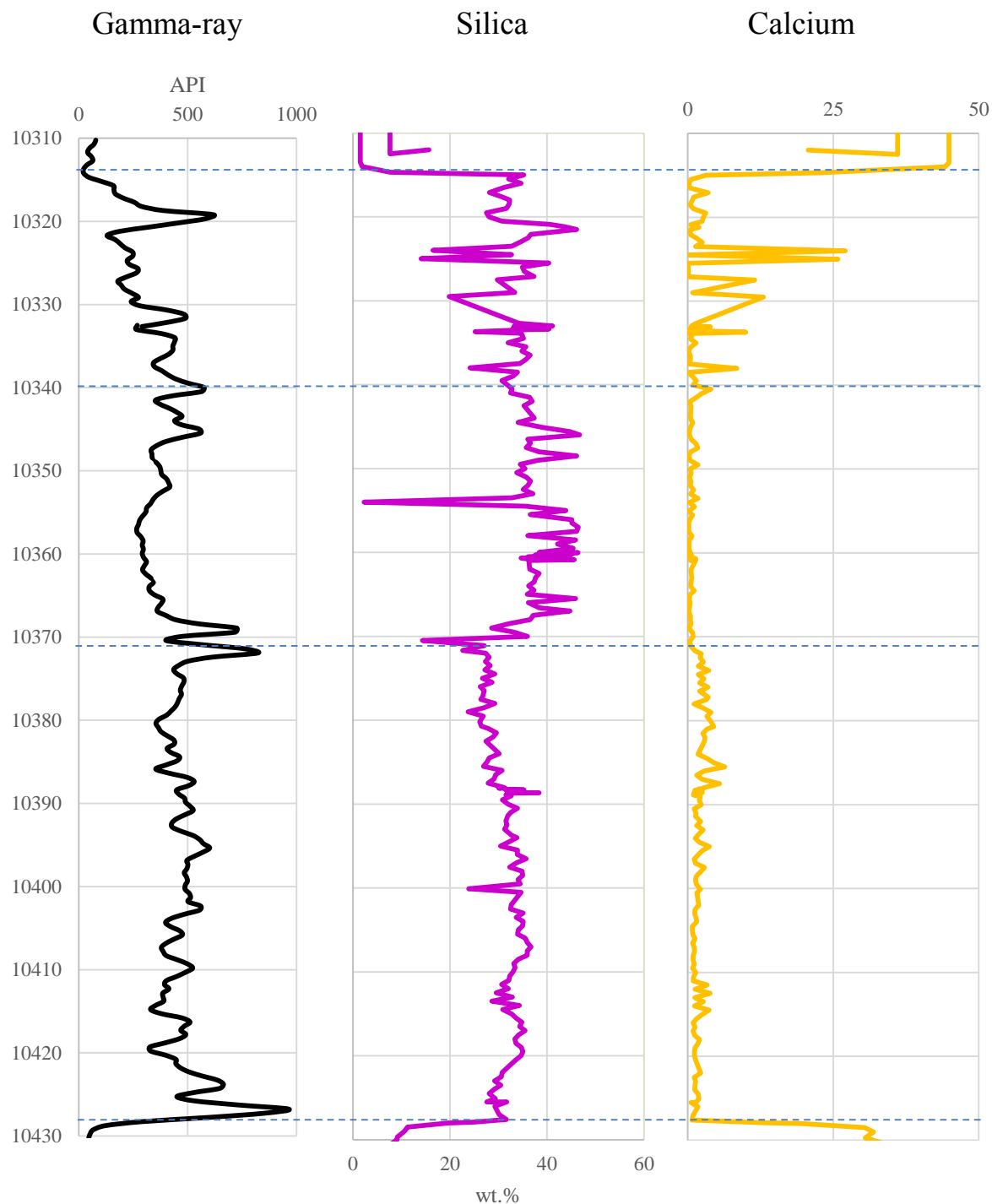


Figure 15. Gamma-ray profile and uncorrected concentration values for silica (Si) and calcium (Ca) (wt.%), Rother 1H-5X. Si has the greatest concentration throughout the core. Interval 1 from 10428 to 10372 ft. averages 30 wt.% for Si while Ca is consistent at 5 wt.%. In interval 2 (10372–10340 ft.), Si increases to 40% while Ca decreases to approximately 1%. Si and Ca fluctuate in concentrations and exhibit an inverse relationship in interval 3 (10340–10314 ft.).

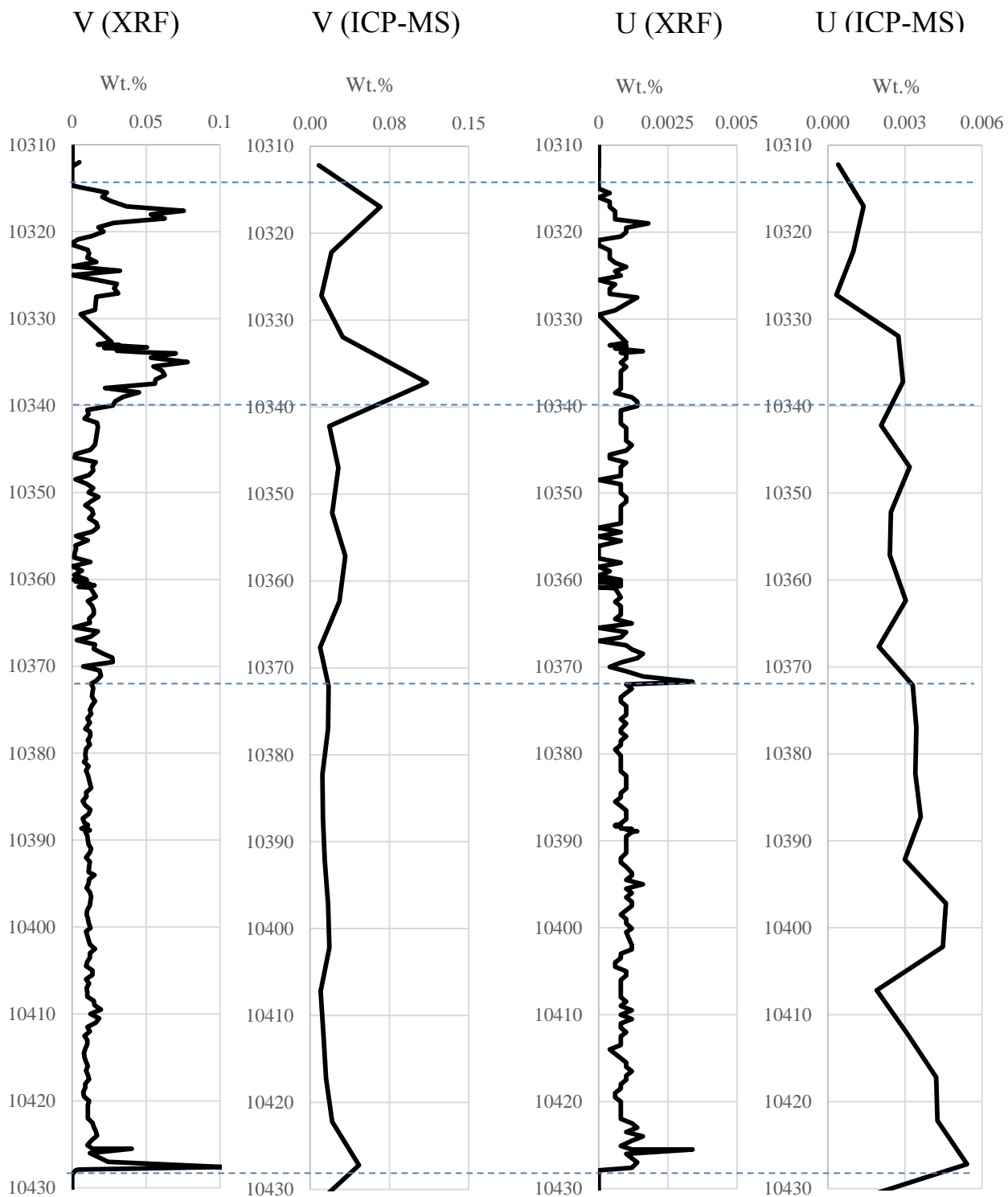


Figure 16. Profiles of vanadium (V) and uranium (U) (measured in wt.%) from XRF results are compared to the provided ICP-MS data, Rother 1H-5X. Concentrations for V are consistent for both data sets while the U concentrations have a greater variation, primarily between 10430 and 10372 ft. The ICP-MS values are higher overall, by nearly 10%.

Yost 1H-18X Core Description

Yost 1H-18X well is located in Sec. 30 T16N R8W in Kingfisher County, Oklahoma (Figure 1B). The core is continuous with a complete Woodford Shale section from 9389–9436 ft., a thin cored interval of Hunton carbonate of only 0.75 ft. from 9435.25 to 9436 ft. and Mississippian carbonate above 9389 ft. (Figure 17). Core depths are less than 2 ft. shallower than the wireline log depths. For most of the core, a natural vertical fracture splits it into two sections. The Woodford Shale in the Yost 1H-18X core is greyish black to black in color, and N1 to N2 on the GSA color chart.

The lowermost Woodford interval (9436–9418) in the Yost core contains a sharp unconformity with the Hunton Group that is marked by clay and phosphate clasts, sand-sized quartz and calcite sediment, and a color change a mix of medium grey, olive grey, and pale yellowish brown (N7, 5 Y 4/1, and 10 YR 6/2) to black (N1). Pyrite bands, laminae, and nodules are common throughout this interval, which is identified as the pyrite-rich (PR) zone (Figure 18). Silica-cemented bands (no greater than 1 cm thick) are scarce within the interval, and occur at depths of 9423, 9428, and 9430 ft. Pyrite laminae are mostly less than 0.1 cm thick and best seen when the core is wet. Pyrite nodules (pyritized sedimentary or biotic features greater than 0.1 cm) are scattered throughout the section; no larger than 0.1 x 1 cm. Most of this interval in thin section is silt to sand-sized quartz and calcite grains, along with silicified radiolarians, flattened *tasmanites*, and amorphous organic material (Figure 19). The upper contact with the next interval is a graded pyrite band (1 cm), with silt to sand-sized pyrite and a few small peloidal clasts.

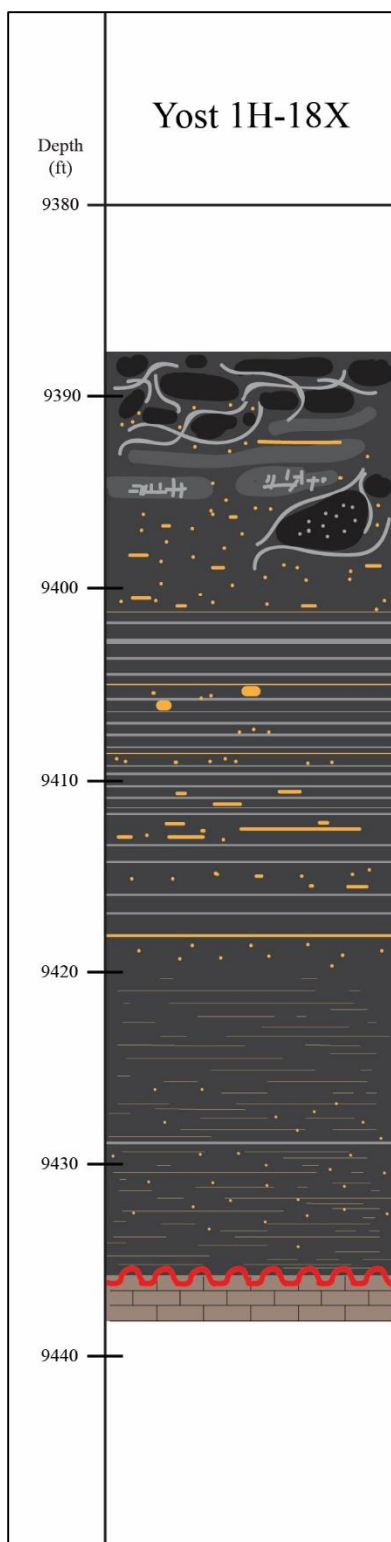


Figure 17. Schematic description of lithology and depositional and authigenic features in the Newfield Yost 1H-18X core, depth 9389 to 9437 ft.

Stratigraphy

	Mississippian		Hunton Group
	Woodford Shale		

Sedimentary Features

	Scattered pyrite		Carbonate-filled Fractures
	Pyrite bands		Glauconite zone
	Pyrite laminae		Phosphate/clay clasts
	Pyrite nodules		Soft-sediment deformation
	Silica-cemented bands		Unconformity

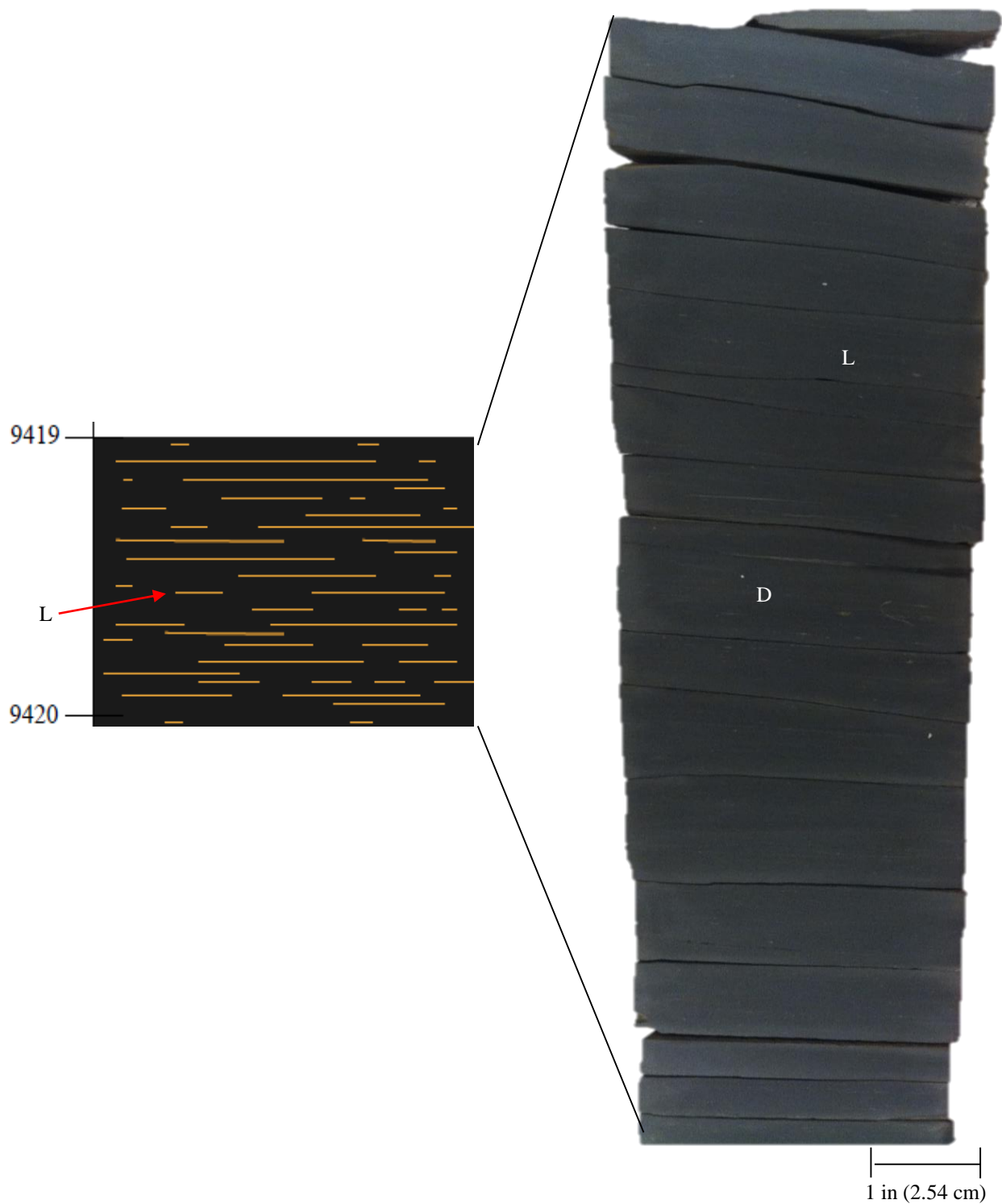


Figure 18. Pyrite-rich (PR) interval, Yost 1H-18X, depth 9419-9420 ft. This representative 1 ft. (30.48 cm) section includes pyrite laminae of less than 0.1 cm thick (L) and disseminated pyrite (D), which are characteristic.

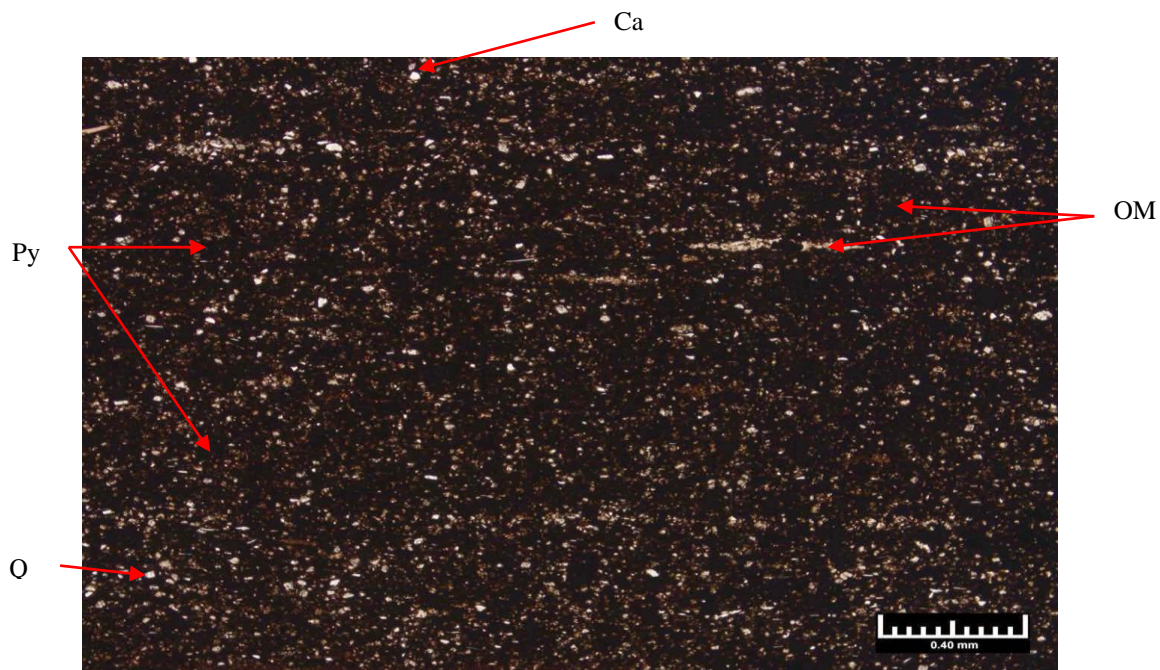


Figure 19. This section photomicrograph of the PR interval, Yost 1H-18X, depth 9424 ft. in plane-polarized light. The darker material is a mixture of pyrite (Py) and organic material (OM), while the lighter material is silt-sized calcite (Ca) and quartz (Q) grains with organic material.

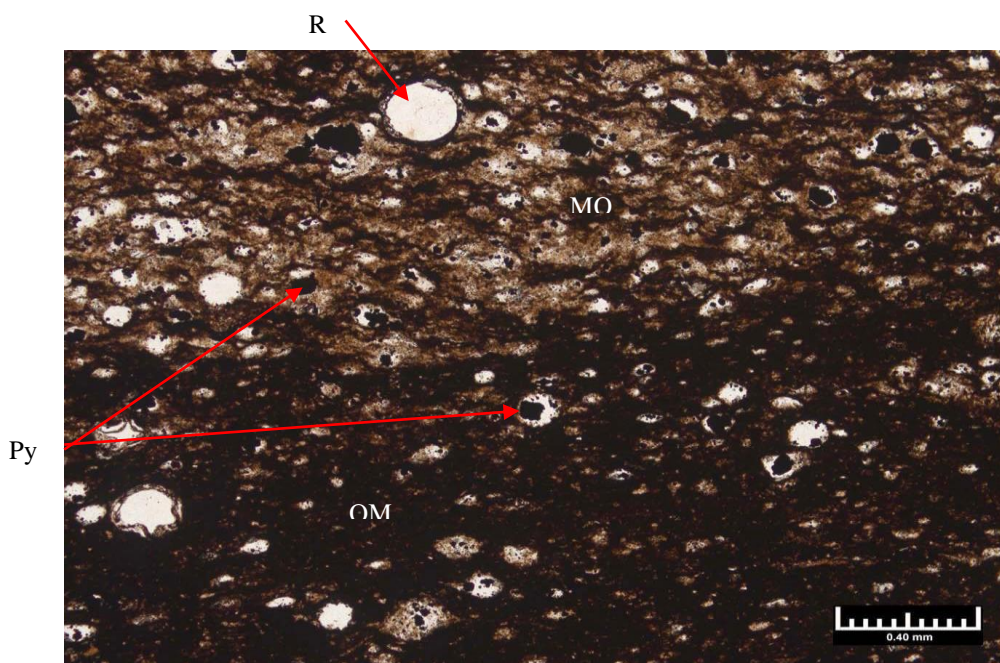


Figure 20. Thin section photomicrograph of the margin of a silica band, plane polarized light. The circular grains are silicified radiolarians (R). Those filled with angular dark grains are partially replaced by pyrite (Py). The dark matrix in the lowermost half of the slide is organic material while the tan to brown upper one-half is mostly microcrystalline quartz (MQ). The source of the silica cement has been attributed to the dissolution of radiolarians (Schieber et al., 2000). Yost 1H-18X, 9406 ft.

The second interval, at depths of 9418–9402 ft., is rich with silica-cemented bands and is labeled the silica-rich (SR) interval. Pyrite occurs within silica-rich bands and as separate pyrite-rich intervals without obvious silica cement. Silica bands average about 1.2 cm in thickness, whereas pyrite bands are around 0.5 cm. Figure 20 is a photomicrograph of a sample from 9406 ft. that shows the contact of one of these silica bands and the adjoining shale. The bright circles are silicified radiolarians, while the black spots are secondary pyritization within radiolarians. Some silica bands are cut by small calcite-filled vertical fractures that terminate in the adjacent more clay-rich beds above and below (Figure 21). Although silica bands often contain an accumulation of pyrite, silt-sized pyrite and nodules are also distributed through the section. Nodules mostly occur in the silica bands, but a few larger pyritized biogenic features are observed near the top of this section. The contact between the silica-rich (SR) interval and the overlying section is placed above the last high concentrations of silica-cemented bands at 9402 ft.

The uppermost interval at 9402–9389 ft. exhibits the most variability in facies. Soft-sediment deformation, phosphate and clay clasts, calcite-filled fractures, and disseminated pyrite are common. There are no silica-cemented bands, but pyrite layers, 0.5 to 1 cm thick, occur at the depths of 9395, 9398, 9400, and 9402 ft. Figure 22 is a photomicrograph of the pyrite band at 9400 ft. which includes skeletal fragments such as sponge spicules and possible shell fragments, flattened *tasmanites*, and silica grains along with the pyrite, which are the darker areas. A significant feature in this section between 9396–9397 ft. is a large phosphate nodule (5 x 10 cm) enclosed in deformed beds. Other

phosphate nodules are fractured and contain inclusions of pyrite and calcite-filled spherical features. Veins and fractures of calcite also occur in the enclosing beds. Near the top of this carbonate-rich (CR) interval, pyrite laminae and bedding planes dip approximately 9 degrees. The contact with the overlying Mississippian carbonate occurs at 9388 ft., correlating to a change in lithology and color to a light–normal olive grey (5 Y 6/1 – 5 Y 4/1). Immediately along the contact is a distinct glauconitic zone.

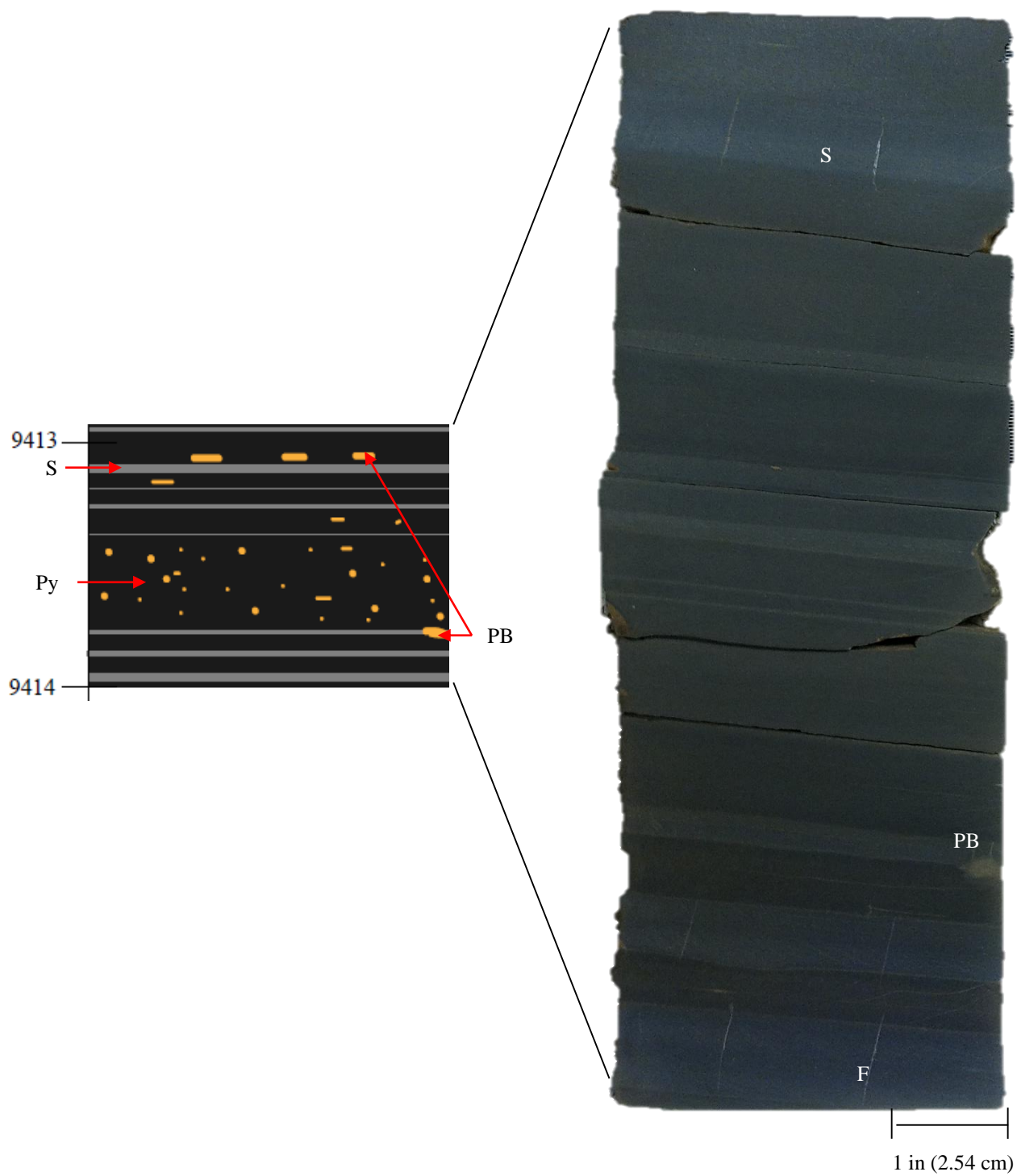


Figure 21. Silica-cemented bands (S) with pyritized burrows (PB) and scattered pyrite (Py) characteristic of the silica-rich (SR) interval. Calcite-filled fractures (F) are evident, Yost 1H-18X, depth 9413-9414 ft.

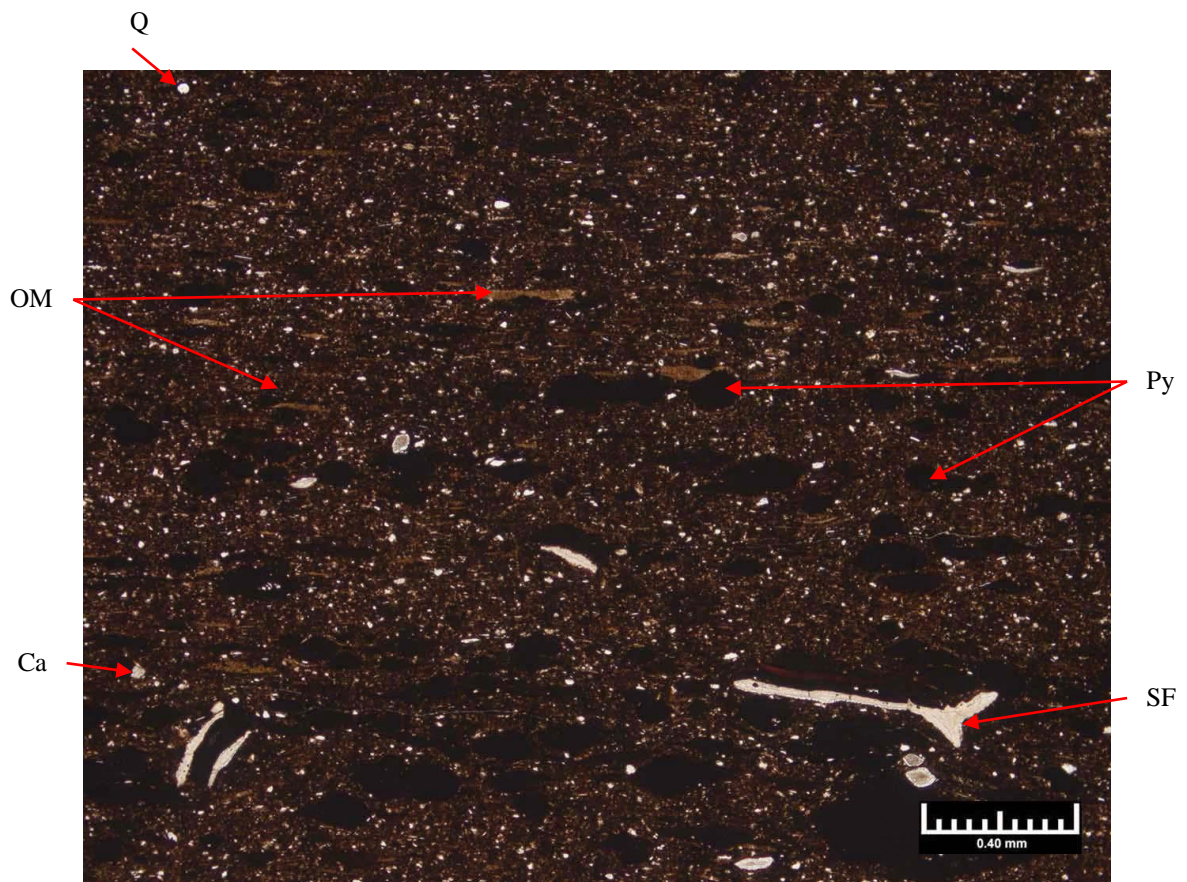


Figure 22. Photomicrograph of a pyrite band in which the dark areas are pyrite (Py), brown is organic material (OM), clear is silt-sized calcite (Ca) and quartz (Q), and white grains are skeletal fragments (SF). Yost 1H-18X, depth 9400 ft. (PPL)

Yost 1H-18X Gamma-ray Characteristics

The lowermost pyrite-rich zone of the Yost 1H-18X well ranges from 9438 to 9421 ft. (Figure 23). Gamma-ray values for this interval consistently average around 600 API units. In the intermediate silica-rich zone (9421–9404 ft.), gamma-ray values are higher near the base (700 API units), decrease across the middle to approximately 300 API units from 9418 to 9408 ft., and then increase toward the top at 9404 ft. where they

reach 700 API units. The gamma-ray measurements across the uppermost carbonate-rich zone, 9402 to 9392 ft., are highest at the base (700 API units) and gradually decrease upward to 200 API units. This interval exhibits greater fluctuation in gamma-ray values than the other units.

Yost 1H-18X Chemostratigraphy

The Yost core was scanned using the Niton XRF and the normalized concentrations of selected metals plotted with the gamma-ray curve to make a chemostratigraphic profile (Figure 23). The gamma-ray curve is approximately 2 ft. deeper than the core depths. The plotted metals are V/Ti, U/Ti, Zn/Ti, and Cu/Ti. The V/Ti plot exhibits more distinct changes across each zone and is less enriched in the pyrite-rich interval where it averages 0.05 wt.%, increases in the silica-rich (SR) interval to around 0.1 wt.%, and is greatest in the carbonate-rich (CR) interval from 0.1-0.5 wt.%. Both U/Ti and Zn/Ti are relatively stable throughout the core whereas Cu/Ti ratios fluctuate more, but are still similar in all three sections. A slight increase in normalized U, Zn, and Cu occurs at 9416 ft. (9418 ft. log), but that is the interval where additional measurements were collected to help identify higher frequency changes across a silica-cemented zone.

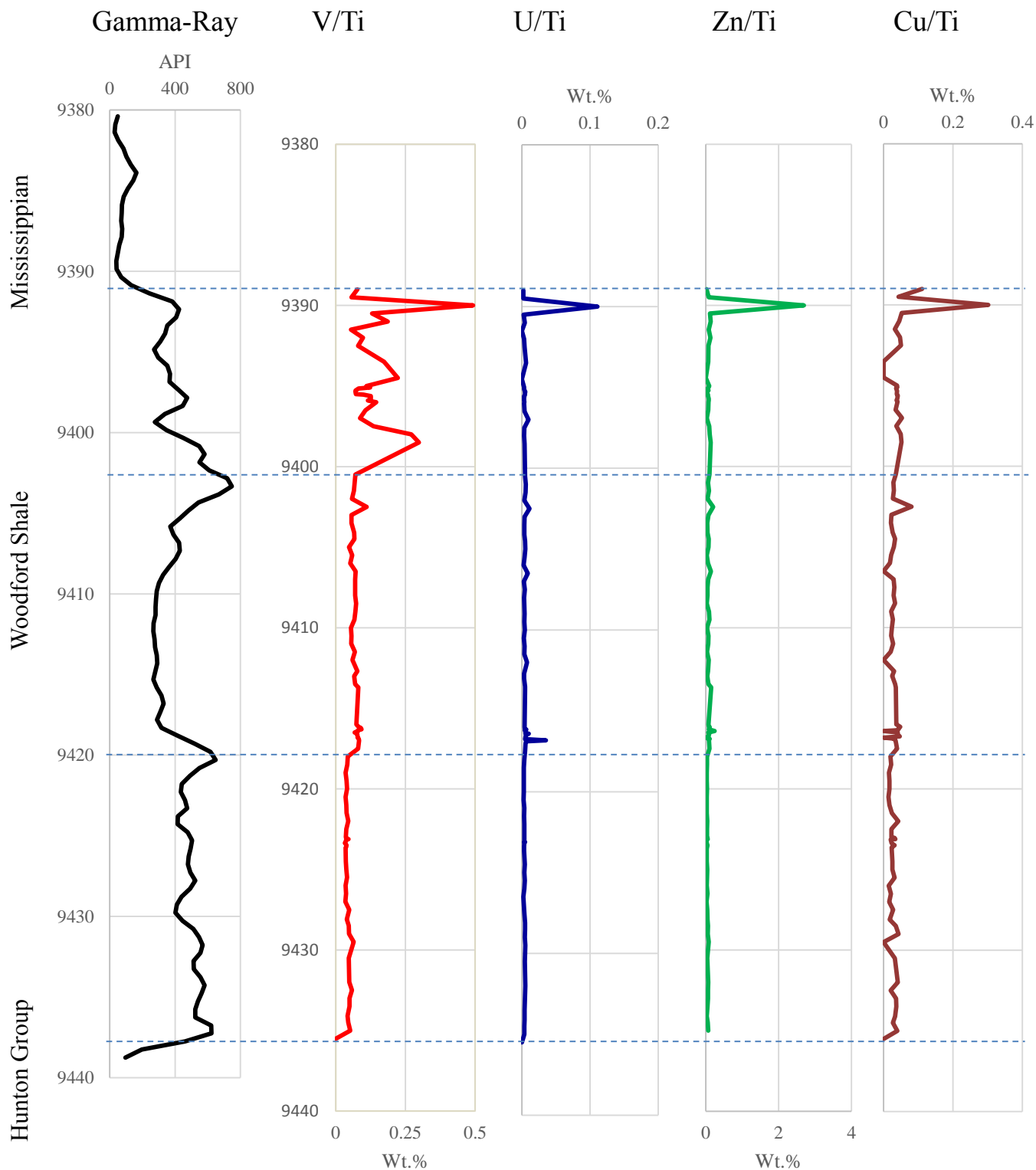


Figure 23. Gamma-ray profile and normalized trace metal concentrations in wt.% for Yost 1H-18X. Gamma-ray depth is approximately 2 ft. lower than core depth. The gamma-ray signature for the lowermost interval (9438–9420 ft.) averages approximately 600 API units and corresponds to consistently lower values in the V, U, Zn, and Cu concentrations. Interval 2 from 9420 to 9402 ft. peaks at 700 API and decreases to 300 API units. The V/Ti concentrations slightly increases across this interval, while concentrations of other elements change less. The third interval gamma-ray (9402–9391 ft.) fluctuates from 700 API to 300 API before returning to normal levels in the superjacent Mississippian limestone. Normalized V and Cu concentrations also fluctuate while U and Zn remain consistent. The peaks at the top of the trace-element graphs correlate to the contact with the limestone.

In addition to examining redox and organic productivity proxies, Si and Ca (uncorrected) were analyzed to evaluate the influence of authigenic cements on rock properties (Figure 24). Generalized patterns emerge that indicate when Si is high, Ca is low; when Si peaks drop, Ca suddenly increases. In the pyrite-rich (PR) zone, Si increases where silica bands occur in the core. As expected, Si increases in the silica-rich (SR) zone from 9420 to 9404 ft. Silica displays variable concentrations in the CR zone and decreases to low values at 9391 and 9397 feet (log depths). Sharp increases in Ca correspond to these drops in Si concentration (Figure 24). Calcium is relatively constant across the pyrite-rich (PR) and silica-rich (SR) intervals, but displays the previously depicted inverse relationship with silica. This relationship is subtle in the PR and SR zones, but very apparent in the CR interval at 9391 and 9397 ft.

The concentrations of Mo, Fe, K, Al, and S are higher in the Yost 1H-18X than the Rother 1H-5X, but the Rother core contains more Ca. Weatherford International analyzed seven samples from the Woodford Shale section in the Yost well using both XRF and ICP. When graphed, the concentrations of trace metals in their samples were too few and too widely separated to make a meaningful pattern.

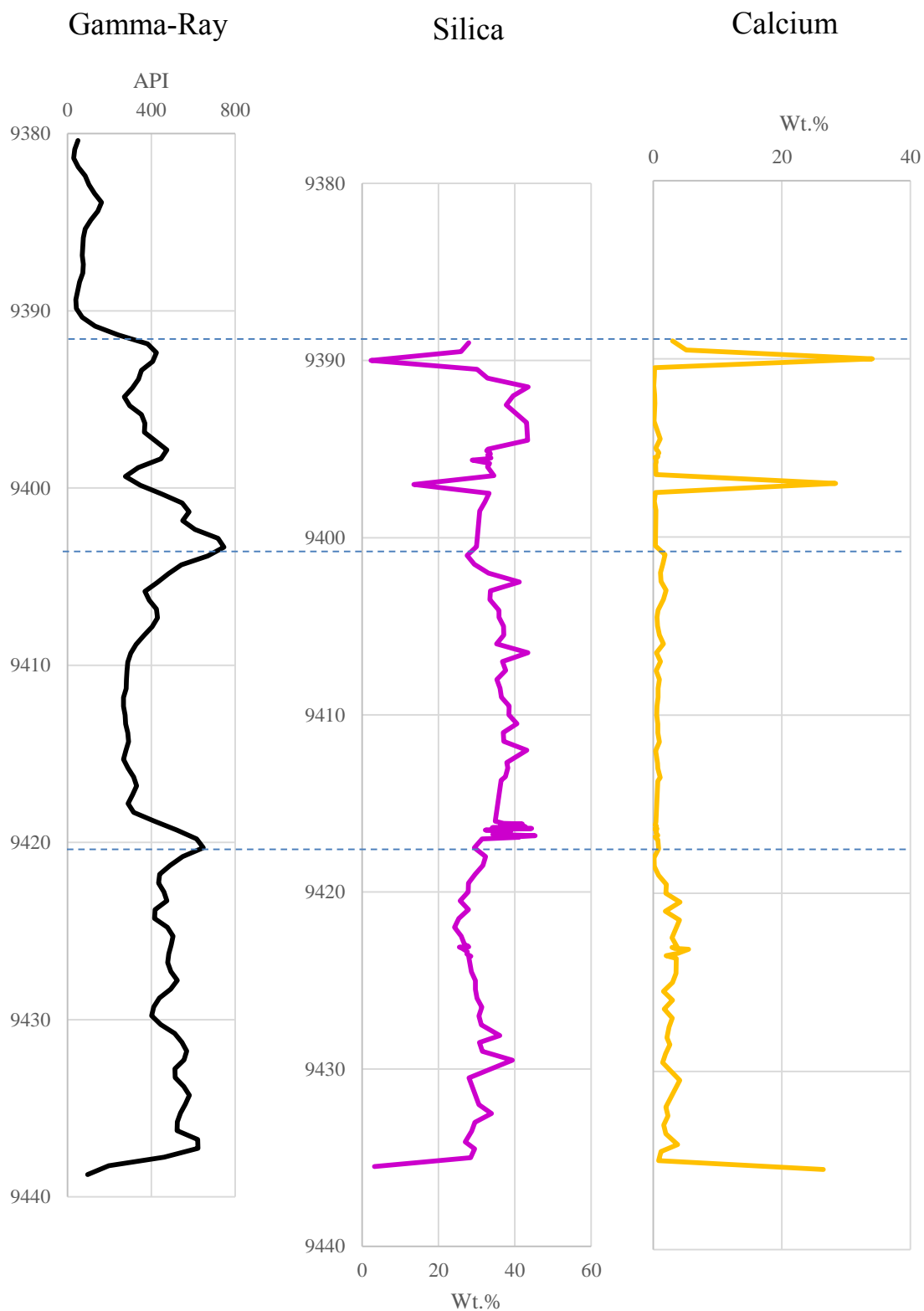


Figure 24. Gamma-ray profile and uncorrected silica and calcium concentrations, Yost 1H-18X. The gamma-ray depths are 2 ft. low to the core depths. Interval 1 (9436–9418 ft. on the element profiles) averages 30 wt.% for Si and decreases from 9430 to 9420 ft. before increasing to the end of the interval. Ca is consistent around 3 wt.%. In interval 2 (9418–9402 ft.), Si increases to approximately 35 wt.%. Ca decreases to a consistent 1 wt.%. From 9402 to 9389 ft. (interval 3), Si and Ca values fluctuate and exhibit an inverse relationship.

Matthews 2-8H Core Description

The Matthews 2-8H well is located in Barber County, Kansas, Sec. 8 T33S R10W (Figure 1B). The Matthews was cored in several intervals including the Mississippian carbonate “Kinderhook” shale, the Woodford Shale, and pre-Woodford beds. This study focuses on 70 feet of core from 4811 to 4881 ft. that includes 34 ft. of the “Kinderhook”, 33.7 ft. of the Woodford Shale, and 2.5 ft. of an unconformity sandstone and 1.5 ft. of Ordovician shale that overlies a thick carbonate section (Figure 25). The Pre-Woodford unconformity sandstone and Ordovician beds are a very light grey to medium light grey (N8–N6) and change to olive grey (5 Y 4/1), the Woodford Shale is dark grey to black (N3–N1), and the “Kinderhook” is mostly greyish black (N2).

The lower section of the Woodford Shale in the Matthews core extends from 4876 to 4856 ft. The Woodford has a sharp unconformable contact with the underlying sandstone. The basal Woodford contact contains phosphate and carbonate clasts, laminated sandstone and carbonate facies, silt to sand-sized grains of calcite and quartz, and green grains that may be glauconite.

The lower zone of the Woodford Shale, identified here as the lower pyrite-rich (LPR) zone, contains pyrite laminae, pyrite nodules, disseminated silt-sized pyrite, and a few pyrite bands at 4860–4867 ft. (Figure 26). Horizontal zones of concentrated silt-sized pyrite occur at 4874 and 4863 ft., but the pyrite is not abundant enough to be defined as a layer. A large pyrite nodule occurs at 4872 ft. that is 1 x 2 cm, but all other nodules are less than 1 cm. Pyrite laminae are usually less than 0.1 cm and the defining characteristic of this interval. Also in the LPR zone at 4867 ft. are a few anomalous pyrite features shaped like two semi-circles that are <1 cm in length. Thin section photomicrographs

show that the LPR is primarily silt to sand-sized quartz and pyrite grains, *tasmanites*, and silt lenses (Figure 27). The contact of the LPR zone with the next interval was placed along a 1 cm thick pyrite band. Figure 28 is a thin section photomicrograph of this pyrite band and reveals the constituents include conodonts, unknown bone fragments, flattened *tasmanites*, silt-sized quartz grains, and pyrite. Some pyrite grains have a phosphate coating (Figure 28).

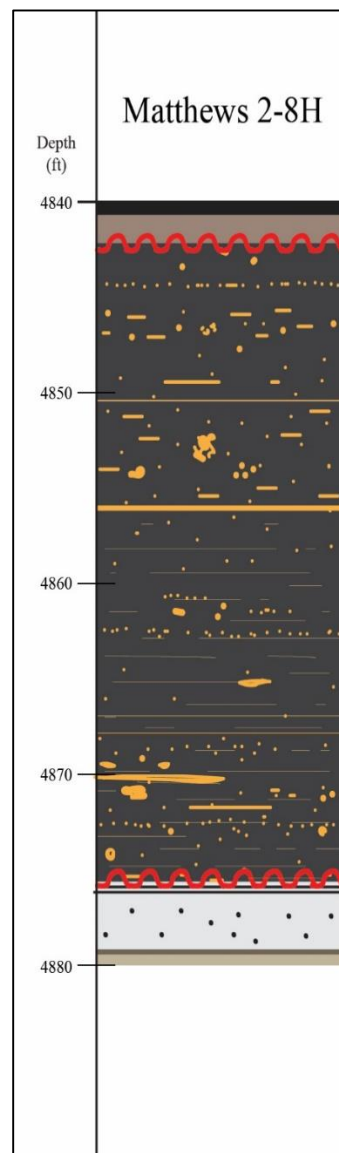


Figure 25. Schematic description of lithology and depositional, biogenic, and authigenic features in the Tug Hill Operating Matthews 2-8H core.

Stratigraphy

	Mississippian		Hunton Group
	Woodford Shale		Pre-Woodford Beds

Sedimentary Features

	Scattered pyrite		Carbonate-filled Fractures
	Pyrite bands		Glaucinite zone
	Pyrite laminae		Phosphate/clay clasts
	Pyrite nodules		Soft-sediment deformation
	Silica-cemented bands		Unconformity

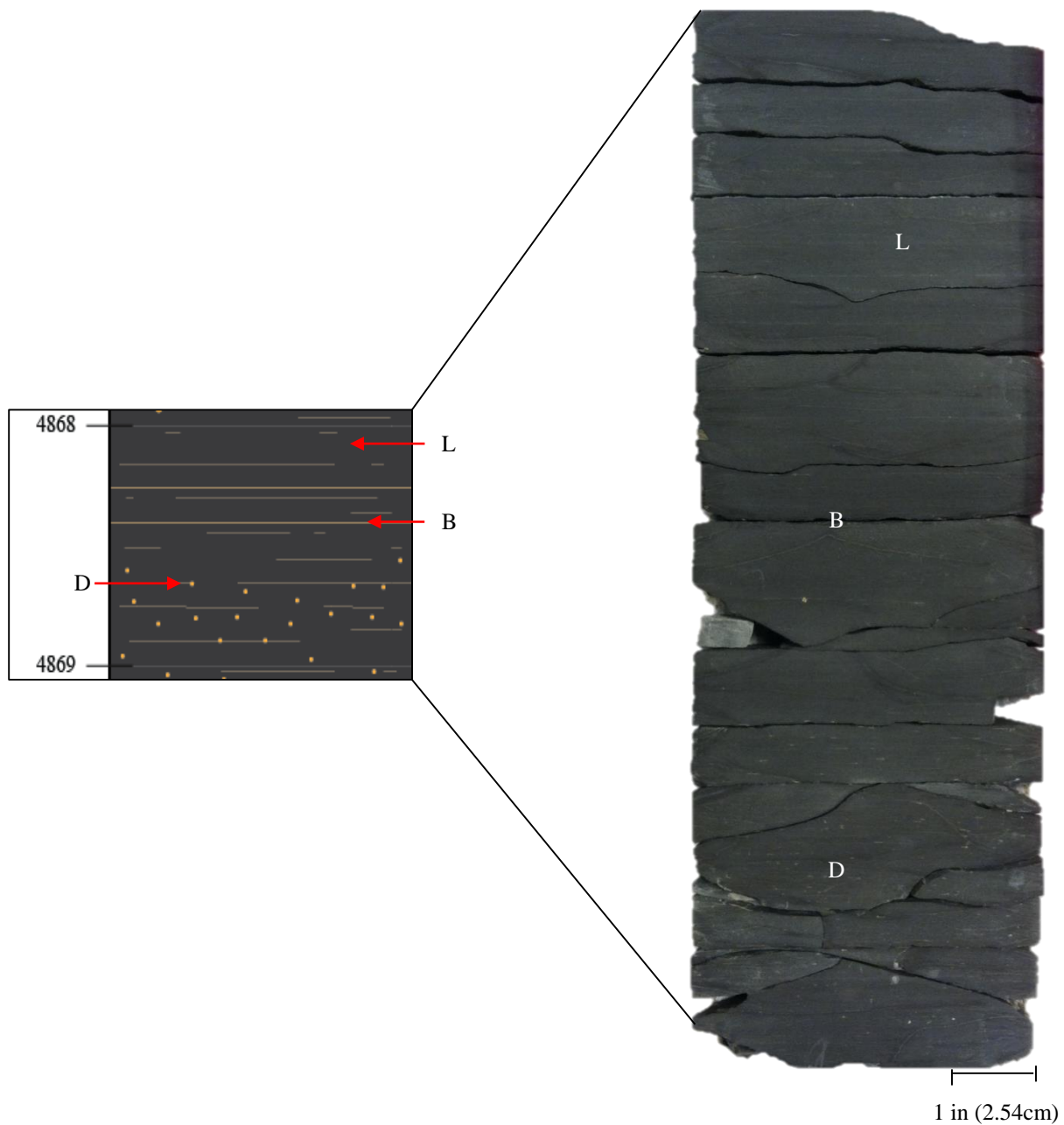


Figure 26. Pyrite laminae (L), pyrite bands (B), and disseminated sand-sized pyrite (D) that are common within the lower pyrite-rich (LPR) interval, Matthews 2-8H, depth 4868–4869 ft.

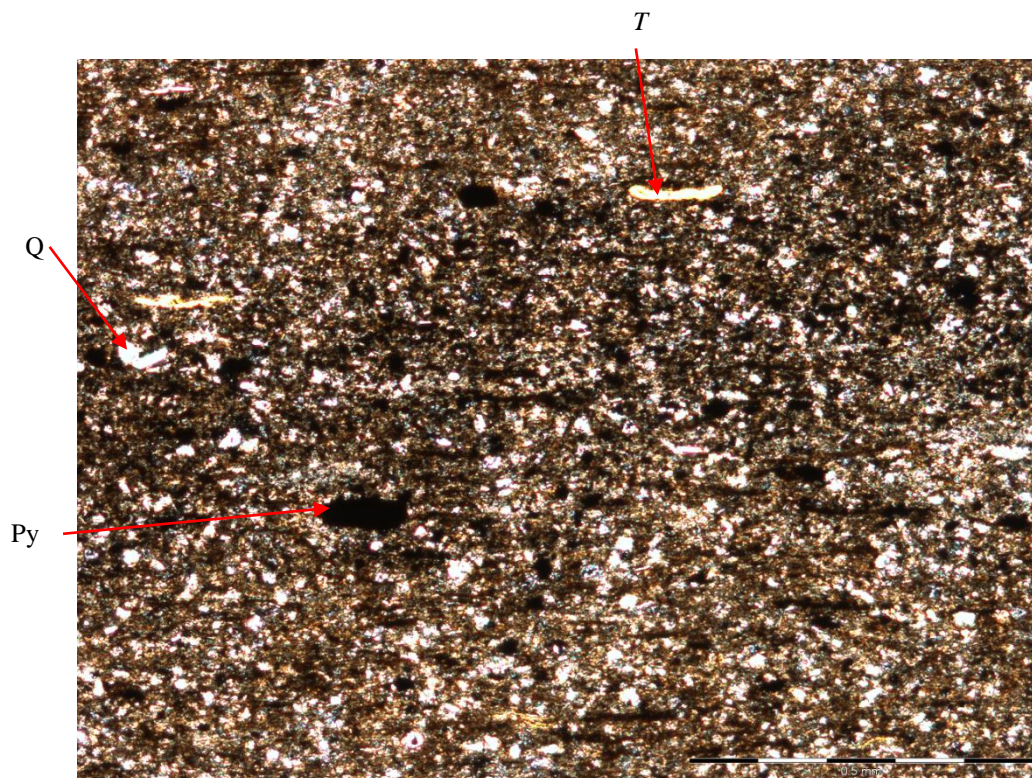


Figure 27. Thin section photomicrograph of the LPR interval, Matthews 2-8H, depth 4863. Most of the interval is made up of silt to sand-sized quartz grains (Q), pyrite (Py), and organic material that includes *tasmanites* (T).

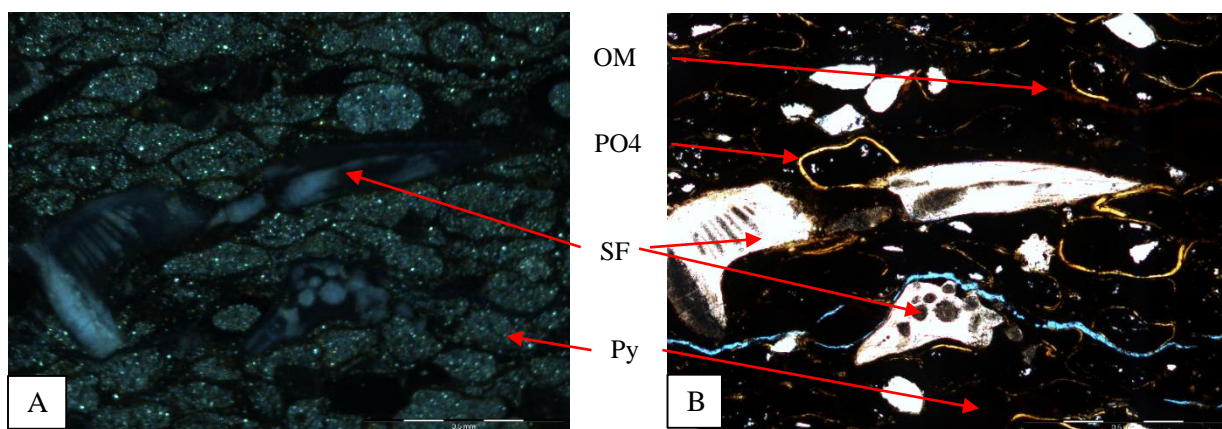


Figure 28. Thin section photomicrographs of the pyrite band that represents the contact between the LPR and the UPR, Matthews 2-8H, depth 4855 ft. (A) Reflected light was used to identify the individual pyrite grains (Py). (B) Plane-polarized light of the same area as A. The white pieces are skeletal fragments (SF), the brown is amorphous organic material (OM), and the yellow is phosphate (PO4) that coats pyrite grains.

The upper Woodford section (4856–4842 ft.) is also pyrite-rich and identified here as the upper pyrite-rich (UPR) zone. This zone contains disseminated silt to sand-sized pyrite and pyrite nodules, but lacks the pyrite laminae evident in the LPR. Thin section analysis reveals that the UPR also includes features such as silt lenses, agglutinated forams, *tasmanites*, and amorphous organic matter (Figure 29). Pyrite bands are not common in the UPR, but do occur at 4844, 4851, and 4855 ft. (Figure 30). The pyrite nodules are spherical, less than 1 cm in diameter, and occur singularly or in groups. Color changes from black to dark gray, which are noticeable when the core is wet, occur at 4846 and 4848 feet (Figure 31). The unconformable contact between the Woodford and the Mississippian “Kinderhook” includes one foot (30.48 cm) of dark greenish grey mudrock (5 GY 4/1) and a lag deposit of phosphate clasts and sand-sized grains that marks the base of the “Kinderhook” black shale. This Mississippian shale appears to be very similar to the Woodford as another black shale with scattered pyrite, but thin section petrography reveals the “Kinderhook Shale” is more clay-rich than the Woodford (Figure 32).

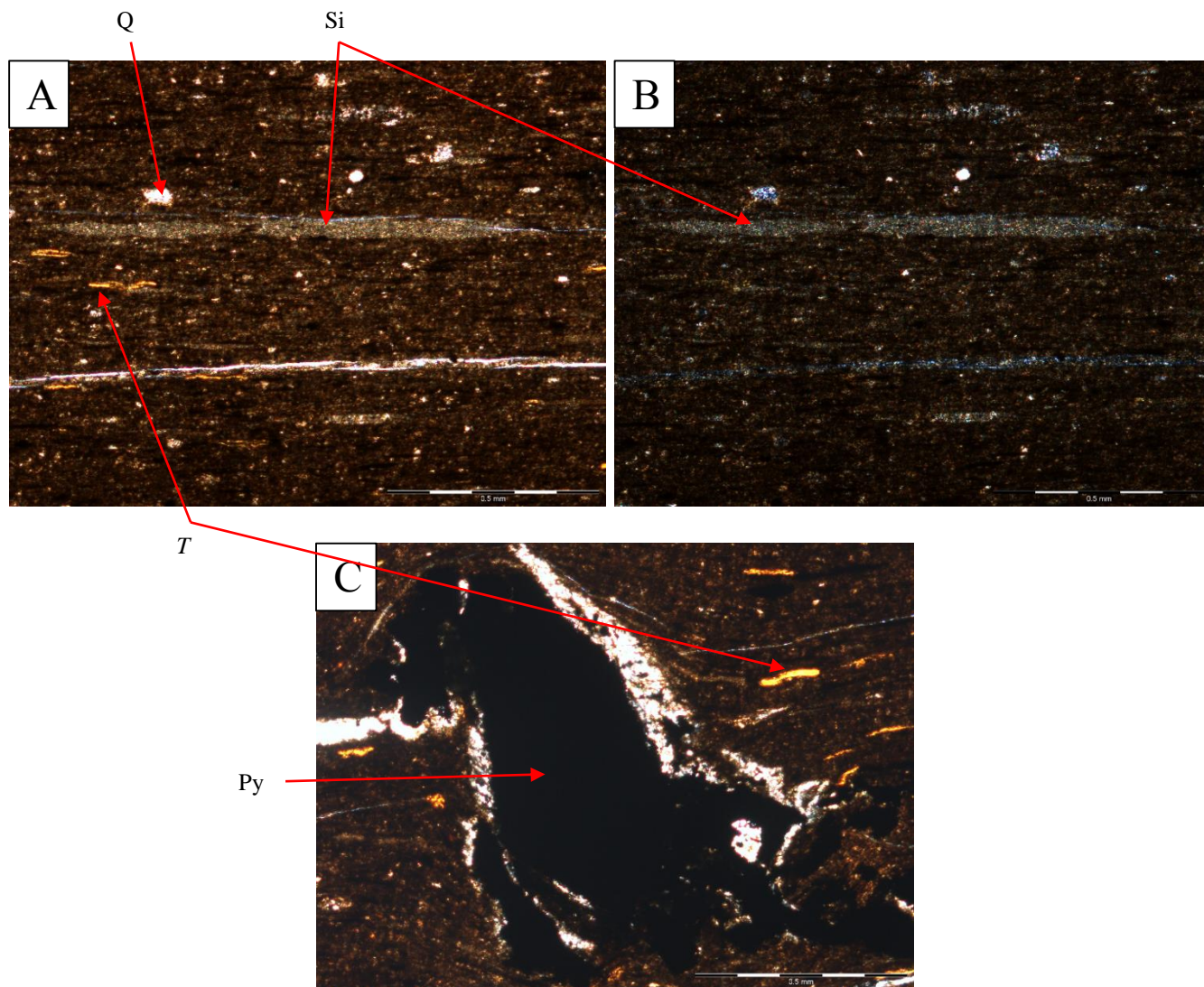


Figure 29. Thin section photomicrographs of silt lenses (A-B) and pyrite (C), Matthews 2-8H, depth 4848 ft. (A) Plane-polarized view of silt lenses (Si), *tasmanites* (T), and quartz grains (Q). (B) Cross-polarized light view of A. (C) Plane-polarized photomicrograph of a pyrite grain (Py). This pyrite grain disrupts bedding in the surrounding matrix.

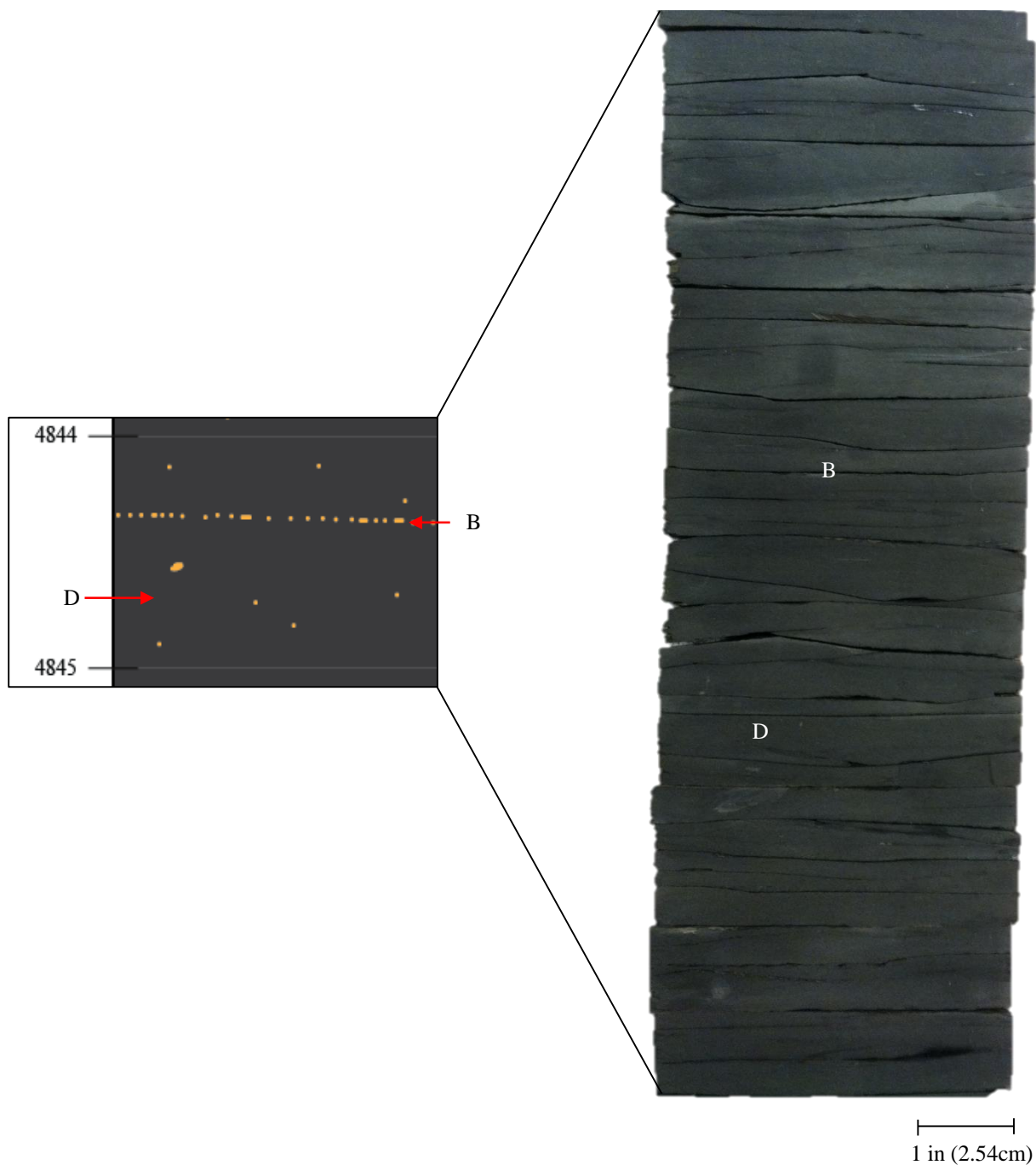


Figure 30. Disseminated silt-sized pyrite (D) and one of the few pyrite bands (B) found in the upper pyrite-rich (UPR) zone, Matthews 2-8H, depth 4844–4845 ft. The clay-rich UPR zone does not contain many obvious sedimentary or biogenic features.

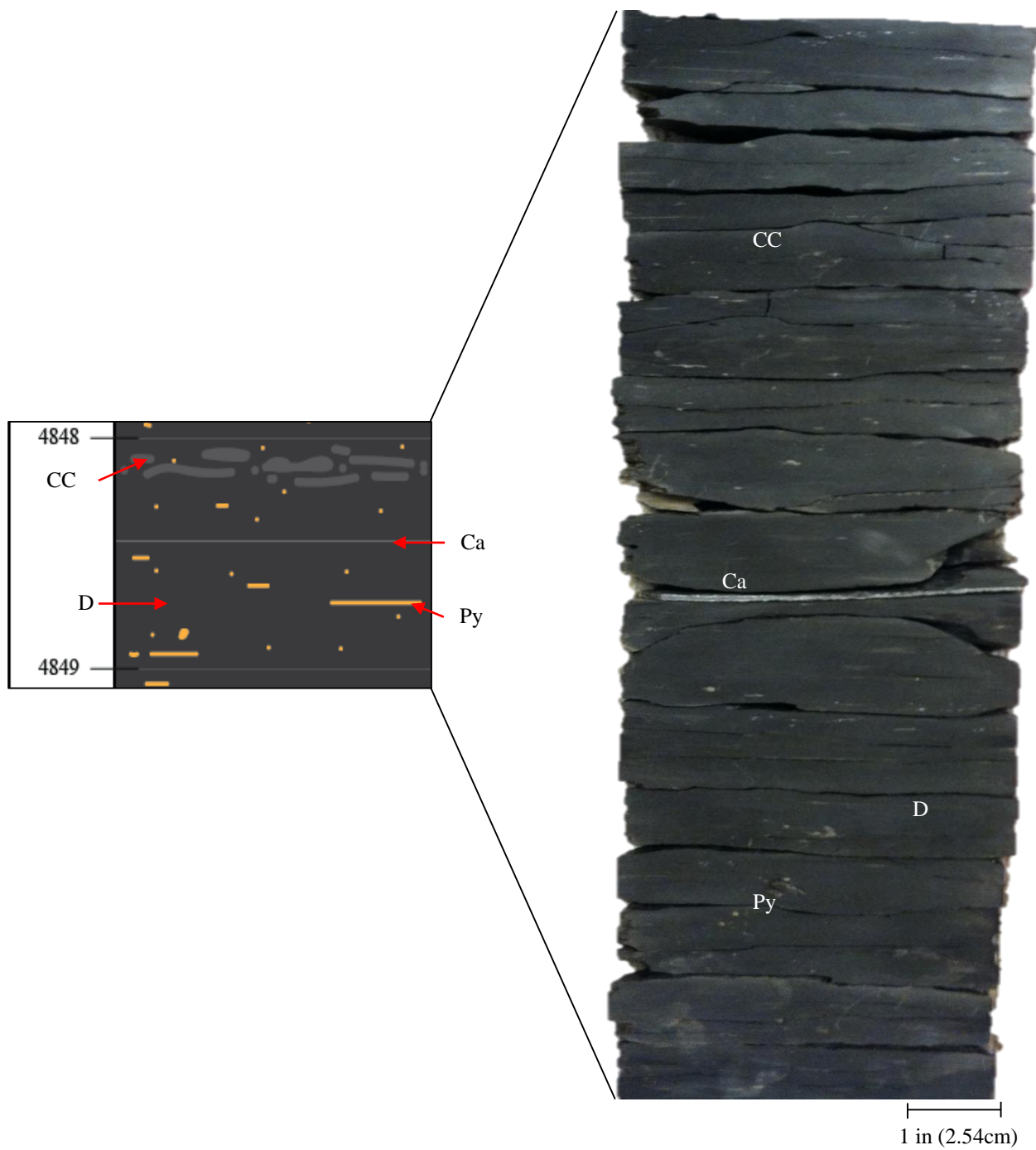


Figure 31. Disseminated pyrite (D), calcite-band (Ca), and scattered pyritized features (Py), Matthews 2-8H, depth 4848 ft. At the top of this section, there is a slight color change (CC) from black to dark grey.

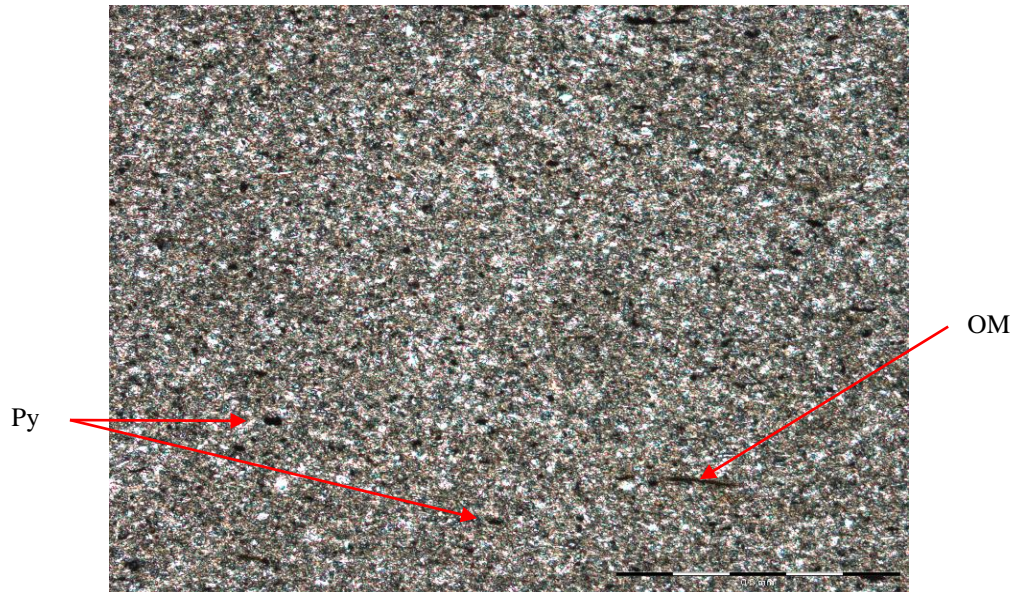


Figure 32. Thin section photomicrograph of the “Kinderhook Shale”, Matthews 2-8H, depth 4836 ft. Constituents include pyrite grains (Py) and organic material (OM). The dark colored “Kinderhookian Shale” appears to be more clay rich than the subjacent Woodford Shale.

Matthews 2-8H Gamma-ray Characteristics

The lowermost interval of the gamma-ray signature for Matthews 2-8H (4880 to 4876 ft.) records the pre-Woodford beds. The gamma-ray curve peaks at 420 API units at 4877 ft. (Figure 33). From 4877 to 4875 ft. the gamma-ray decreases to less than 140 API units which corresponds to sandstone below the Woodford Shale. The lowermost Woodford Shale interval (LPR, at core depths 4875 to 4856 ft.) has high volumes (>300 API wireline open hole log) that decreases to approximately 225 API at 4860 feet and increases to >500 API by 4856 ft. The highest gamma-ray value (620 API units) occurs at 4854 ft. within the uppermost Woodford Shale interval (UPR). Gamma-ray values decrease to the top of the Woodford section at 4842 ft. The uppermost interval of this core from 4842 to 4811 ft. is the Mississippian “Kinderhook Shale”. “Kinderhook”

gamma-ray values are consistent around 140 API units with a peak at 4826 ft. of approximately 180 API units.

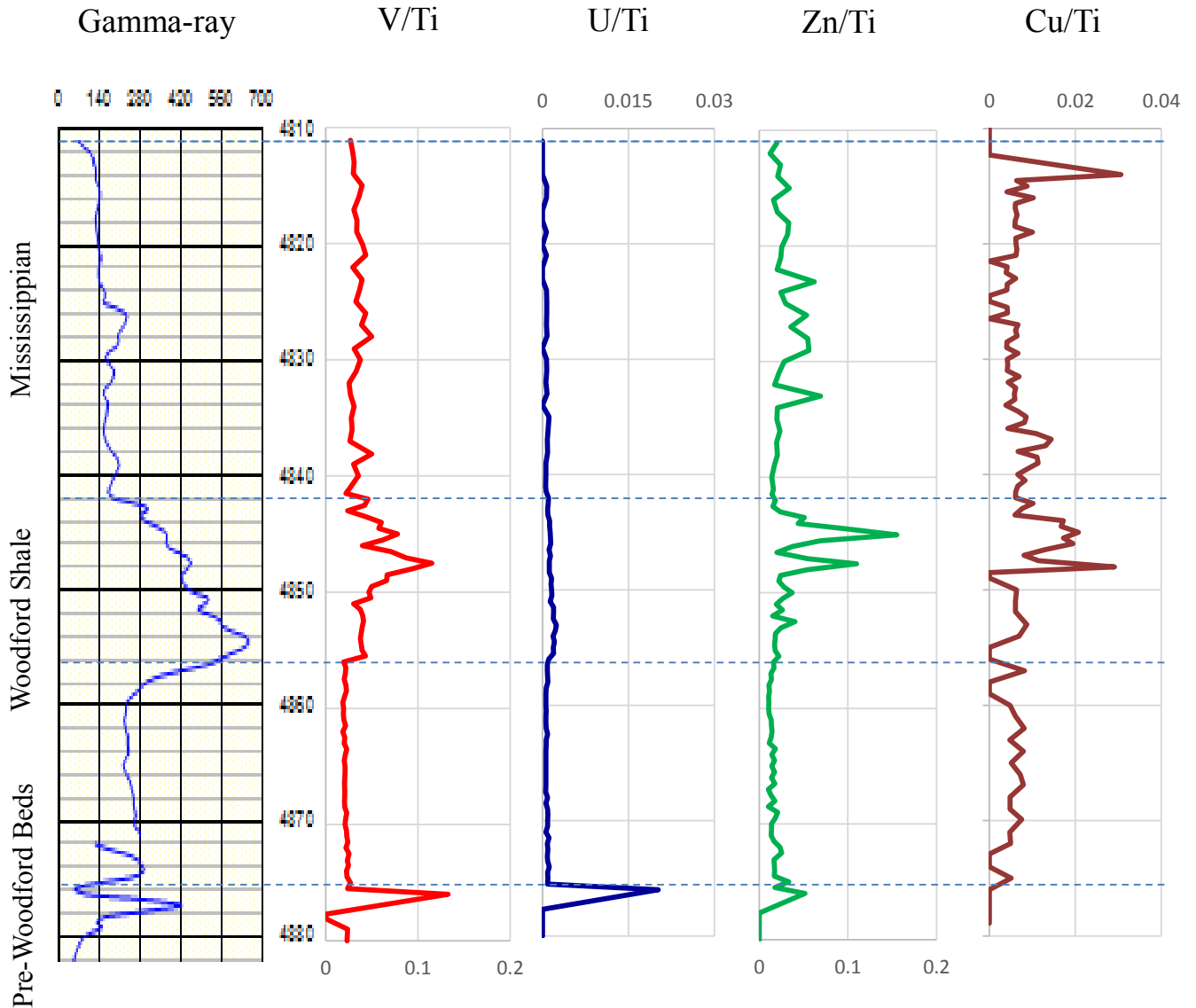


Figure 33. Gamma-ray profile and normalized trace element concentrations for the primary proxies (V, U, Zn, Cu), Matthews 2-8H. The lowermost interval from 4880 to 4876 ft. contains the Pre-Woodford beds, which corresponds to peaks in V/Ti, U/Ti, and Zn/Ti profiles. Interval 2 (4876–4856 ft.) has consistent trace-element concentrations while the gamma-ray values vary from 280 to 150 API units. From 4856 to 4842 ft. the gamma-ray values peak at 580 API before decreasing to 200 API. The normalized V, Zn, and Cu values share peaks at 4847 and 4845 ft. while U/Ti only has a slight increase in concentration. The top interval (4842–4811) is the Mississippian “Kinderhook” section and all graphs share consistent values, with a few peaks in Zn and Cu.

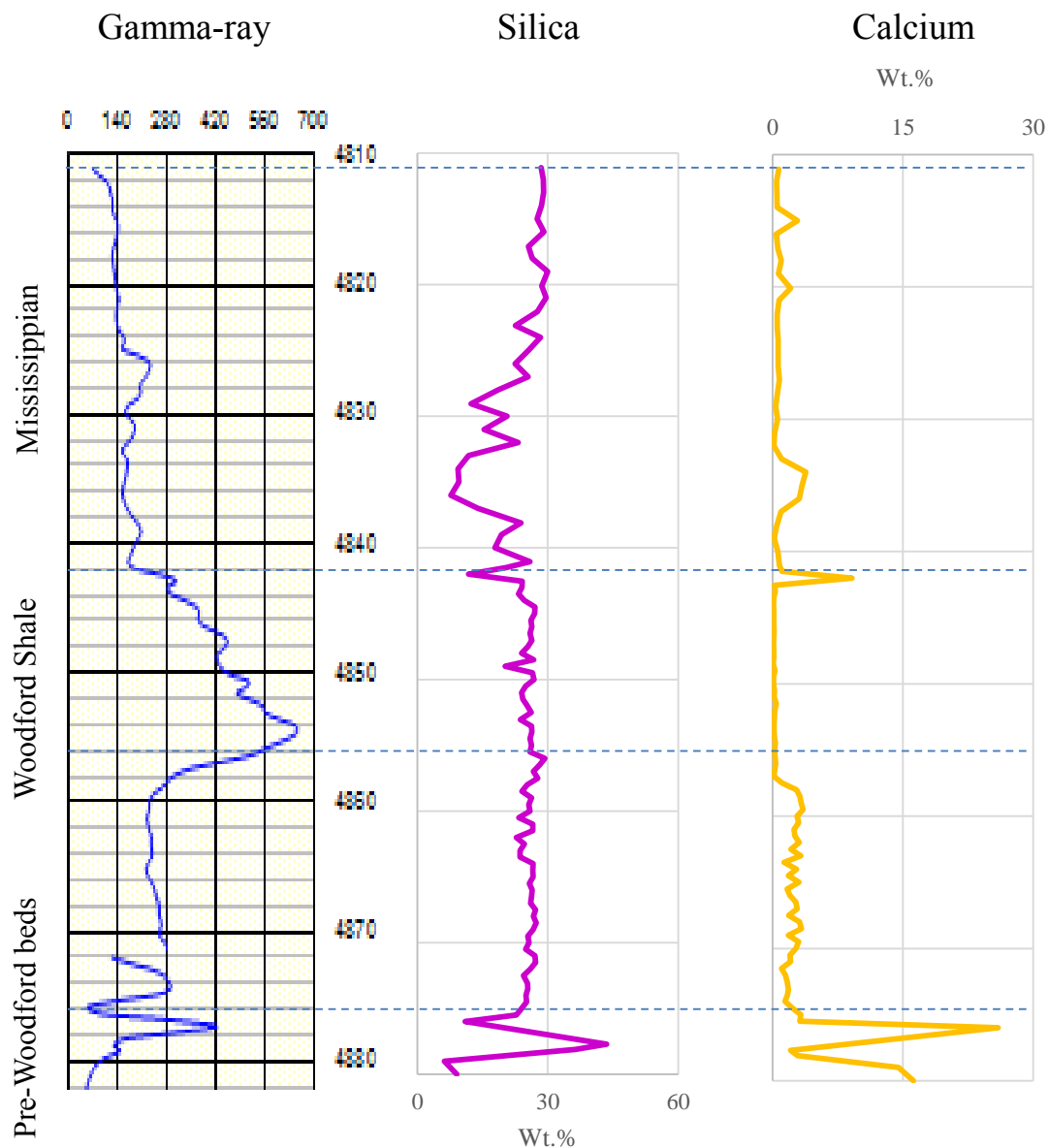


Figure 34. Gamma-ray profile and uncorrected silica (Si) and calcium (Ca) concentrations, Matthews 2-8H. At 4878 ft., there is a sharp gamma-ray peak that correlates to peaks in the Si and Ca, as well as the previous trace element profiles. The first interval (4876–4856 ft.) has relatively consistent Si values, averaging around 25 wt.%. Ca concentrations are around 3% for most of the interval and then decrease to 1%. Interval 2, from 4856 to 4842 ft., Si values remain similar to the subjacent interval, with low values at 4842.5 and 4849 ft. Ca values are less than 1% for the interval except at 4842.5 ft. where is peaks at 9%. In the Mississippian Kinderhook Shale section (4842 to 4811 ft.), Si and Ca share an inverse relationship at 4835 feet. For the remainder of the core, values stay relatively consistent.

Matthews 2-8H Chemostratigraphy

The Matthews 2-8H chemostratigraphic profile includes 43 ft. of the Mississippian “Kinderhook shale” (Figure 33). The “Kinderhook” was sampled every 1 ft. (30.48 cm) as a general overview of the section in order to compare it to the Woodford Shale. At the base of the core (4878 ft.), the trace elements share a large spike in concentrations that match the peak in the gamma-ray in the pre-Woodford beds. For the LPR (4876–4856 ft.), the V/Ti curve is consistent at 0.03 wt.%, while the normalized U, Zn, and Cu profiles are also relatively consistent. With the increase of gamma-ray in the UPR (4856–4842 ft.), the V/Ti, Zn/Ti, and Cu/Ti concentrations exhibit the largest increases. V peaks at 0.12 wt.%, Zn at 0.16 wt.%, and Cu at 0.03 wt.%. There is a slight increase in U values in this interval, but U remains significantly low throughout the entire core. The Mississippian “Kinderhook” section from 4842 to 4811 ft. has generally consistent concentrations for V and U. Zn and Cu values fluctuate, but have a small range of 0.01–0.05 wt.%. These percentages are less than the values recorded for the Rother and Yost cores, which were 0.05–0.2 wt.% and 0.1–2.5 wt.%, respectively.

Comparing the uncorrected Si and Ca concentrations (Figure 34), Si is higher concentration throughout the examined core, averaging nearly 30%. Both Ca and Si graphs show a sharp increase in concentration at 4876 ft. as do the other graphed trace elements. The Ca profile begins at 3 wt.% for the LPR interval, but decreases to 1% for the remainder of the core except between 4842 and 4832 ft. In this section within the “Kinderhook” interval, Si and Ca share an inverse relationship in which Ca increases

where Si decreases. However, this is the only zone where the concentration of these elements seem to be related to each other.

Wireline Log Analysis

By examining the open-hole wireline logs, specifically porosity logs, mechanical properties of the Woodford Shale can be estimated. Neutron logs measure the amount of hydrogen in rock, therefore as clay increases, hydrogen increases and neutron porosity increases. Density logs use higher energy gamma-rays (from Compton Scattering) to measure formation electron density which is related to bulk density. The photoelectric effect (PE) curve uses lower energy gamma-ray to determine mineralogy and therefore formation lithology. Each mineral has a specific PE value, such as quartz (1.81), calcite (5.08), illite (3.5), and pyrite (17) (Asquith and Krygowski, 2004). Using the PE curve in combination with the neutron porosity curve provides insight into the relative ratio of clay minerals to silica and calcite.

The neutron log for the pyrite-rich (PR) interval of the Rother 1H-5X (10442–10386 ft.) has the highest neutron porosity (note that open hole log depths for the Rother 1H-5X are approximately fifteen feet deep to core depths) with values that consistently exceed 20 porosity units (pu) (Figure 35). The PE curve across the PR interval averages 2.97 barns/electrons (b/e). In the silica-rich (SR) zone from 10386 to 10354 ft., neutron porosity decreases to 16 pu, which corresponds to the increase in Si evident in figure 35 at depth 10370-10342 feet. The average PE value across the SR interval is 2.31 b/e, but is approximately 2.0 from 10377 to 10370 ft. In the carbonate-rich (CR) zone (10354–10331 ft.), the neutron porosity log values increase, ranging from 24 to 16 pu. The PE

values average 2.34 b/e (Figure 35). The density porosity curve across the Woodford Shale in the Rother core appears to fluctuate less than the neutron porosity. The density porosity averages approximately 14 pu from 10442 to 10410 ft. where it declines to a low 8 pu at 10400–402 ft. At the top of this section, the density curve averages approximately 11 pu from 10410 to 10388 ft. where it increases to a value of approximately 14 pu, which it maintains to the Woodford-Mississippian limestone contact at 10332 ft. (Figure 35).

The wireline logs for the Rother 1H-5X share a similar pattern with the Yost 1H-18X (Figure 36). In the Yost pyrite-rich (PR) interval from 9444 to 9426 ft., the neutron log averages 22 pu, the density begins around 12 pu before decreasing to 5 pu and rebounding back to 12 pu, while the PE curve average is 3.21 b/e. The neutron in the silica-rich (SR) interval (9426–9410 ft.) is suppressed as it is in the Rother and decreases to 16 pu (Figure 36). Density porosity averages 12 pu and the PE value for the SR interval is 2.34 b/e. The CR interval (9410–9397 ft.) has the highest neutron values of >28 pu, but also contains a five feet thick interval with 18 pu (depth 9406–9401 ft.). Density readings in the CR interval increase to 15 while the PE value is 2.77 b/e (Figure 36).

The Matthews 2-8H core begins with a sharp decrease in the neutron and density logs (Figure 37) to nearly zero units from 4880 to 4878 ft. that corresponds to the sandstone below the Woodford Shale. The PE curve also decreases to 2.5 b/e in this section. In the lower pyrite-rich (LPR) interval (4878–4856 ft.) of the Woodford Shale, the neutron porosity value begins high at 39 pu (4878 ft.) and gradually decreases to 25 pu around 4860 feet before quickly increasing again at 4856 ft. Density porosity is much

lower, having average values of 9–10 pu from 4878 to 4860 feet; at 4856 ft., it increases to 21 pu (Figure 37). The PE curve remains around 3.3 b/e across the LPR interval. In the upper pyrite-rich (UPR) zone from 4856 to 4845 ft., the neutron and density curves mirror each other at 36 and 18 pu, respectively. From 4845 to 4842 feet, the neutron and density porosity values drop to 25 and 6 pu, respectively. The PE value is approximately 3.2 for this unit. Across the Mississippian “Kinderhook” shale interval from 4842 to 4811 ft., the neutron, density, and PE curve consistently track each other and display low variability. The neutron porosity averages around 27 pu, the density 9 pu, and the PE, 3 b/e (Figure 37).

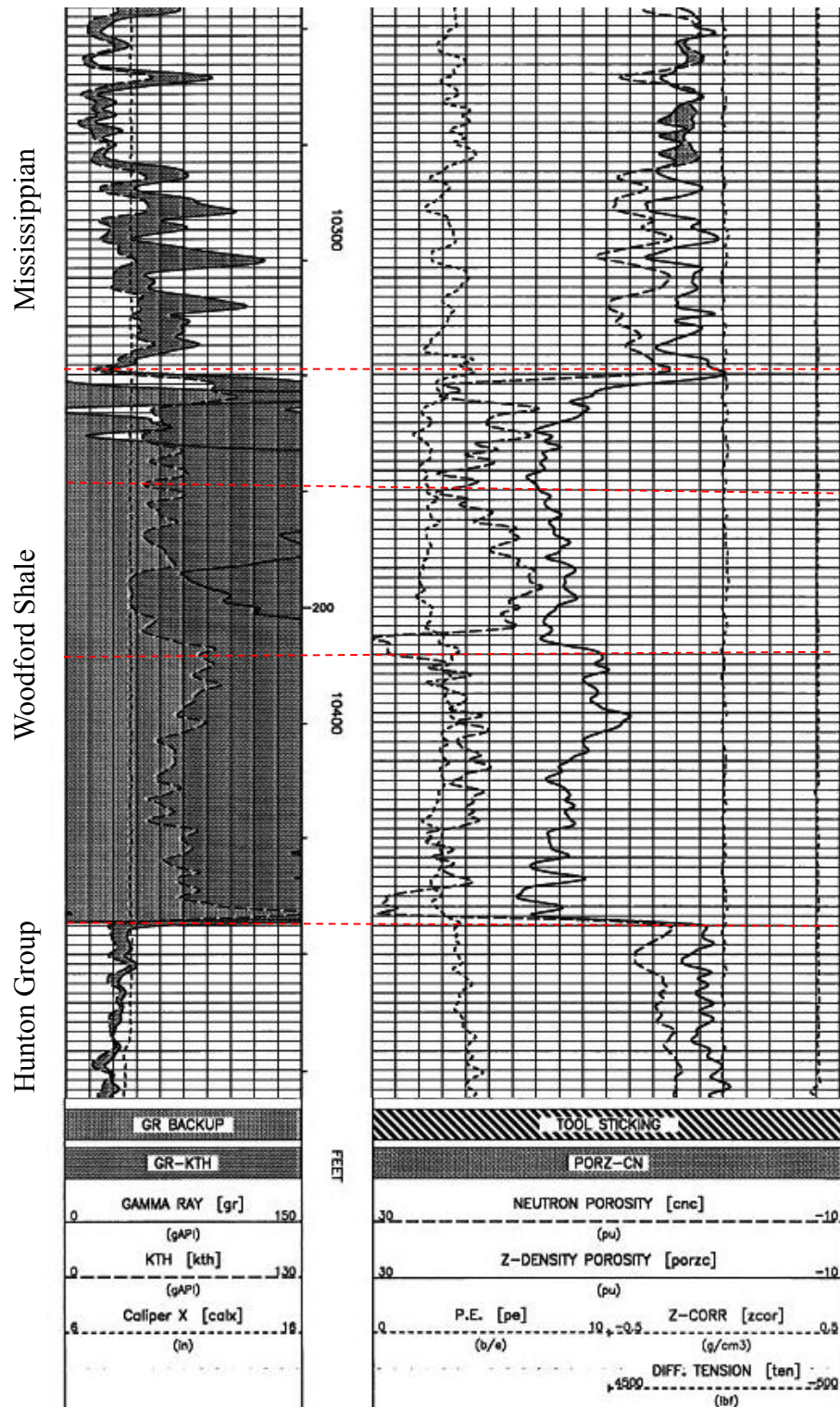


Figure 35. Portion of wireline log across part of the Hunton Group, the Woodford Shale, and part of the base of the Mississippian lime, Rother 1H-5X. Neutron porosity is greater than 20 porosity units (pu) across the lower PR interval (10442–10386 ft.). Across the second interval (10386–10354 ft.), the pu is suppressed, decreasing to 16 pu, before increasing to 22 pu. The third interval from 10354 to 10329 ft. decreases to 16 pu at 10337 ft., peaks at 24 pu (10332 ft.), and then decreases to nearly 0 pu as it reaches the Mississippian. The density log is relatively consistent except for decreasing between 10414 and 10385 ft. The PE values for the Woodford remain between 2.3 and 3 barns/electrons (b/e). Note that open hole wireline log depths are twelve to fifteen feet deeper than core depths.

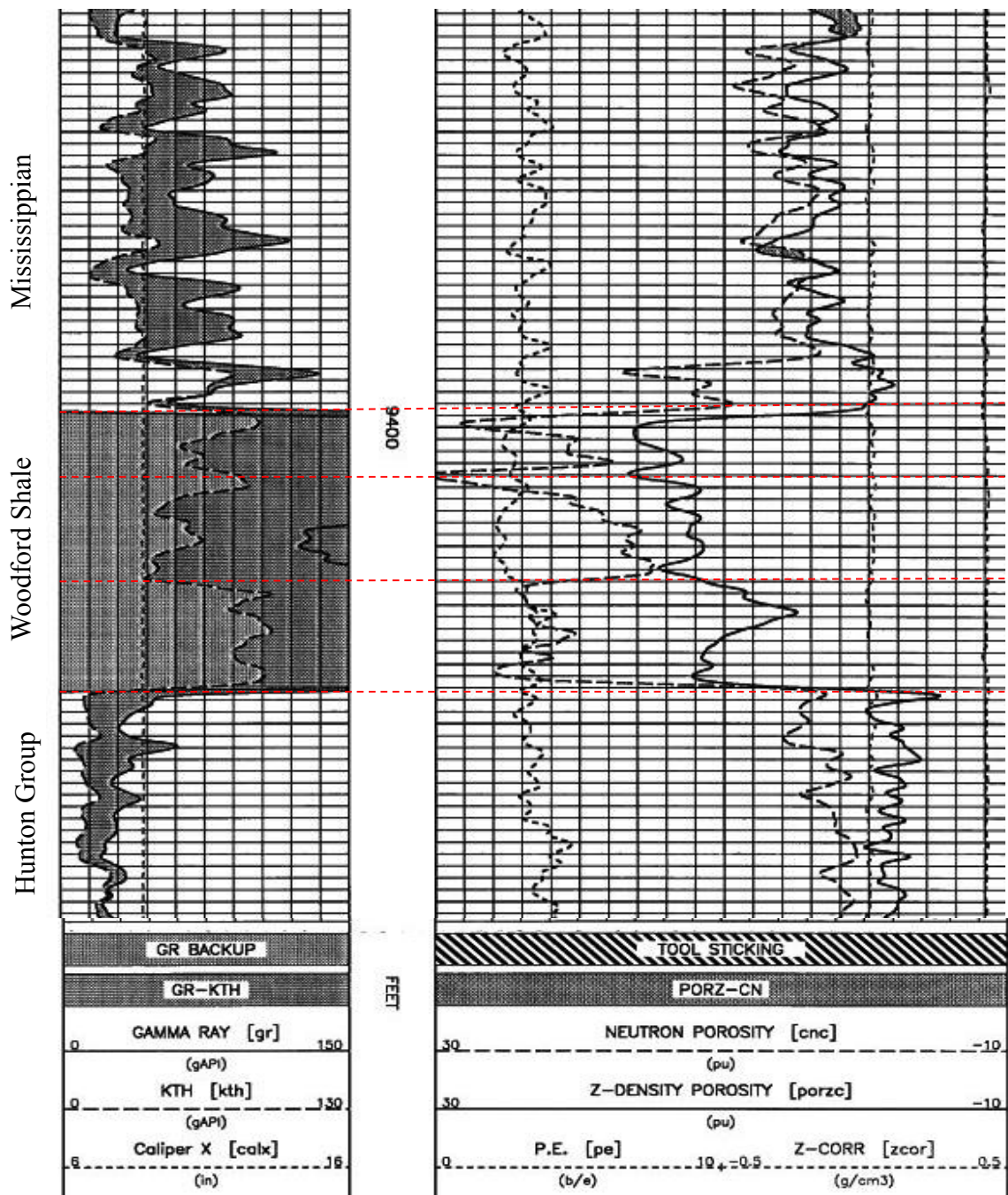


Figure 36. Portion of wireline log across part of the Hunton Group, the Woodford Shale, and part of the Mississippian lime, Yost 1H-18X. Neutron porosity in the Woodford Shale begins with an average of 23 pu in the first interval (9445 to 9426 ft.), decreasing to 15 pu in the second interval (9426–9408 ft.), before fluctuating between 18 and 30 in the third interval from 9408 to 9397 feet. Density porosity curves from 12 to 5 in the first interval, rebounding to 12 pu before averaging around 14 pu for the remainder of the Woodford. The PE curve is relatively consistent, with only a slight decrease in the second interval. Note that open hole log depths for the Yost are approximately six to seven feet deep to core depths.

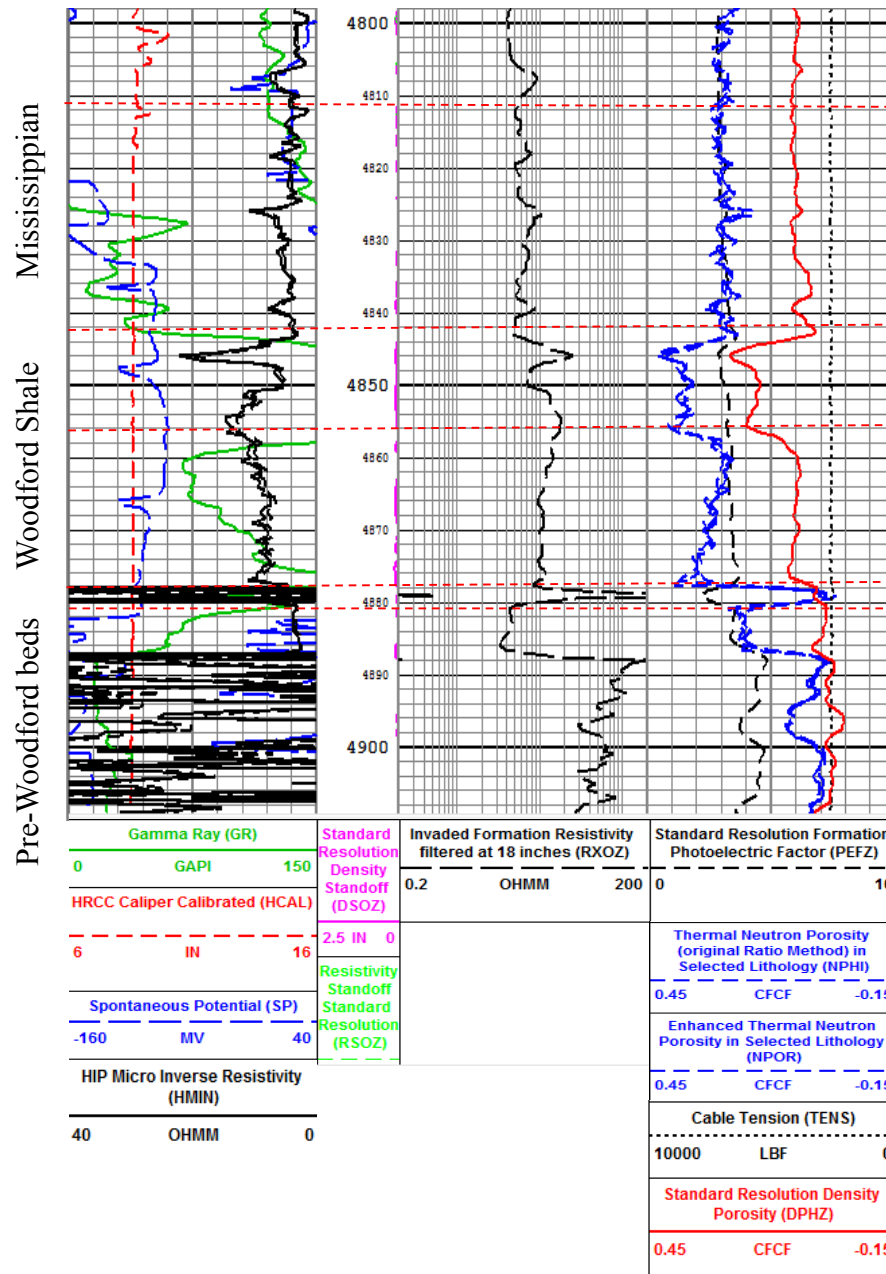


Figure 37. Portion of wireline log across part of the pre-Woodford beds, the Woodford Shale, and the Mississippian “Kinderhook Shale”, Matthews 2-8H. There is a sharp decrease in the gamma-ray values, neutron and density porosity readings and PE values in the unconformity sandstone below the Woodford Shale. Within the lower pyrite-rich interval (LPR) of the Woodford Shale, neutron porosity is >35 pu and gradually decreases to 25 pu at 4860 ft. before increasing to >39 pu at 4856 ft. The density log remains consistent in this section at 9 pu. Across the upper pyrite-rich interval (UPR), 4856 to 4842 feet, neutron porosity is >33 pu from 4856 to 4845 feet, where it decreases to 27 pu at 4842 ft. The density curve tracks the neutron curve and averages 18 pu before decreasing to about 6 pu at 4842 feet. In the “Kinderhook shale” section (4842–4811 feet), the neutron and density curves consistently track each other around 27 and 9 pu respectively. The PE curves averages 3 and 4 b/e across the Woodford and “Kinderhook” section.

Scanning electron microscope (SEM)

To better understand the difference in the rock fabric and porosity for pyrite-rich and silica-rich zones, SEM images were acquired for samples from these intervals. A sample of the silica-rich interval in the Rother core was taken from 10,365 ft. (Figure 38). Two-dimensional (2D) images of the milled surface show micrometer to nanometer pores that appear randomly in the matrix or between pyrite grains (Figure 38). In the 2D images, micrometer pores appear to be scattered randomly, whereas nanometer pores are concentrated around constituents such as framboid pyrite. Compositional images include pyrite clusters viewed on the 2D surface and a quartz grain as a 3D image (Figure 44 B/C, D). Pyrite within the SR interval appears to be a mixture of larger euhedral crystals and framboid clusters.

The second sample of the Rother core examined using SEM is from 10385 ft. within the PR interval (Figure 39). Porosity occurs at the micrometer to nanometer scale and is concentrated around mineral grains. Shrinkage porosity associated with pyrite grains is evident in Figure 45C. The most recognized constituent in the PR interval is pyrite that occurs as framboids and larger euhedral crystals.

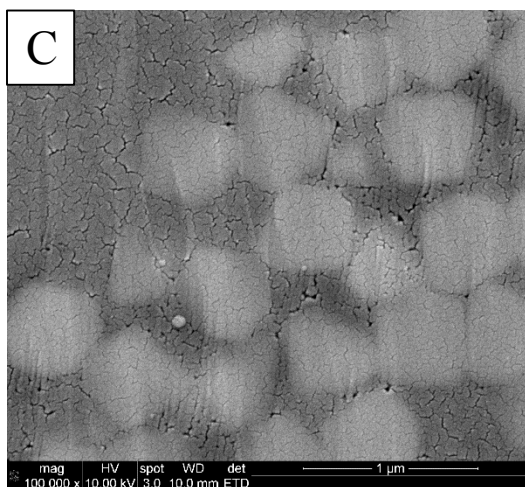
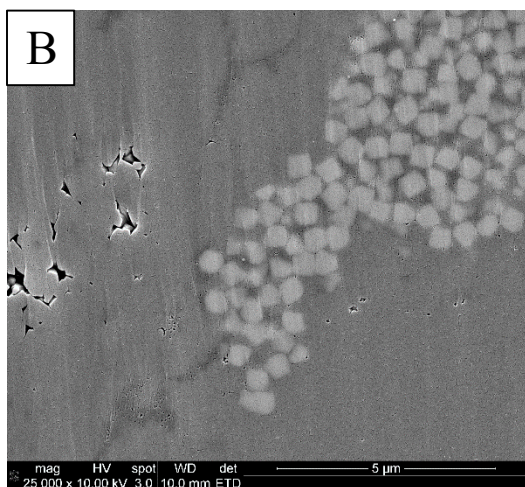
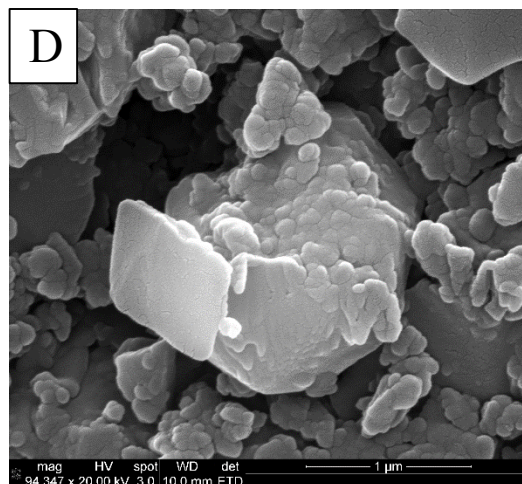
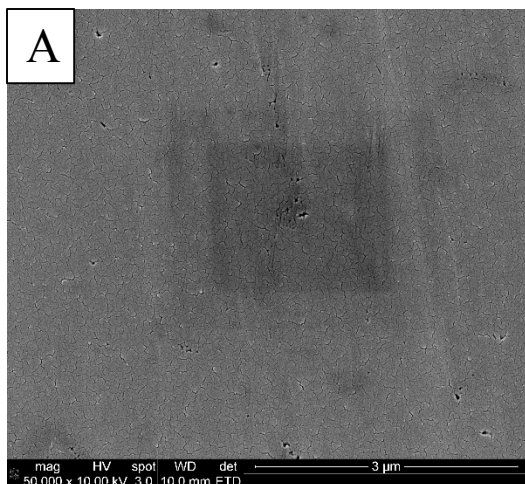


Figure 38. 2D and 3D SEM images of the silica-rich interval, Rother 1H-5X core, depth 10365 ft. (A) Random porosity within the matrix at nanometer scale. (B) Framboidal pyrite and micrometer scale porosity. (C) Framboidal pyrite with nanometer porosity between pyrite grains. (D) 3D image of a quartz grain within the clay matrix.

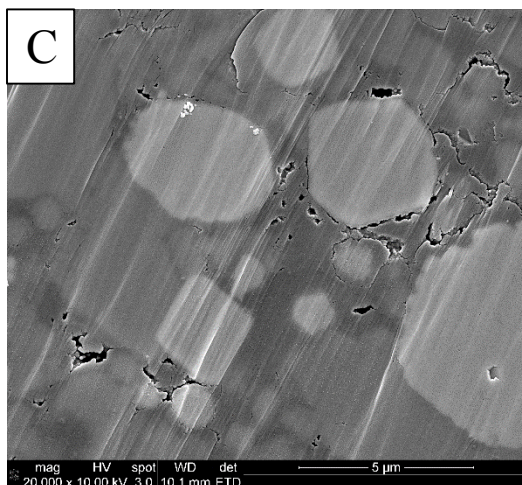
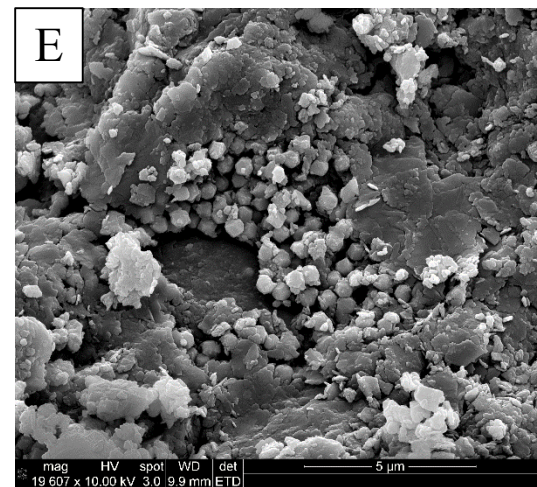
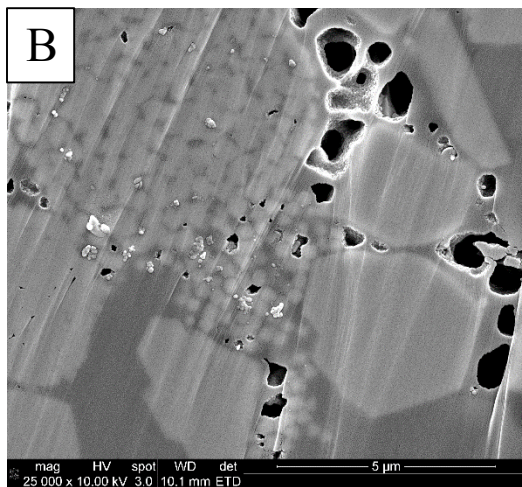
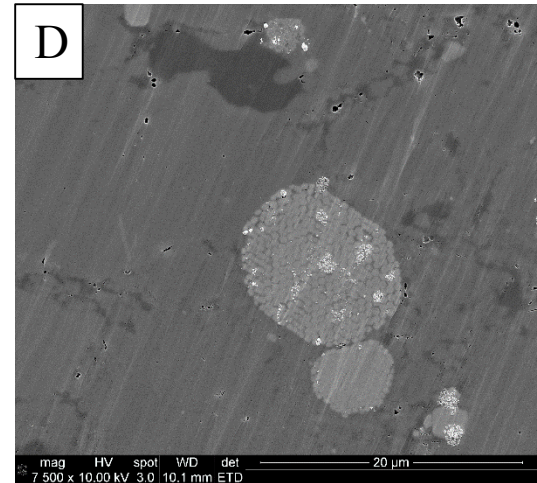
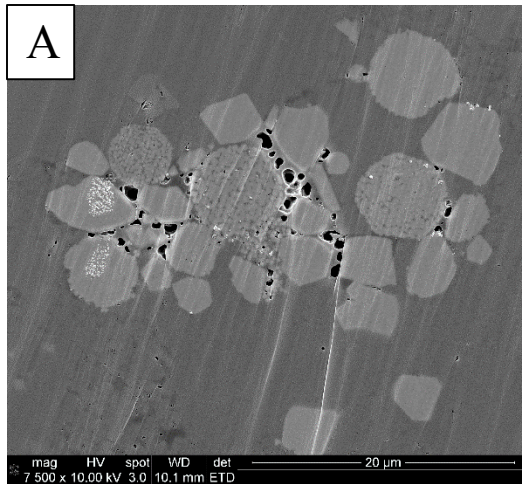


Figure 39. 2D and 3D SEM images of samples from the pyrite-rich zone, Rother 1H-5X, depth 10385 ft. (A) Pyrite cluster of framboidal and euhedral pyrite. Porosity is micro to nanometer scale. (B) Close up of pyrite cluster A., showing framboidal pyrite, euhedral pyrite, and associated porosity. (C) Euhedral pyrite with porosity of undetermined origin. (D) Framboidal pyrite cluster within two-tone matrix. (E) 3D image of framboidal pyrite with intercrystalline porosity and clay minerals.

CHAPTER V

DISCUSSION

Anderson 12 no.1 core

To help correlate the Rother 1H-5X and Yost 1H-18X wells in Oklahoma to the Matthews 2-8H well in Kansas, a core described by Callner (2014) was used to provide information in the gap between Oklahoma and Kansas. The Anderson 12-1 well is located in Garfield County, Oklahoma, Sec. 6 T20N R5W. This 124 ft. core (6824 to 6945 ft.) includes an incomplete Woodford Shale section (missing 14 ft.) which was described as “medium grey to black shale containing a variety of sedimentary and diagenetic features” (Callner, 2014). Based on the description of these features, the core was divided into nine sedimentary and diagenetic intervals and six chemostratigraphic intervals. The gamma-ray curve is distinctly different from curves for the Rother 1H-5X and Yost 1H-18X wells. Based on high TOC levels, sedimentary features such as bundled laminae that may indicate tidal rhythmites and interpretation of the trace metal analysis, the Anderson 12-1 was interpreted to be inbound of the continental shelf edge (Callner, 2014).

The Anderson 12-1 does not correlate cleanly with the three intervals defined

in the Rother 1H-5X and Yost 1H-18X, or the generalized intervals in the Matthews 2-8H in Kansas. At the base of the lowermost interval for the Anderson core, there is an increase in TOC that matches up with a color change and sedimentary features identified as storm deposits, bioturbation, and clasts. The remainder of this lower interval matches with the PR interval of the other wells, with pyritized features prominent as well as consistent trace metal concentrations. The SR interval (sedimentological/ diagenetic unit 7 of Callner (2014)) was thin; only about 10 ft. thick. There was no significant suppression of gamma-ray across this interval in the Anderson core so this correlation is based solely on core description. The upper section of the core matches the core descriptions and fluctuations in trace-element proxies of the CR of the Rother 1H-5X and Yost 1H-18X cores and the UPR in the Matthews 2-8H.

Inferences from redox indices (U, V, Mo) and organic productivity proxies (Zn, Cu)

The trace metals U, V, and Mo are commonly used as paleoenvironmental proxies, specifically for bottom water chemistry and redox states (Cruse and Lyons, 2004; Tribovillard 2006; Lyons et al., 2009; Scott and Lyons, 2012; Musa 2013; Puckette, 2013). Mo is one of the more significant trace elements used to distinguish between sulfidic (euxinic) and non-sulfidic (anoxic) water column conditions (Lyons et al, 2009; Scott and Lyons, 2012). High concentrations of Mo within sediment can only come from hydrothermal vents, Mo-enriched terrigenous material, or through enrichment of euxinic water column chemistry (Scott and Lyons, 2012). Because there is no indication of hydrothermal activity or Mo-enriched detrital input related to the Woodford

deposits in this area, euxinic water column conditions would be the most likely process to explain high Mo concentrations in these samples (Figure 40). According to Algeo and Maynard (2004), when U and V are enriched without Mo, conditions tend to be anoxic, but not sulfidic. When Mo, V, and U are enriched, the depositional environment is likely euxinic, but when these trace elements are depleted, conditions may be most likely suboxic to oxic (Figure 41; Algeo and Maynard, 2004; Tribovillard et al., 2006; Lyons et al., 2009; Scott and Lyons, 2012).

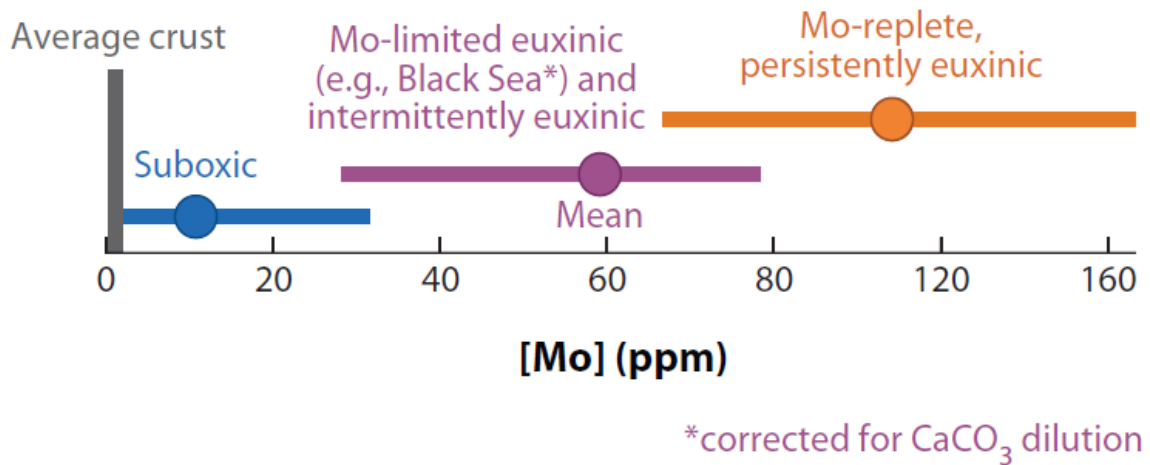


Figure 40. Schematic of ranges of Mo concentrations observed in modern day environments. When Mo concentrations reach over 80 ppm (0.0008 wt.%), bottom water conditions are usually euxinic. Modified from Lyons et al. (2009).

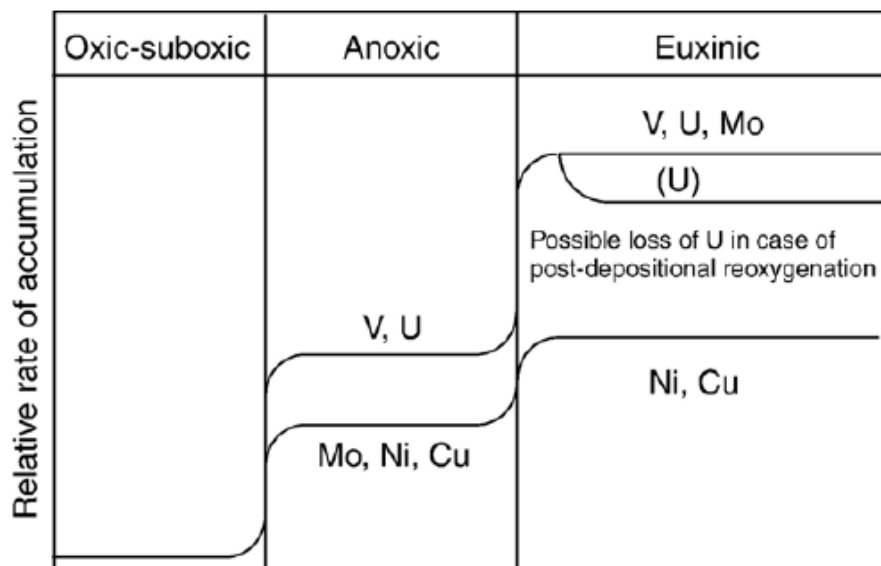


Figure 41. Schematic of trace element behavior in redox conditions. This diagram is based on concentration values. When there are higher concentrations of V and U yet lesser amounts of Mo, Ni, and Cu, redox conditions are primarily anoxic. When concentration levels of V, Mo, and U are significantly higher than Ni and Cu, conditions are euxinic. (Tribovillard et al., 2006, modified from Algeo and Maynard, 2004).

Concentrations of Mo were recorded by the XRF for all three wells, but no correction factor was provided by the standard. However, Mo concentrations were available from the inductively coupled plasma mass spectrometer (ICP-MS) along with concentrations for over 40 trace elements and oxides. When ICP-MS results were compared with the XRF concentrations from the Rother 1H-5X (Figure 16), ICP-MS values correlated within one standard deviation of the XRF results. Therefore, it appears that the commercial ICP-MS data is consistent to the lab XRF data. Figure 42 shows the gamma-ray profile and ICP-MS concentration profiles for Mo, V, and U for the Rother core. Intervals defined in the gamma-ray and trace element profiles correlate with the

intervals defined in core description. In the pyrite-rich interval (PR), Mo and V average 0.01 wt.% while U is around 0.004 wt.%. These matching concentrations of Mo and V with the low U are indicative of a euxinic environment (Algeo and Maynard, 2004; Lyons et al., 2009; Scott and Lyons, 2012). Mo in the silica-rich (SR) interval averages around 0.008 wt.%, V increases to approximately 0.03 wt.%, and U decreases in concentration to less than 0.003 wt.%. From these values, the paleoenvironment was primarily anoxic, but potentially euxinic as well. For the carbonate-rich (CR) interval, all trace element profiles decrease in concentration. Mo decreases to 0.0 wt.% while V and U remain very low before all begin to increase again. This separation as well as extremely low values indicate that this paleoenvironment was suboxic, but based on the high amount of preserved organic material seen in core description, it is interpreted that conditions were primarily anoxic.

Only 7 ICP-MS samples were provided for the Yost 1H-18X core. Mo concentrations ranged from nearly 0 to 0.016 wt.%, V from 0.0002 to 0.1 wt.%, and U from 0 to 0.0008 wt.%. XRF concentration profiles for the Yost core are similar to the Rother results. ICP-MS concentration data was not provided for the Matthews core.

Organic productivity can be estimated using the trace element proxies Zn and Cu. Both behave similar to micronutrients in the water column, where upon decay of organic material, these trace elements can be released into the pore water or wrapped up with pyrite in reducing (euxinic) conditions (Algeo and Maynard, 2004; Tribovillard et al., 2006; Musa, 2013). As a result, enriched Zn and Cu values indicate an increase in organic productivity. Stability in these concentrations may also indicate euxinic conditions. Zn/Ti and Cu/Ti values for the Rother 1H-5X are mostly constant for the PR interval, increase

slightly in SR, and increase again in CR. Zn/Ti and Cu/Ti values in the Yost 1H-18X do not exhibit major variations in values from a baseline of 0.1 wt.% across most of the Woodford interval. Zn/Ti values for the Matthews 2-8H increase at the LPR/UPR contact to 0.16 wt.%, but then return to low values of 0.02 wt.%. Cu/Ti values for the Matthews core for also increase at the LPR/UPR border but remain higher from 0.01 to 0.03 wt.% from the contact through the Mississippian section of the core.

From this analysis, Si and Ca are abundant in the Woodford Shale in both the Rother and Yost cores. Silica percentages exceeded 40% specifically within the SR interval of each of these two cores, whereas Ca reached over 20% in the CR intervals. In contrast, Woodford samples from the Matthews 2-8H core were consistently measured at less than 30% Si while Ca averaged 1–3%. The silica content in the Woodford Shale in the Matthews core is produced mostly from silt-sized quartz grains and an occasional radiolarian. In contrast, the silica evident in thin section in the Rother and Yost cores includes the silica-cemented bands of radiolarian beds as well as detrital quartz silt. The lack of radiolarian beds in the Matthews core from Kansas supports the interpretation that paleogeographically, the Woodford Shale in the Matthews was much higher on the continental shelf.

The relationship between the paleoredox and the origin of centimeter scale banding in the SR zone of the Woodford Shale was examined using high frequency sampling. XRF measurements were taken for silica-rich and clay-rich bands in the Rother (10360 ft.) and the Yost (9416 ft.) (Figure 43). Trace element analysis showed that even at higher frequency sampling, concentrations of the paleoredox proxy elements remained similar across the selected one foot (30.48 cm thick) intervals of the silica-cemented

banding from the Rother and Yost cores. Normalized V values ranged from 0.04 to 0.1 wt.% for both Rother and Yost samples. Uranium concentrations were lower in the Rother and ranged from 0.0025 to 0.005 wt.%, whereas U values in the Yost ranged from 0.01–0.04 wt.%. Zn ranged from 0 to 0.3 wt.% for both wells and Cu 0 to 0.05 wt.%. Therefore, it appears that the silica bands produced by radiolarian blooms operated independently of bottom water chemistry. Instead, this silica source was potentially controlled by the availability of nutrients as a reflection of the paleogeographic position on the shelf.

Total organic carbon (TOC) was provided for all three wells, yet due to a scarcity of samples for the Matthews, only data from the Rother and Yost wells were graphed. The four TOC samples for the Matthews occur within the LPR (4862, 4866, 4870, 4874 ft.) and average 2.8%. Figure 44 shows the gamma-ray, TOC, and major trace element profiles for the Rother. TOC values in the PR interval are the highest, beginning at nearly 10% before decreasing to less than 5% around 10,372 feet. Concentrations of TOC decrease to 2% before slowly increasing back to 5% at 10,340 ft. TOC remains around 5% in the CR interval until 10320 feet, where it decreases to about 1% at 10311 ft. The decrease in TOC from the PR interval to the SR interval is matched by a decrease in gamma-ray values within the SR interval that may reflect increased silica-cementation.

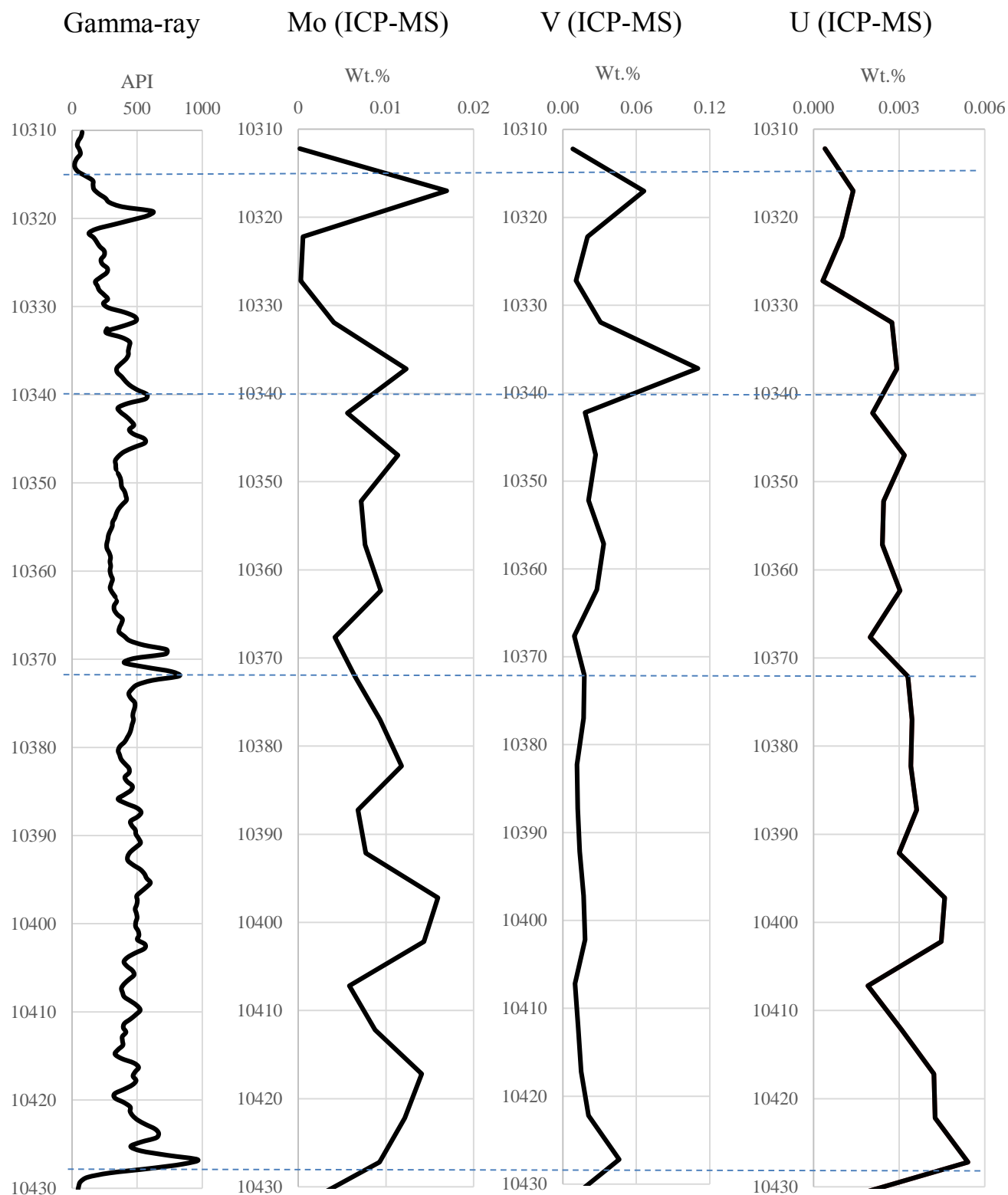


Figure 42. Gamma-ray profile and ICP-MS concentrations of Mo, V, and U, Rother 1H-5X. In the PR interval (10428–10372 ft.), Mo concentrations average 0.01 wt.% with a peak of 0.012 wt.% at 10396 ft. The average in the SR interval is 0.008 % from 10372 to 10340 ft. Mo concentrations in the CR interval (10340–10314 ft.) ranges from 0 to 0.017 wt.%. The Mo and U concentrations have similar patterns while V concentrations are similar in the CR interval. These concentrations confirm primarily anoxic redox conditions, with potential for euxinic conditions in the PR and SR zones, while potentially suboxic in the CR interval (Algeo and Maynard, 2004; Scott and Lyons, 2012).

The peak in TOC values of nearly 10% at the base of the PR interval matches the peaks in the trace element profiles immediately above the contact with the underlying Hunton Group. TOC values for the PR interval in the Yost core range from 3.5 to 7% (Figure 45). TOC concentrations decrease slightly in the SR zone to 3.5– 4%, which correlates to a decrease in gamma-ray values. In the CR interval, TOC values increase to approximately 6% before decreasing to <2% in the Mississippian carbonate (Figure 45).

The trace element analysis along with gamma-ray and TOC values are interpreted to suggest that the bottom water chemistry during deposition of the pyrite-rich (PR) zone was mostly euxinic. In contrast, water chemistry during deposition of the silica-rich (SR) interval was primarily anoxic with possibility of euxinia. The depletion of concentrations of the paleoredox proxies in the CR zone is interpreted to suggest that the waters were most likely suboxic to anoxic. The preservation of high TOC within the PR interval correlates with the consistent concentrations of the trace elements, which may indicate that organic matter preservation was controlled by the bottom water chemistry (Puckette et al., 2013).

Comparison of Wireline Logs for mechanical rock properties

The integration of data from wireline logs, core descriptions, and thin section petrography allow interpretation of mechanical properties. The decrease in density porosity toward the top of the PR interval of the Rother core (10442–10386 ft.) and Yost core (9444 to 9426 ft.) correlate to pyrite-rich intervals in the form of nodules, bands, and

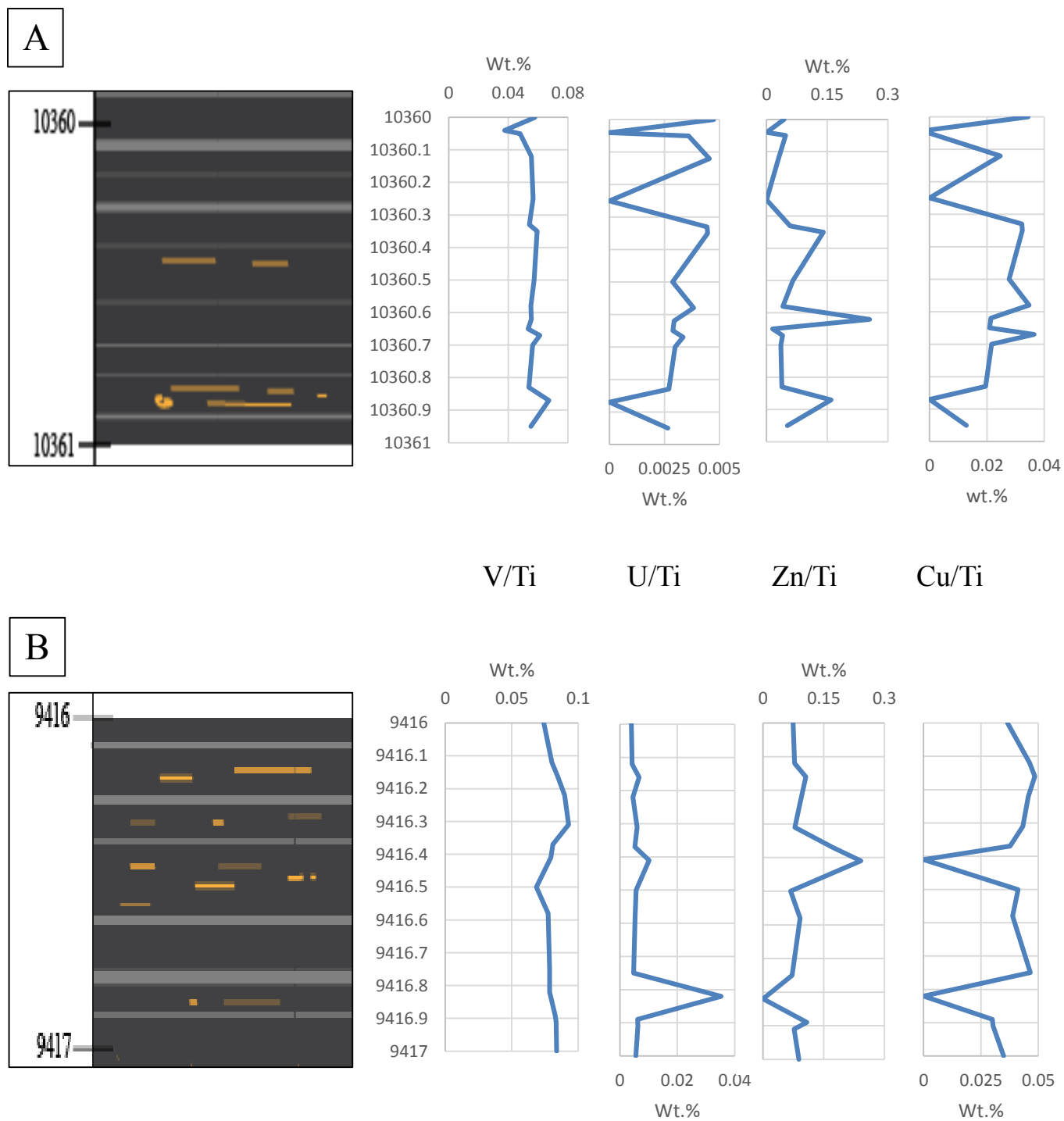


Figure 43. Schematic core description and normalized trace element concentrations (V, U, Zn, Cu) of high frequency XRF sampling for the SR interval, (A) depth 10360 ft. for Rother 1H-5X, and (B) depth 9416 ft. for Yost 1H-18X.

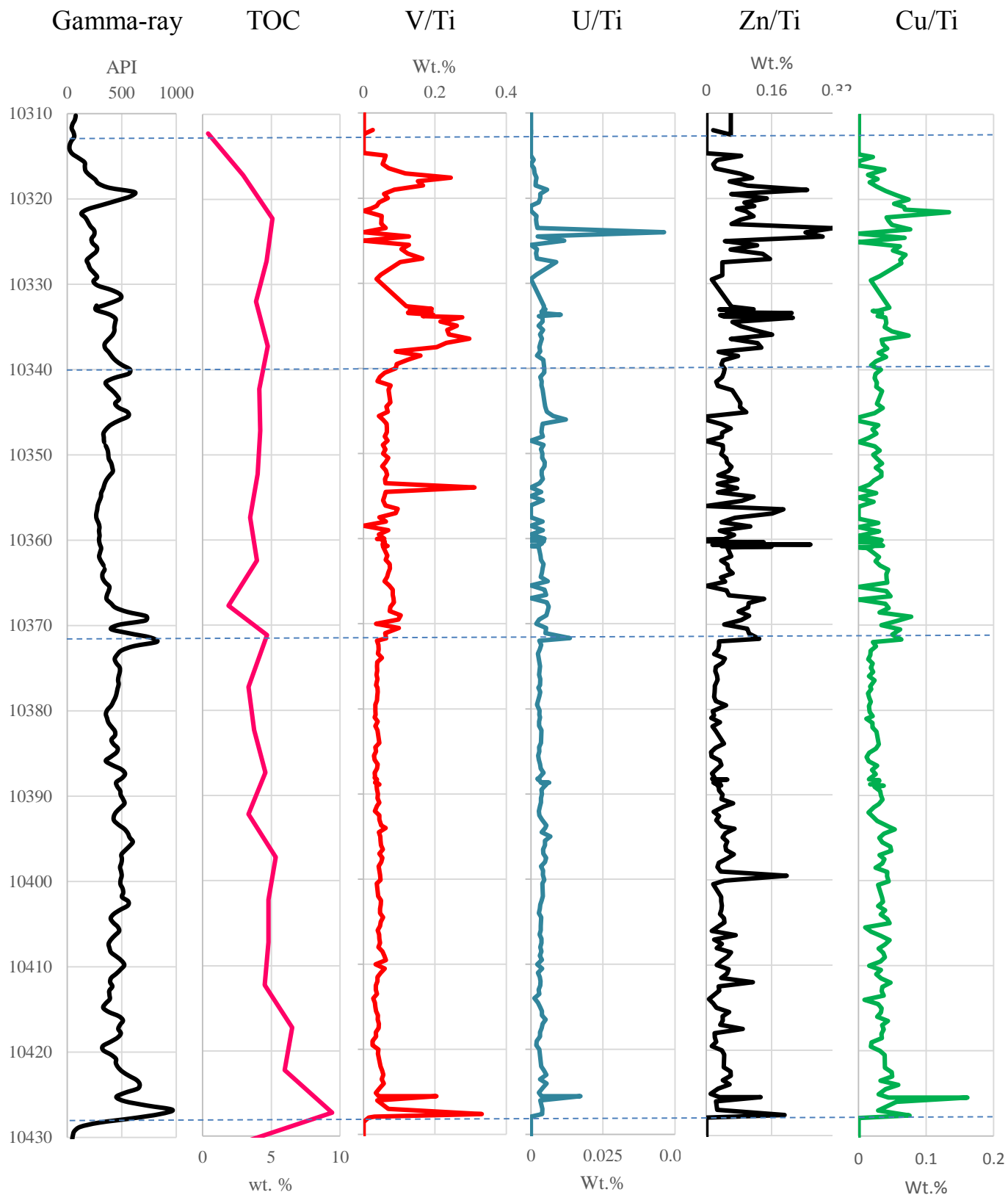


Figure 44. Gamma-ray profile with TOC and significant normalized trace element profiles for Rother 1H-5X core. In the PR interval, TOC concentrations are the greatest, beginning at nearly 10% before decreasing to 4%. There is a slight decrease within the SR interval before stabilizing around 4%. TOC values are consistent around 5% in the CR before decreasing to negligible values in the Mississippian carbonate interval.

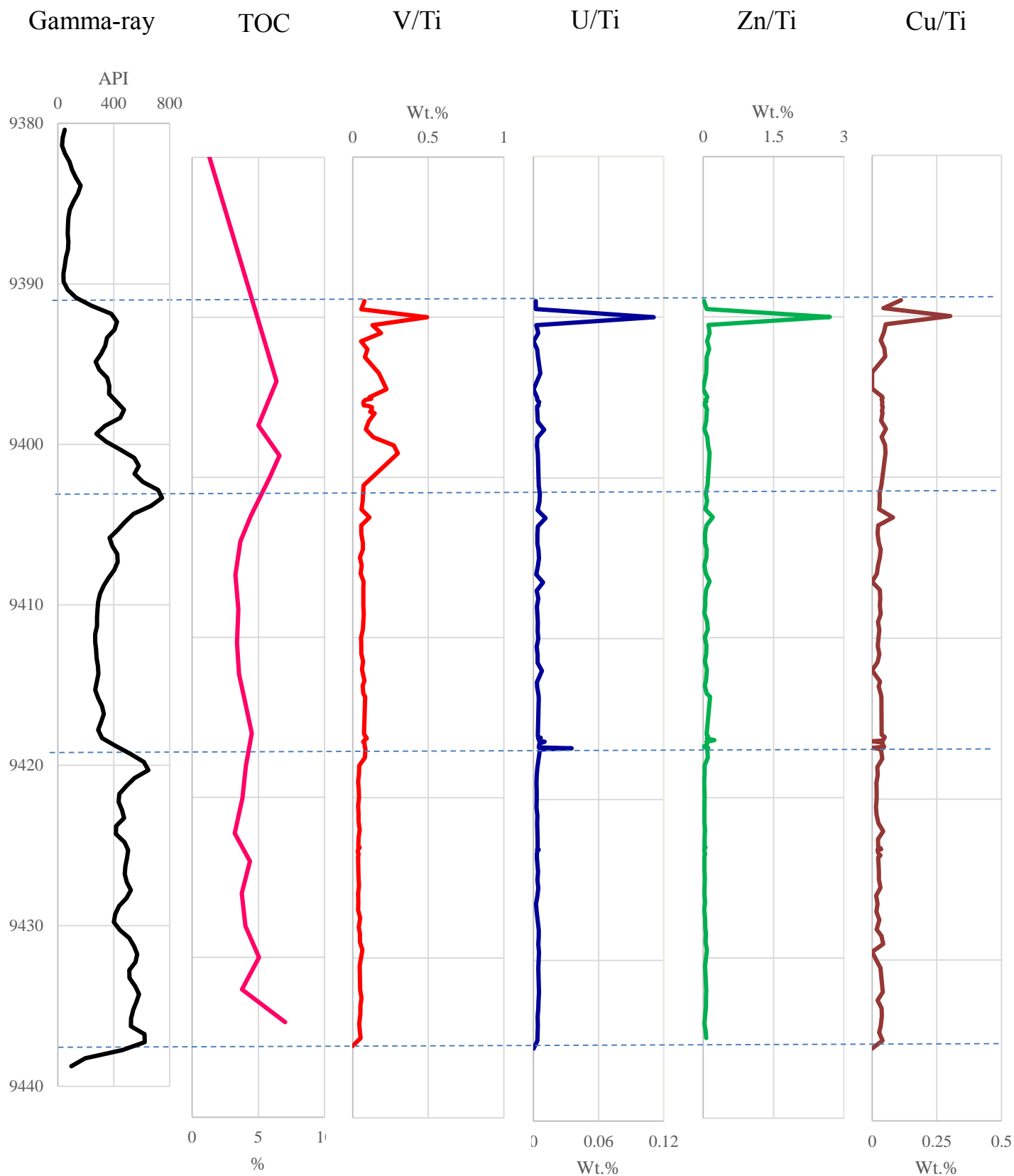


Figure 45. Gamma-ray profile with TOC and significant normalized trace element profiles (V, U, Zn, Cu) for Yost 1H-18X core. In the PR interval (9436 to 9426 ft.), TOC concentrations, range from 4 to 7%. TOC values decrease within the SR zone (9426–9402 ft.) to approximately 3.5%, which correlates to the decrease in gamma-ray values. In the CR interval from 9402 to 9388 ft., the three values are >5%.

laminae. The PE curve for the Rother in the pyrite-rich (PR) averages 3.0 b/e, whereas the PE curve in the Yost averages 3.5 for this zone and exceeds 4.0 from 9434–37 feet, yet no carbonate is apparent. These intervals have the highest average PE levels, which confirms the supposition of high amount of clay and pyrite. In the silica-rich (SR) zone in both the Rother and Yost wells, the suppression of the neutron log and the increase of density values may indicate that this interval has the least amount of clay and less pyrite, as well as a higher silica content that increases the brittleness. The PE values across the SR zone decrease toward 2.0, which supports the interpretation of a lower clay content and higher silica content (Figures 35 and 36). This silica-rich zone has a distinct wireline log signature, making it easy to correlate with wireline well logs where no core is available.

SEM interpretations

SEM images reveal some defining characteristics of the two lowermost intervals of the Rother 1H-5X core. The abundant framboidal pyrite is indicative of sulfidic pore waters below the sediment-water interface. When compared with the trace element analysis, the pyrite morphology confirms that the redox conditions for the pyrite-rich (PR) and silica-rich (SR) intervals were mostly anoxic to euxinic. Porosity occurs at the micrometer to nanometer scale in the matrix and between framboids. Rock fabric appears to be similar for both intervals, but larger pores are most abundant in the pyrite-rich interval, which is attributed to less silica cement in the PR interval compared to the SR interval.

CHAPTER VI

SUMMARY AND CONCLUSIONS

Traditionally, the petroleum industry has mostly considered dark, organic-rich shales in terms of their source rock potential. However, with improvements in drilling, production, and completion technology, dark organic-rich shales like the Woodford Shale can now be characterized as self-sourcing reservoirs and the target of exploration and development. The Woodford Shale is a premier source rock in the Midcontinent Region of North America and an active exploration and development play. Therefore increasing understanding of the petrography and composition of the Woodford Shale has great implication for the petroleum industry.

The primary objective of this study was to generate a more accurate model of the depositional processes that formed the Woodford Shale in northern Oklahoma and southern Kansas. This was accomplished by detailed description of core, thin section petrography, x-ray fluorescence, analysis of wireline logs, and scanning electron microscopy (SEM). These techniques were used to image depositional and diagenetic features and interpret their origin. In the three cores described for this project, generalized subunits were identified based on the relative abundance of pyrite, clay, silica cement, their geochemical signatures, and their resultant wireline log signatures. The

three subunits recognized in the cores from Oklahoma may match up with the commonly used tripartite system used by much of the petroleum industry and reiterates the need for conodont biostratigraphy to define the stratigraphic position of the Woodford within the global stratigraphic framework (Frasnian-Famennian to Tournaisian). The three generalized intervals recognized in the Rother and Yost cores are in ascending order pyrite-rich (PR), silica-rich (SR), and carbonate-rich (CR). The pyrite-rich (PR) interval was the most argillaceous and contained pyrite laminae, bands, and disseminated silt to sand-sized pyrite grains <0.1 mm. X-ray fluorescence trace element analysis revealed that this interval had consistent concentrations of U, V, Cu, and Zn as well as the consistently higher concentrations of TOC. Based on the elevated concentrations of U and V from XRF and ICP-MS, as well as Mo concentrations from ICP-MS relative to Cu, the pyrite-rich interval is interpreted as representing deposition in anoxic to euxinic conditions. The scarcity of benthic biogenic features such as burrows, seems to support this interpretation. SEM imaging reveals that the pyrite occurs as mostly framboidal clusters and euhedral crystals, which can be an indicator of euxinic pore waters. Further work on the morphology of pyrite is suggested to determine the paleogeochemistry of the ocean water during deposition. This PR interval also appears to have a greater amount of micrometer-scale porosity. Based on modern analogs, geochemical proxies, and pyrite morphology, the PR zone for the Rother 1H-5X and the Yost 1H-18X cores as well as the lower pyrite-rich zone for the Matthews 2-8H are interpreted as representing deposition in mostly anoxic to euxinic conditions.

The silica-rich (SR) zone generates interest for its number of silica-cemented bands. Thin section petrography revealed these bands were microcrystalline quartz

(chert) associated with silicified radiolarians. These radiolarian beds are absent in the Matthews core and common in the Rother and Yost cores, but primarily confined to the SR interval. Pyrite, while not overly common in this zone, does appear within these beds as a secondary diagenetic product, pyritizing the radiolarians. SEM images revealed that pyrite morphology in the SR interval is framboidal and euhedral crystals. Redox elemental proxies U, V, Cu, Zn, and Mo, increase in concentration from the PR interval and TOC values remain high as well. Gamma-ray and neutron logs are suppressed by the reduced clay content in the SR interval, and are used for identifying the zone, which correlates to slightly decreased TOC concentrations. The geochemical signature of silica-rich intervals indicate that the depositional environment was primarily anoxic, with potential episodic euxinic conditions.

The carbonate-rich (CR) zone of the Rother 1H-5X and Yost 1H-18X displays the most variation in fabric due to fracturing, soft-sediment deformation, and depositional features including clasts and disseminated pyrite. This variability is mirrored by the trace element analysis, where the primary proxies all fluctuate in concentration. The upper pyrite-rich interval of the Matthews core does not share the fabric variability of the CR zone of the Rother and Yost cores, but the trace metal concentrations fluctuate. This interval is interpreted as representing anoxic to suboxic depositional conditions.

An important finding of this study is that high-resolution XRF measurements show that the generalized redox interpretation was not refined by measurements taken on the centimeter scale. The increase in radiolarian content and development of silica bands appear to have operated independently of bottom water geochemistry. Thus two geochemical systems were working simultaneously: an upper oxygenated system that

hosted cyclic radiolarian population blooms and collapse, and the lower system with mostly anoxic to euxinic conditions (Figure 46). This combination of organic carbon production in the shallow layers and long-term anoxia to euxinia in the lower layers provide a viable mechanism for generating the high TOC values measured in the Woodford Shale.

The interpreted depositional model for Woodford Shale in these cores confirms that these wells occur along the northern shelf of the Devonian Oklahoma Basin, whose geometry was similar to the present-day Anadarko Basin. The variations in thickness of the Woodford Shale between cores could be the result of several processes. First, thick Woodford Shale such as in the Rother 1H-5X and the Anderson 12-1 cores, may indicate deposition in channels eroded into the pre-Woodford shelf. This mechanism would explain why the Anderson core is further up the shelf, yet it has the thickest Woodford section. A second mechanism for variable Woodford Shale thickness and thinning of subunits away from the basin axis is onlap of the Woodford onto the eroded and karsted pre-Woodford surface. An onlap sequence could account for locally thinning or missing subunits or total section.

Another importance of this study is the improved understanding of the role of silica cementation. The silica-rich interval from the Rother 1H-5X and Yost 1H-18X was sourced from radiolarian blooms, and can be identified by wireline logs. This interval is the most brittle and therefore, the best target interval for hydraulic stimulation. TOC is high in the silica-rich interval, however, the subjacent pyrite-rich interval has the better porosity as well as higher TOC, making it a better source and better reservoir. Therefore, the lower pyrite-rich section of the Woodford Shale in Oklahoma would be the best target

for production but the silica-rich interval is important for hydraulic stimulation and fracture propagation. In contrast, the Kansas core was too far up the shelf during Woodford time to be influenced by upwelling and radiolarian blooms, which removed the primary silica source, and makes the resultant core more difficult to fracture stimulate.

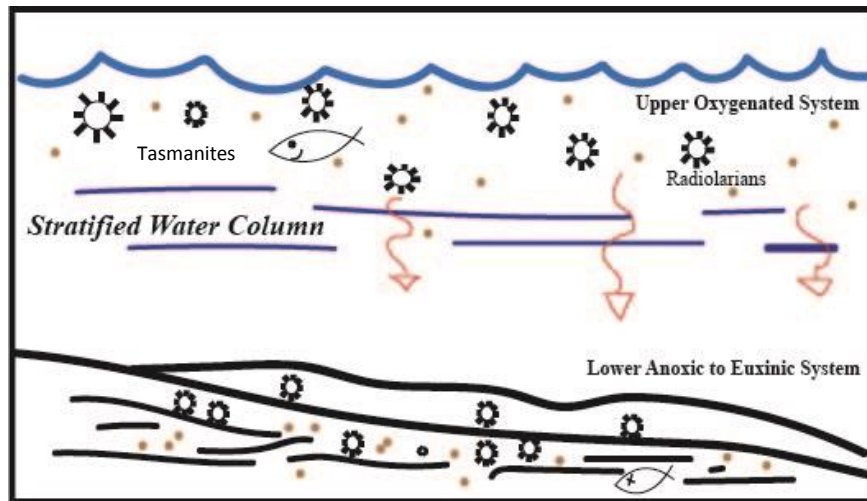


Figure 46. Schematic of generalized two-part system of paleo redox conditions for the Woodford Shale. In the upper part of the water column, an oxygenated system occurs above a pycnocline. Below the pycnocline, the system is anoxic to euxinic conditions, thereby preserving organic material and certain trace elements.

REFERENCES

- Algeo, T.J. and Maynard, J.B., 2004, Trace-element behavior and redox facies in core shales of Upper Pennsylvanian Kansas-type cyclothems: *Chemical Geology*, Vol. 206, p. 289-318.
- Algeo, T.J. and Rowe, H., 2011, Paleooceanographic applications of trace-metal concentration data: *Chemical Geology* 324-325, p. 6-18.
- Arthur, M.A., and Sageman, B.B., 1994, Marine Shales: depositional mechanisms and Environments of Ancient Deposits: *Annual Review of Earth and Planetary Sciences*, v.22, p.499-551.
- Asquith, G., and Krygowski, D., 2004, Basic well log analysis: *AAPG Methods in Exploration*, Vol. 16.
- Barron, L.S. and Ettensohn, F.R., 1981, Paleocology of the Devonian-Mississippian black shale sequence in eastern Kentucky with an atlas of some common fossils: U.S. Department of Energy, p. 1-80.
- Berryman, R.R., 2012, Constraints on development of anoxia through geochemical facies mapping of the Devonian black shales in the Midcontinent: Stillwater, OK, Oklahoma State University, unpublished M.S. thesis.
- Bond, D., Wignall, P., Racki, G., 2004, Extent and duration of marine anoxia during the Frasnian–Famennian (Late Devonian) mass extinction in Poland, Germany, Austria and France: *Geological Magazine*, v. 141, no. 2, p. 173–193.
- Butler, I.B., and Rickard, D., 2000, Framboidal pyrite formation via the oxidation of iron (II) monosulfide by hydrogen sulphide: *Geochimica et Cosmochimica Acta*, Vol. 6, no. 15, p. 2665-2672

Callner, S.A., 2014, An integrated approach to understanding sedimentary structures and depositional processes in Devonian-Mississippian black shale: the Woodford Shale and associated strata in the Southern Midcontinent: Stillwater, Ok, Oklahoma State University, unpublished M.S. thesis.

Calvert, S.E. and Pederson, T.F., 1993, Geochemistry of recent oxic and anoxic marine sediments: Implications for the geological record. In: R.J. Parkes, P. Westbroek and J.W. de Leuw (Editors), *Marine Sediments, Burial, Pore Water Chemistry, Microbiology, and Diagenesis*, Marine Geology, Vol. 113, p. 67-88.

Cardott, B.J., 2012, Thermal maturity of Woodford Shale gas and oil plays, Oklahoma, USA: *International Journal of Coal Geology*, v 103, p. 109-119

Comer, J.B., 2008, Reservoir characteristics and production potential of the Woodford Shale: *World Oil*, v. 229, no 8, p.1-7.

Comer, J.B. and Hinch, H.H., 1987, Recognizing and quantifying expulsion of oil from the Woodford Formation and age-equivalent rocks in Oklahoma and Arkansas: *AAPG Bulletin*, v. 71, p. 844-858.

Cruse, A.M. and Lyons, T.W., 2004, Trace metal records of regional paleoenvironmental variability in Pennsylvanian (Upper Carboniferous) black shales: *Chemical Geology*, v.206, p. 319-35.

Curtis, M.E., Cardott, B.J., Sondergeld, C.H., Rai, C.S., 2012, Development of organic porosity in the Woodford Shale with increasing thermal maturity: *International Journal of Coal Geology*, Vol. 103, p. 26-31.

Dahl, T.W., Ruhl, M., Hammarlund, E.U., Canfield, D.E., Rosing, M.T., Bjerrum, C.J., 2013, Tracing euxinia by molybdenum concentrations in sediments using handheld X-ray fluorescence spectroscopy (HHXRF): *Chemical Geology*, Vol. 360-361, p. 241-251.

Dean, W.E. and Arthur, M.A., 1989, Iron-Sulfur-Carbon relationships in organic-carbon-rich sequences: Cretaceous Western Interior Seaway: *American Journal of Science*, Vol. 289, p. 708-743.

Droser, M.L., and Bottjer, D.J., 1986, A semiquantitative field classification of ichnofabric: Research method paper: *Journal of Sedimentary Research*, Vol. 56, no. 4, p. 558-559.

Ettensohn, F.R., 1992, Controls on the origin of the Devonian-Mississippian oil and gas shales, east-central United States: *FUEL*, vol. 71, p. 1487-1492.

Ettensohn, F.R., Miler, M.L., Dillman, S.B., Elam, T.D., Geller, K.L., Swager, D.R., Markowitz, G., Wook, R., and Brown, L., 1988, Characterization and Implications of the

Devonian-Mississippian Black Shale Sequence, Eastern and Central Kentucky, USA: Pycnoclines, Transgression, Regression, and Tectonism: McMillan, N.J., et al., eds., Devonian of the world, Volume 2: Canadian Society of Petroleum Geologists Memoir 14, p. 323-345.

Gilbert, M.C., 1992, Speculations on the origin of the Anadarko Basin: in Mason, R., ed., Proceedings of the Seventh International Conference on Basement Tectonics: Kingston, Ontario, Kluwer Academic, p. 195-208.

IHS Midcontinent Drilling Wire newsletter, 2014

Jenkyns, H.C., 2010, Geochemistry of oceanic anoxic events: Geochemistry, Geophysics, Geosystems, v.11, Q03004.

Johnson, K.S., 1989, Geologic Evolution of the Anadarko Basin: Oklahoma Geological Survey, vol. 90, p. 3-12.

Johnson, K.S. and Cardott, B.J., 1992, Geologic framework and hydrocarbon source rocks of Oklahoma: Oklahoma Geological Survey, Vol. 93, p. 21-37.

Kirkland, D.W., Denison, R.E., Summers, D.M., Gormly, J.R., 1992, Geology and organic geochemistry of the Woodford Shale in the Criner Hills and Western Arbuckle Mountains: Oklahoma Geological Survey, Vol. 93, p. 38-69.

Lambert, M., 1993, Internal Stratigraphy and Organic Facies of the Devonian-Mississippian Chattanooga (Woodford) Shale in Oklahoma and Kansas, in *Source Rocks in a Sequence Stratigraphic Framework*, Studies in Geology 37, p. 163-176.

Lobza, V., and Schieber, J., 1999, Biogenic sedimentary structures produced by worms in soupy, soft muds: Observations from the Chattanooga Shale (Upper Devonian) and experiments. *Journal of Sedimentary Research*, v. 69, p. 1041-1049.

Löwemark, L., Chen, H.-F., Yang, T.-N., Kylander, M., Yu, E.-F., Hsu, Y.-W., Lee, T.-Q., Song, S.-R., Jarvis, S., 2011, Normalizing XRF-scanner data: A cautionary note on the interpretation of high-resolution records from organic-rich lakes: *Journal of Asian Earth Sciences*, Vol. 40, p. 1250-1256.

Lüning, S. and Kolonic, S., 2003, Uranium spectral gamma-ray response as a proxy for organic richness in black shales: applicability and limitations: *Journal of Petroleum Geology*, vol. 26, p. 153-174.

Musa, M.O., 2013, Factors controlling organic matter preservation and selected metals concentration in the Upper Devonian shales in southern North America (Chattanooga Shale, TN and Woodford Shale, OK): Stillwater, OK, Oklahoma State University, unpublished Ph.D. dissertation.

Over, D.J., 1992, Conodonts and the Devonian-Carboniferous boundary in the Upper Woodford Shale, Arbuckle Mountains, South-Central Oklahoma: *Journal of Paleontology*, Vol. 66, No.2, p. 293-311.

Over, D.J., 2002, The Frasnian/Famennian boundary in central and eastern United States: *Paleogeography, Paleoclimatology, Paleoecology*, Vol. 181, p.153-169.

Paxton, S.T., Cruse, A.M., Krystyniak, A.M., 2006, Detailed fingerprints of global sea-level change revealed in Upper Devonian-Mississippian Woodford Shale of south-central Oklahoma: American Association of Petroleum Geologists Oral Presentation, Search and Discovery Paper:

<http://www.searchanddiscovery.com/documents/2006/06095paxton/index.htm?q=%2BtextStrip%3Agamma+textStrip%3Aarray+textStrip%3Auranium+textStrip%3AWoodford+isMeetingAbstract%3Amtgabsyes>.

Puckette, J.O., Musa, M.O., Boardman, D., Watney, W.L., 2013, Lithologic, biogenic, and geochemical indicators of water chemistry during deposition of the Woodford Shale, KGS-OGS Current #1, Pontotoc County, Oklahoma: Mid-Continent Core Workshop: From source to reservoir to seal, American Association of Petroleum Geologists Mid-Continent Section meeting, Wichita, KS, p.215-224.

Roberts, C.T., and Mitterer, R.M., 1992, Laminated black shale-bedded chert cyclicity in the Woodford Formation, southern Oklahoma, in K.S. Johnson and B.J. Cardott, eds., *Source rocks in the southern Midcontinent, 1990 symposium: Oklahoma Geological Survey, Circular 93*, p. 330-336.

Rowe, H., Ruppel, S., Rimmer, S., Loucks, R., 2009, Core-based chemostratigraphy of the Barnett Shale, Permian Basin, Texas: *Gulf Coast Association of Geological Societies Transactions*, Vol. 50, p. 675-688.

Rowe, H., Hughes, N., Robinson, K., 2012, The quantification and application of handheld energy-dispersive x-ray fluorescence (ED-XRF) in mudrock chemostratigraphy and geochemistry: *Chemical Geology*, 324-325, p. 122-131.

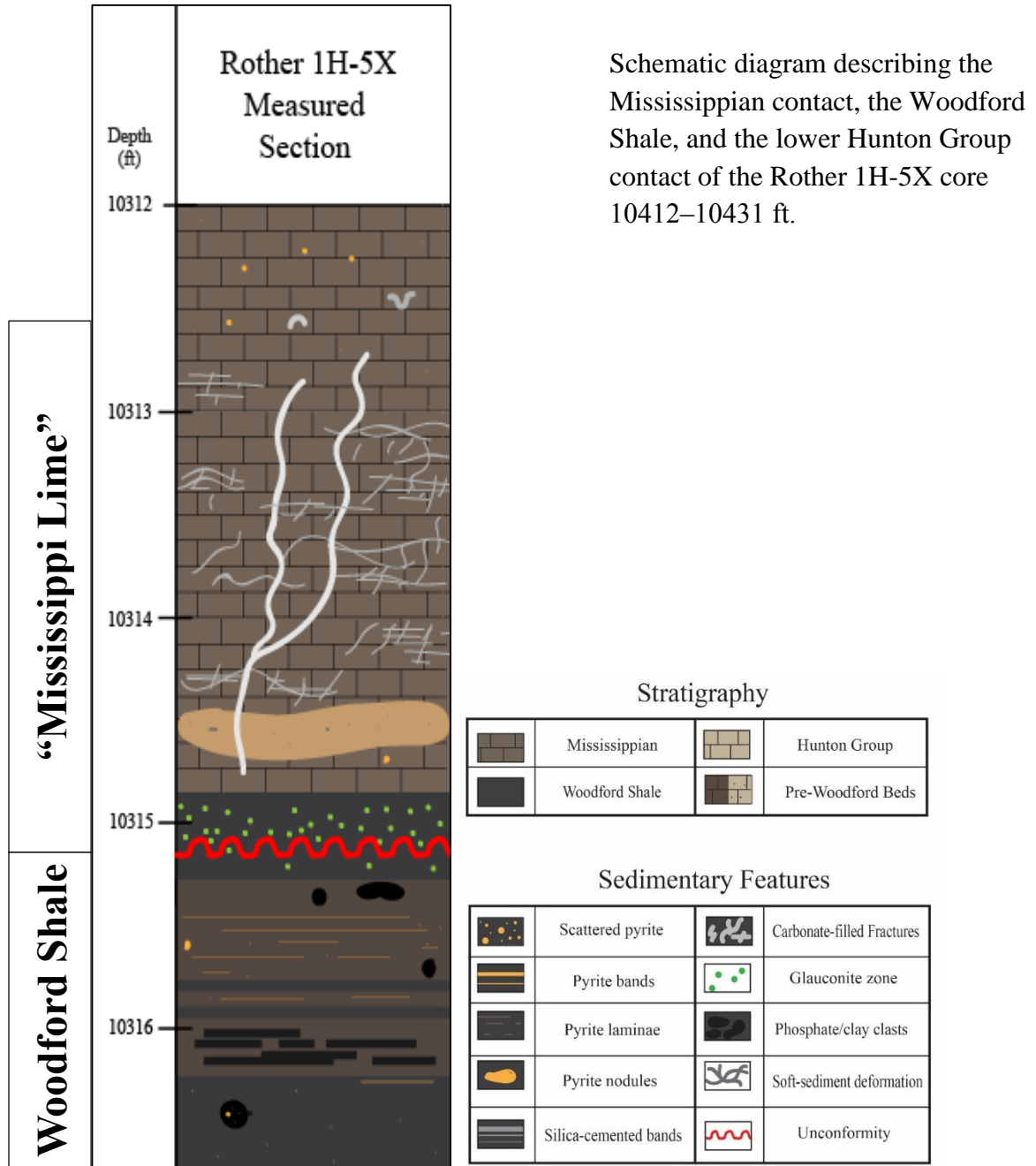
Schieber, J., 1998, Sedimentary features indicating erosion, condensation, and hiatuses in the Chattanooga Shale of Central Tennessee: relevance for sedimentary and stratigraphic evolution. In: J. Schieber, W. Zimmerle, and P. Sethi (editors), *Shales and Mudstones (vol. 1): Basin Studies, Sedimentology and Paleontology*, Schweizerbart'sche Verlagsbuchhandlung, Stuttgart, p. 187-215.

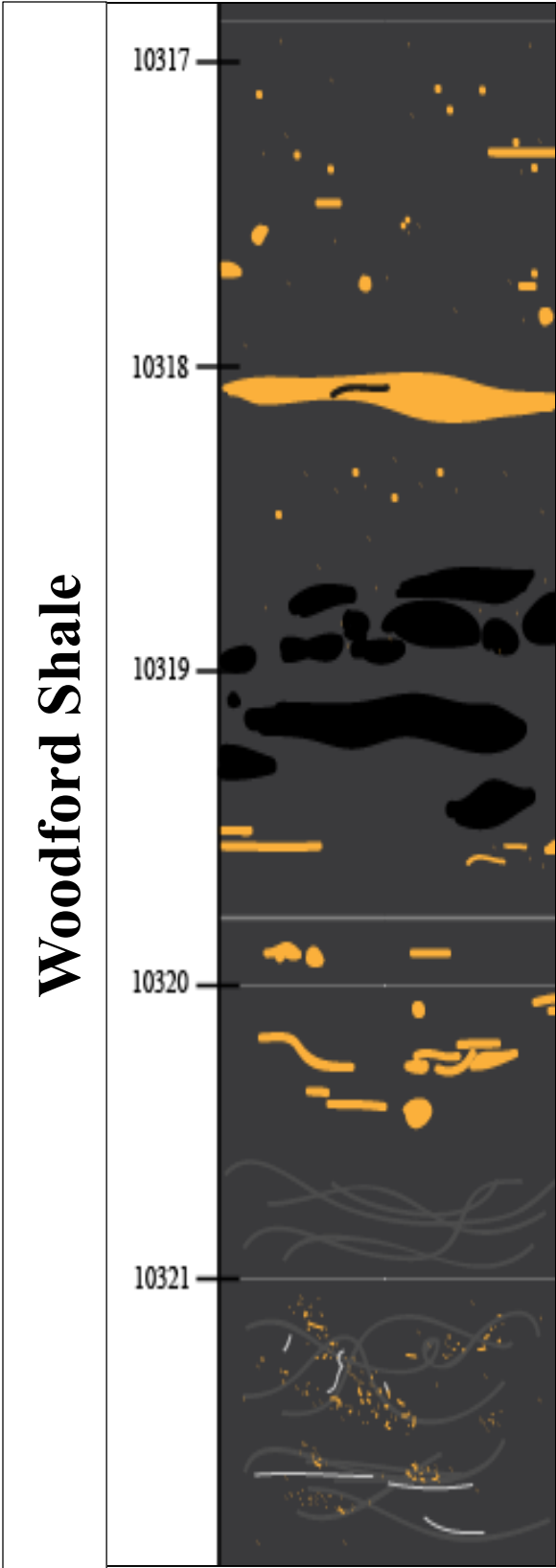
Schieber, J., 2001, A role for organic petrology in integrated studies of mudrocks: examples from Devonian black shales of the eastern US: *International Journal of Coal Geology*, Vol. 47, p. 171-187.

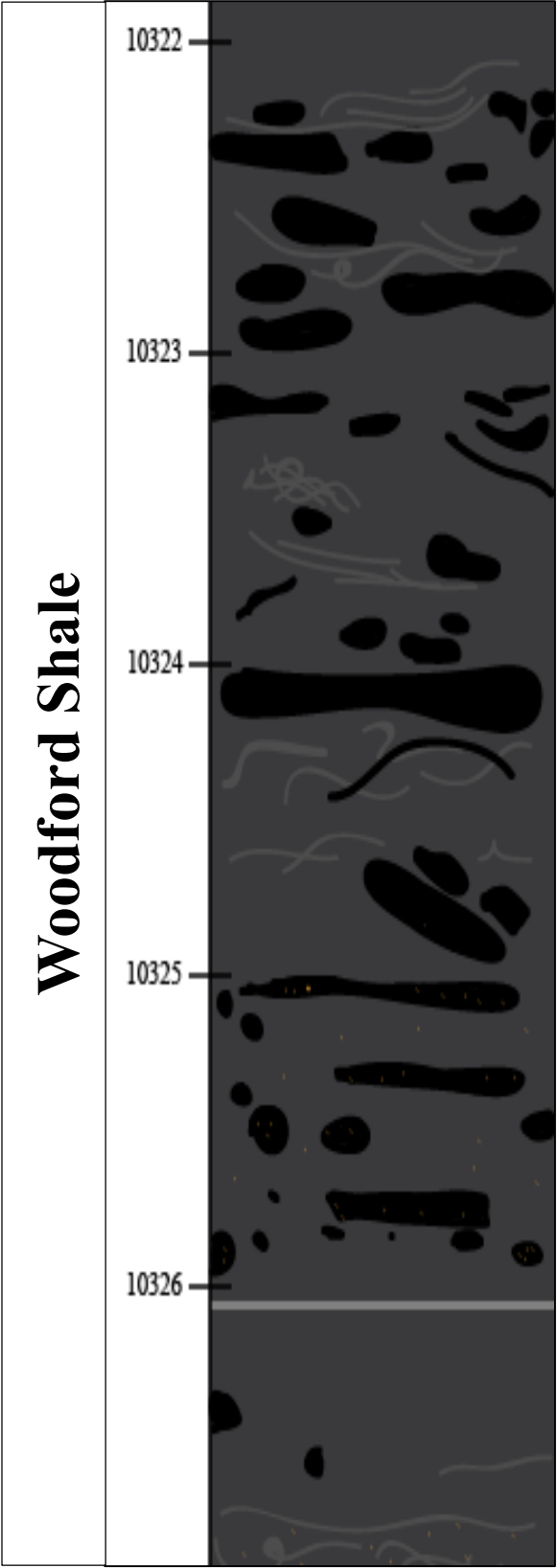
- Schieber, J., Krinsley, D., Riciputi, L., 2000, Diagenetic origin of quartz silt in mudstone and implications for silica cycling: *Nature*, v. 406, p. 981-985.
- Schieber, J., and Riciputi, L., 2004, Pyrite ooids in Devonian black shales record intermittent sea-level drop and shallow water conditions: *Geology*, v. 32, no. 4, p. 305-308.
- Scott, C. and Lyon, T.W., 2012, Contrasting molybdenum cycling and isotopic properties in euxinic versus non-euxinic sediments and sedimentary rocks: Refining the paleoproxies: *Chemical Geology*, Vol. 324-325, p. 19-27.
- Sierra, R., Tran, M.H., Abousleiman, Y.N., Slatt, R.M., 2010, Woodford Shale mechanical properties and the impacts of lithofacies: *American Rock Mechanics Association Symposium*, (ARMA 10-461), p. 1-10.
- Snider, A.L., 2014, Characterization of the Woodford Shale in Southern Noble and Northern Payne Counties Oklahoma: Stillwater, OK, Oklahoma State University, unpublished M.S. thesis.
- Taft, J.A., 1902, Description of the Atoka quadrangle [Indian Territory]: *US Geological Survey Atlas Folio*, v. 79, p.8.
- Thomson, J., I. W. Croudace, and R. G. Rothwell, 2006, A geochemical application of the ITRAX scanner to a sediment core containing eastern Mediterranean sapropel units: In R. G. Rothwell [ed.], *New techniques in sediment core analysis*. Geological Society Special Publication, p. 65-77.
- Tourtelot, H.A., 1979, Black shale – its deposition and diagenesis: *Clays and Clay Minerals*, vol. 27, No. 5, p. 313-321.
- Tribouillard, N., Algeo, T.J., Lyons, T., Riboulleau, A., 2006, Trace metal as paleoredox and paleoproductivity proxies: An update: *Chemical Geology*, vol. 232, p. 12-32.
- Tyson, R.V., Pearson, T.H., 1991, Modern and ancient continental shelf anoxia: an overview: *Geological Society Special Publications*, No. 58, p. 1-24.
- Ulmishek, G.F. and Klemme, H.D., 1990, Effective petroleum source rocks of the world: Stratigraphic distribution and controlling depositional factors: *AAPG Bulletin*, vol.75, p. 1809-1851.
- Wang, Q., and Morse, J.W., 1996, Pyrite formation under conditions approximating those in anoxic sediments I. Pathway and morphology: *Marine Chemistry*, Vol. 52, p. 99-121.
- Wilken, R.T. and Barnes, H.L., 1997, Formation processes of framboidal pyrite: *Geochimica et Cosmochimica Acta*, Vol. 61, no. 2, p. 323-339.

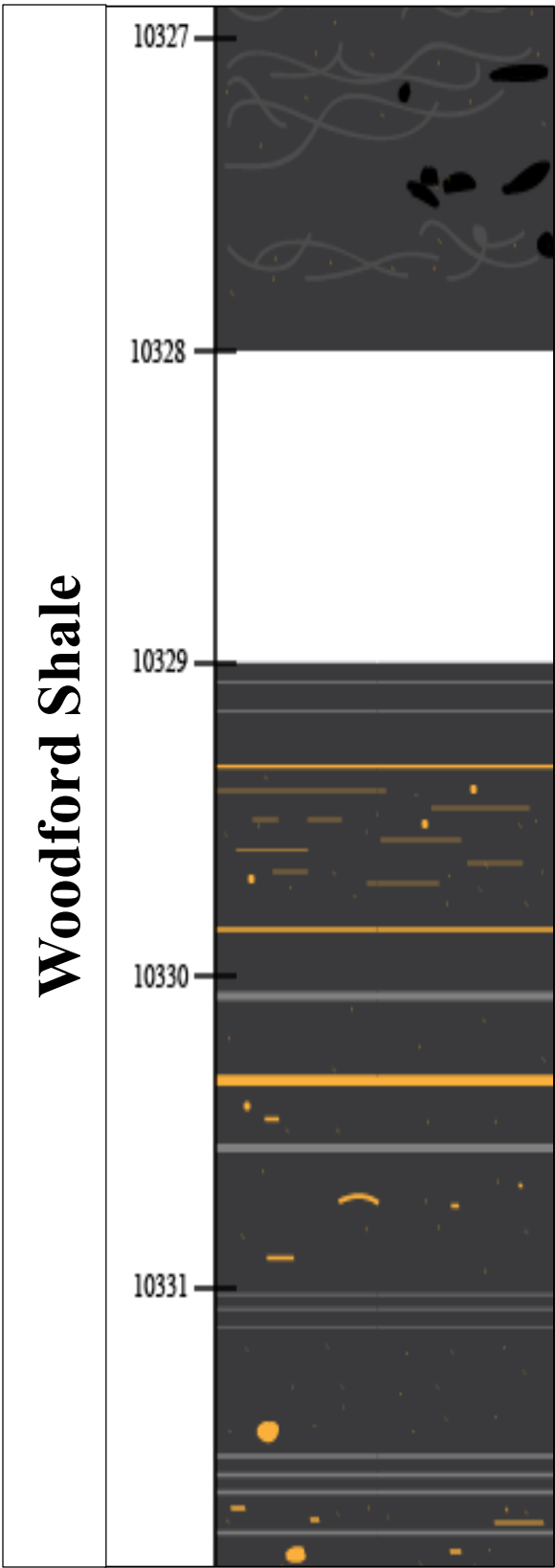
Wilken, R.T., Barnes, H.L., Brantley, S.L., 1996, The size distribution of framboidal pyrite in modern sediments: An indicator of redox conditions: *Geochimica et Cosmochimica Acta*, Vol. 60, no. 20, p. 3897-3912.

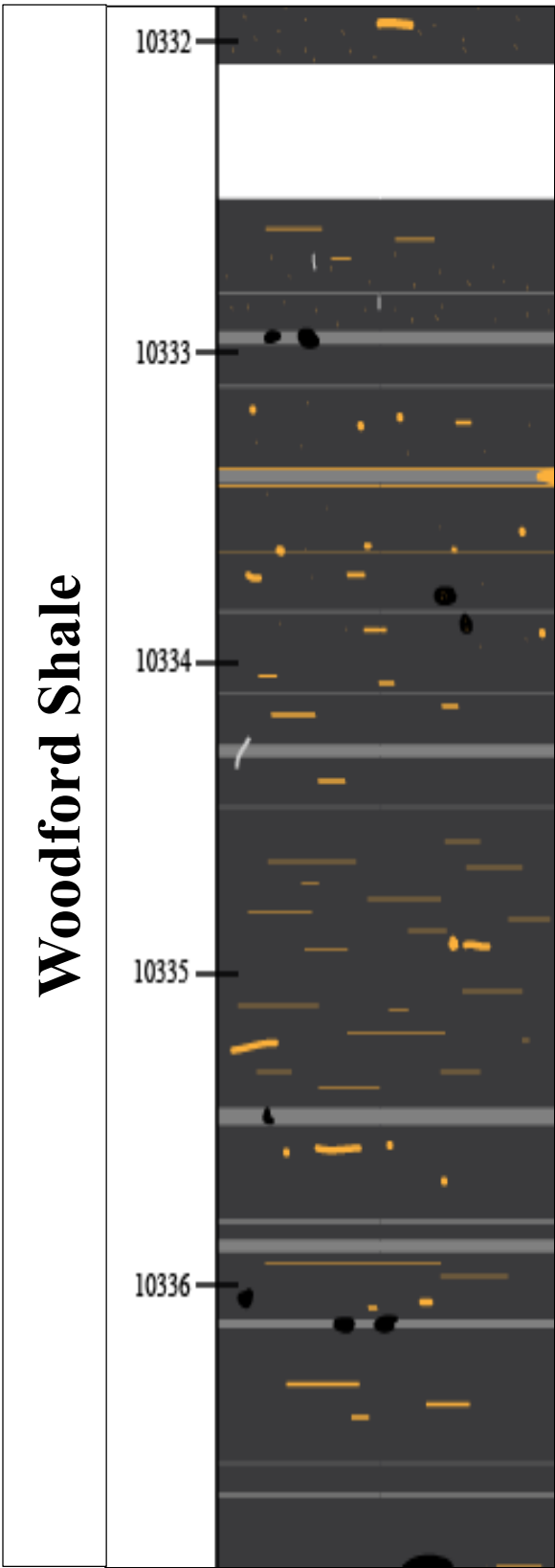
APPENDICES

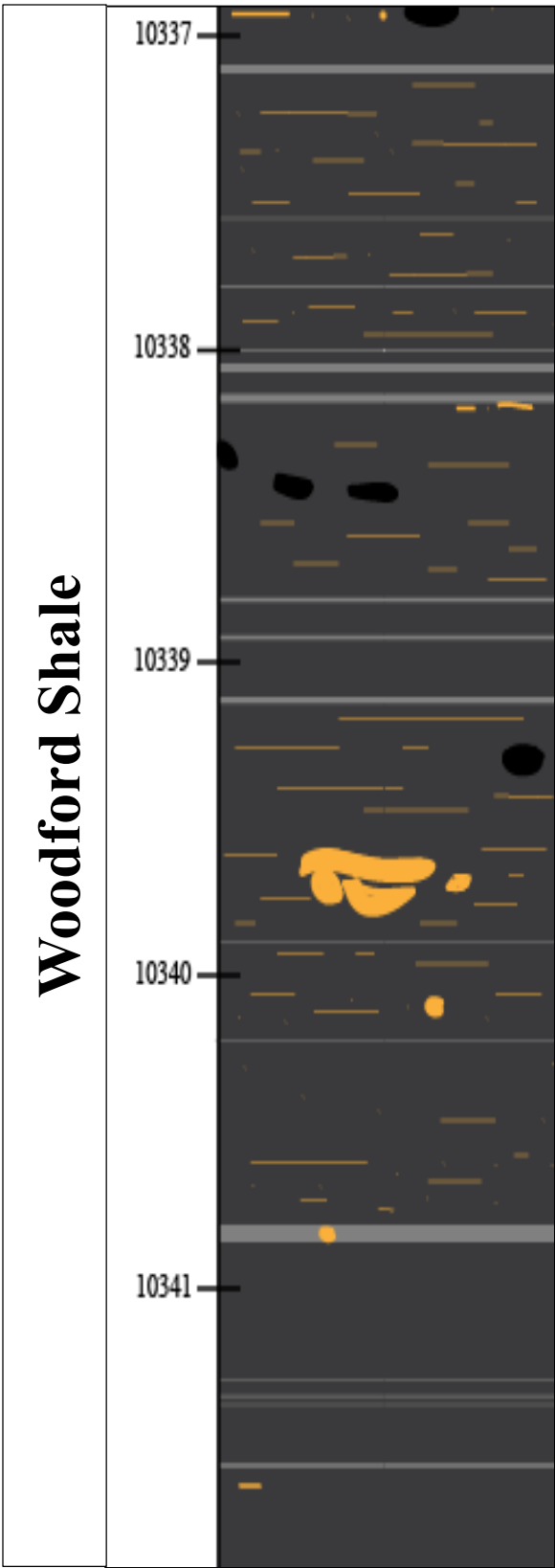


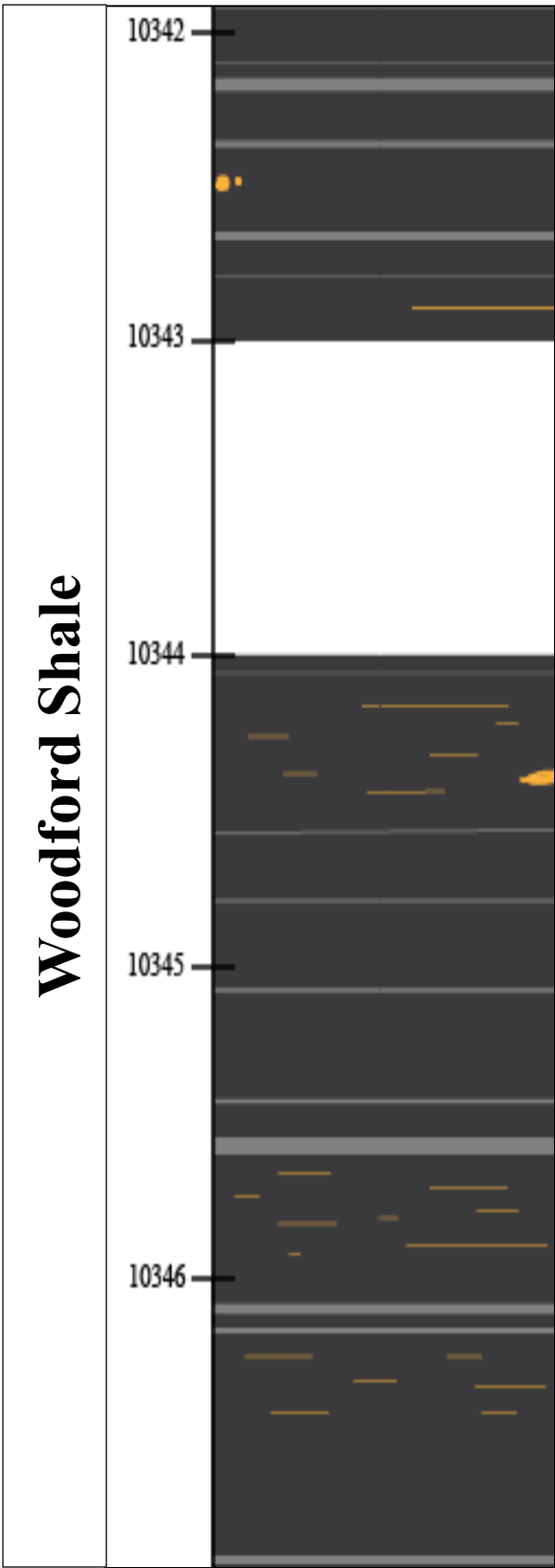


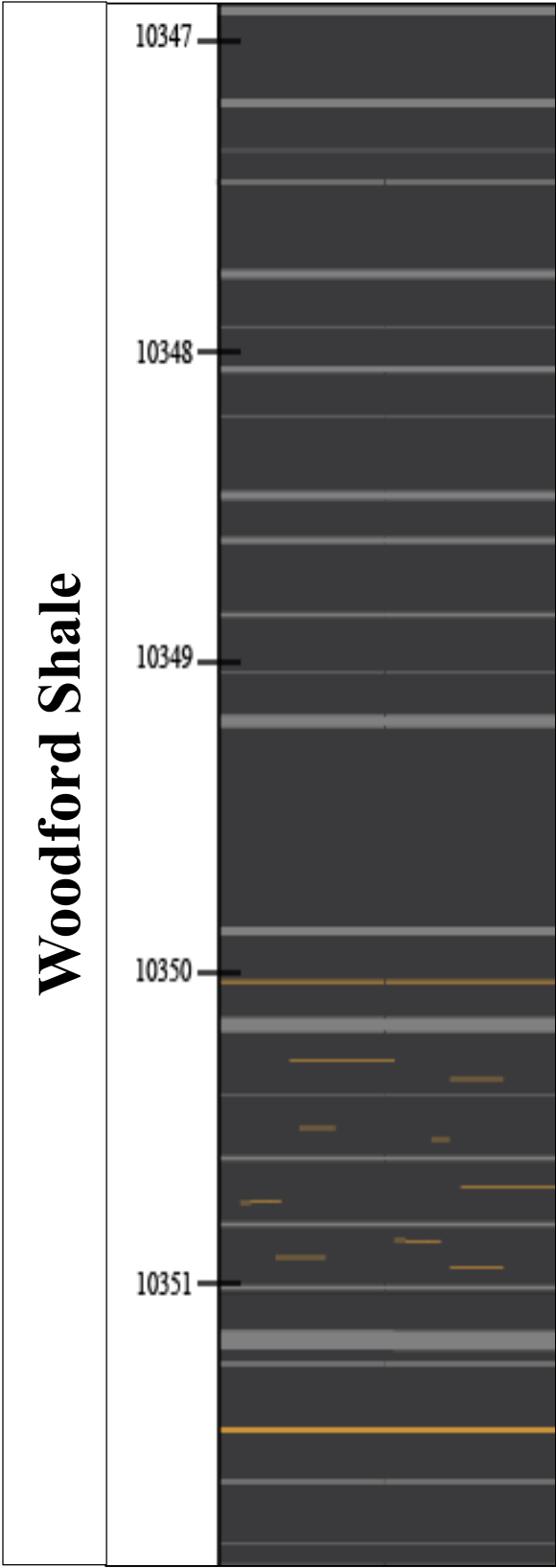


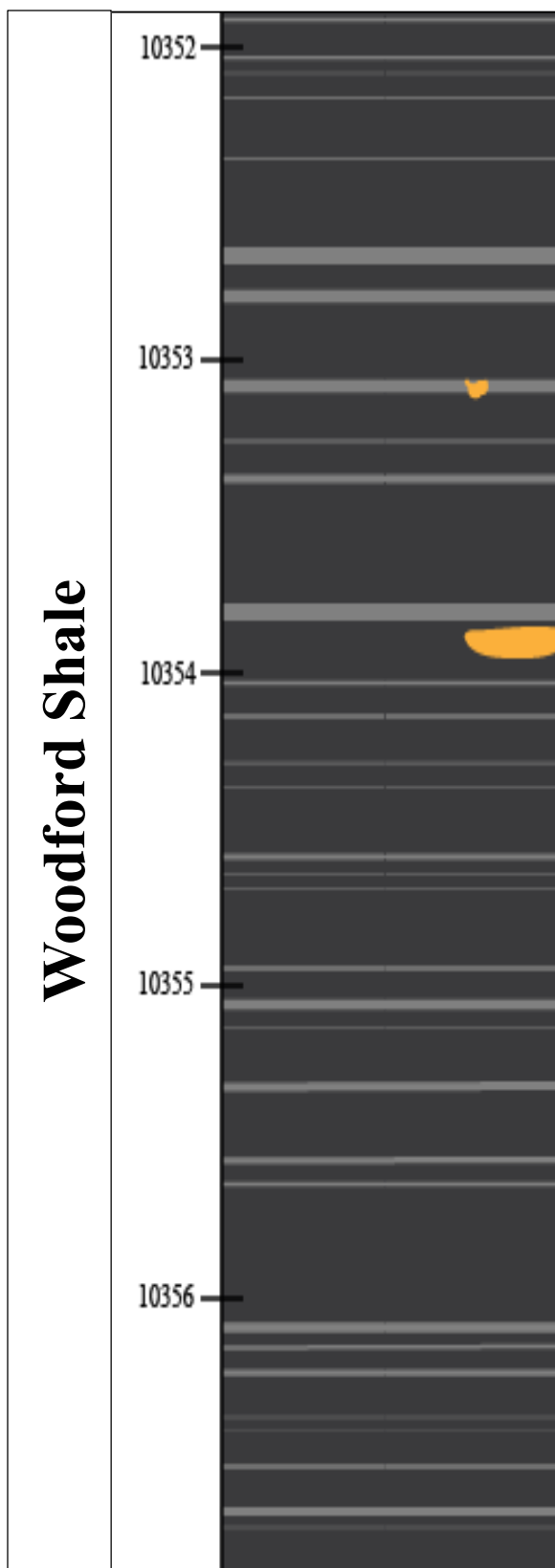


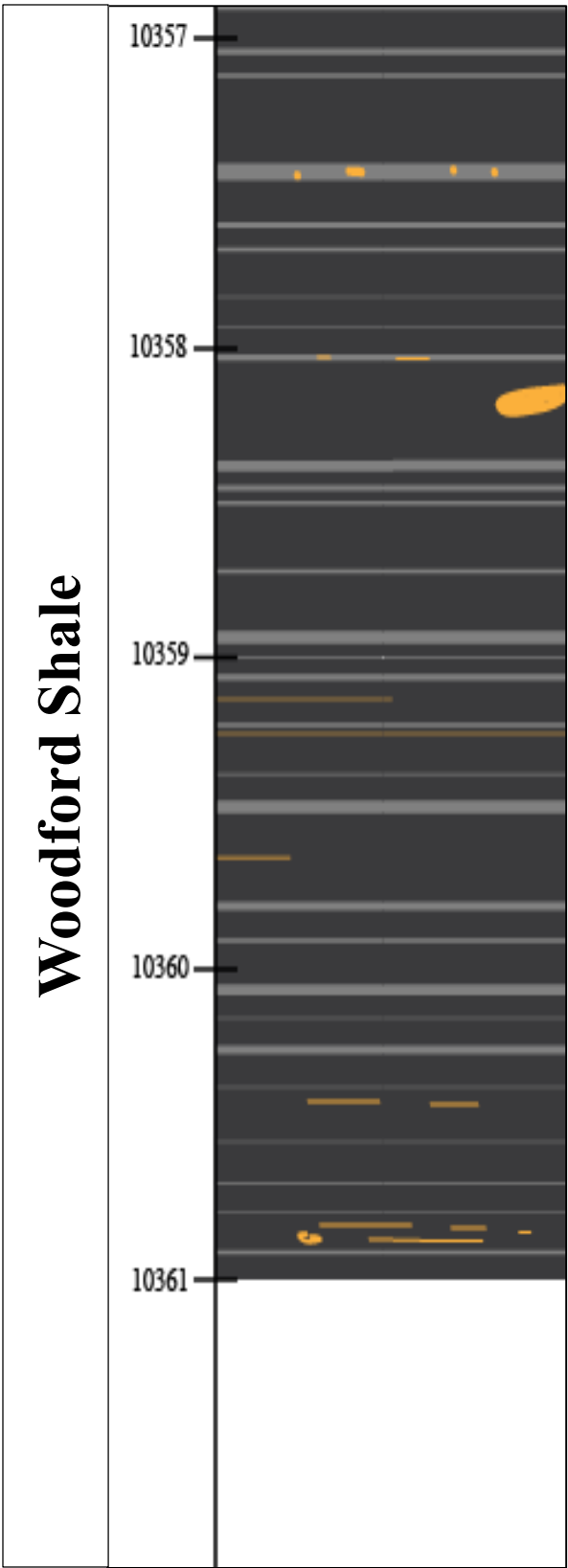


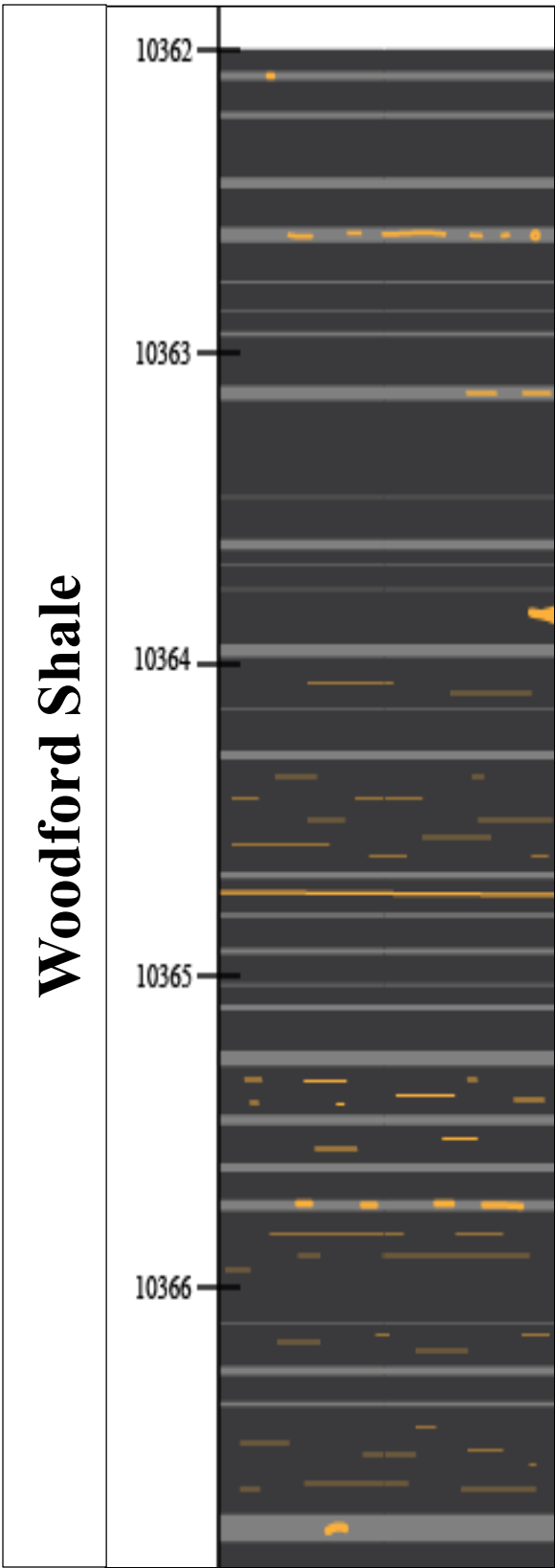


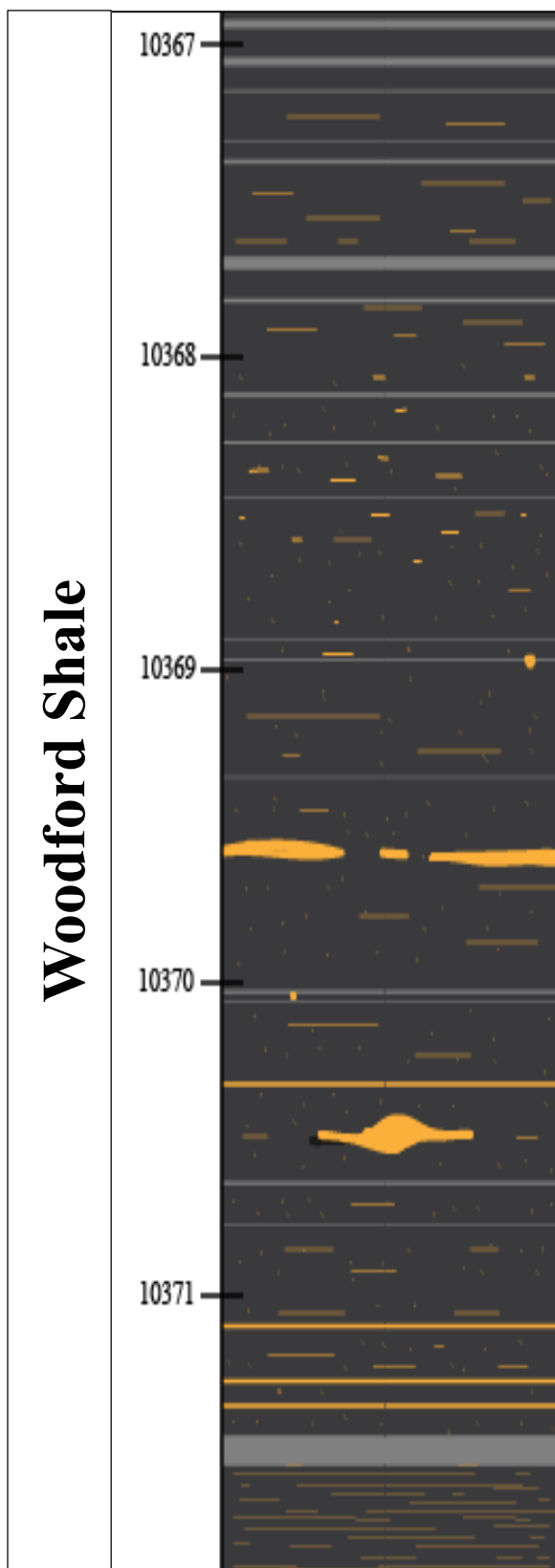


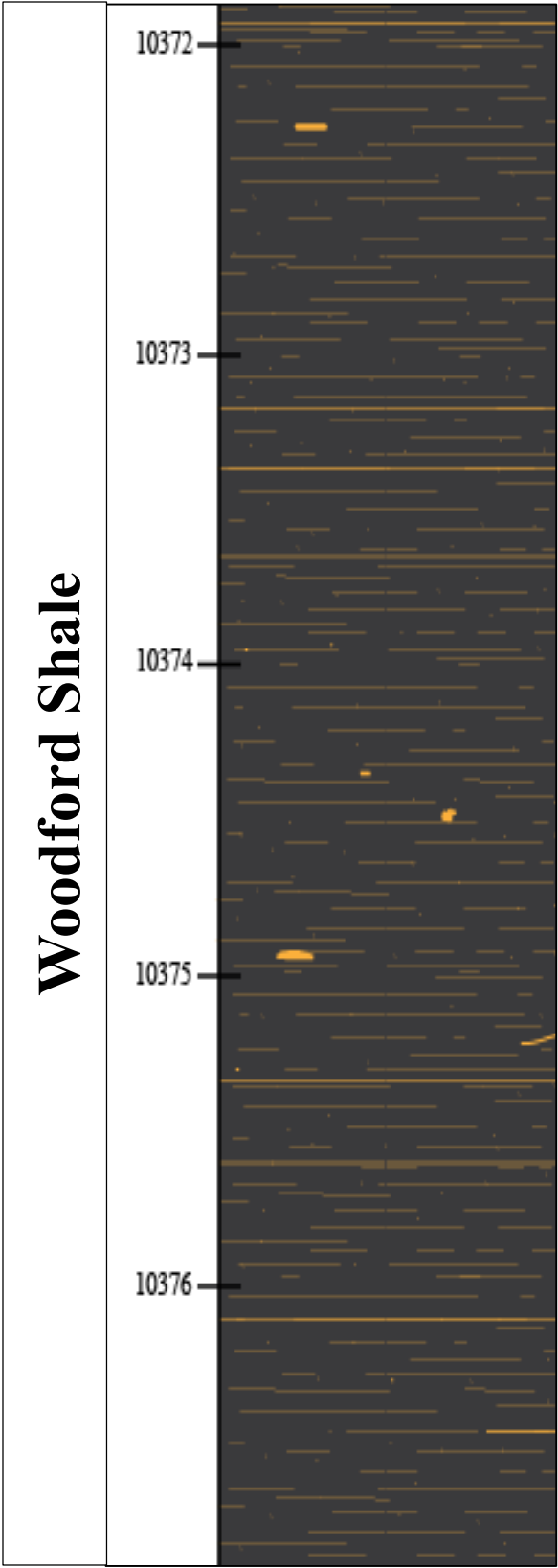


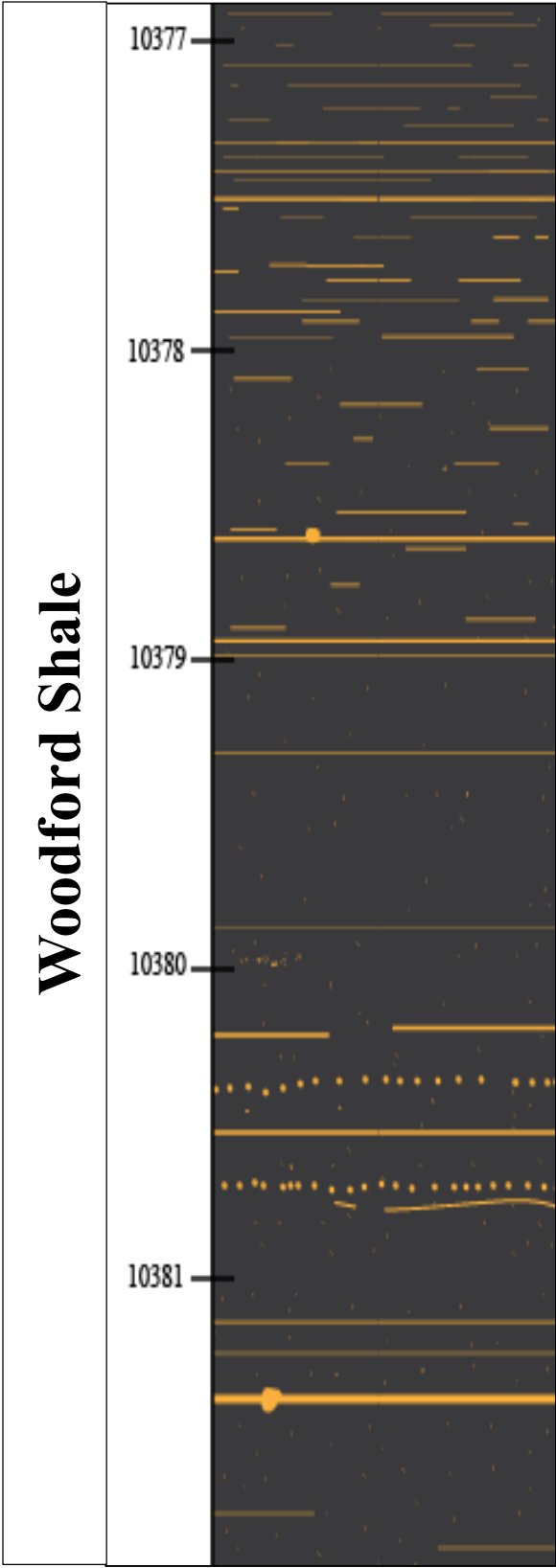


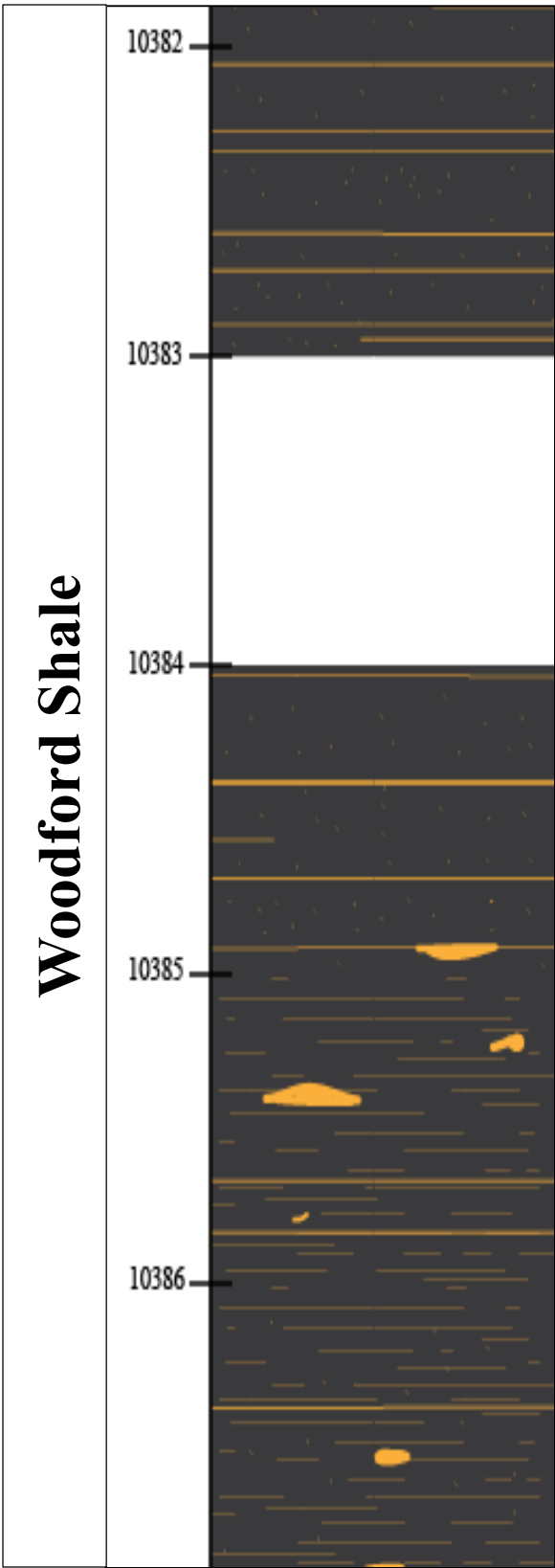


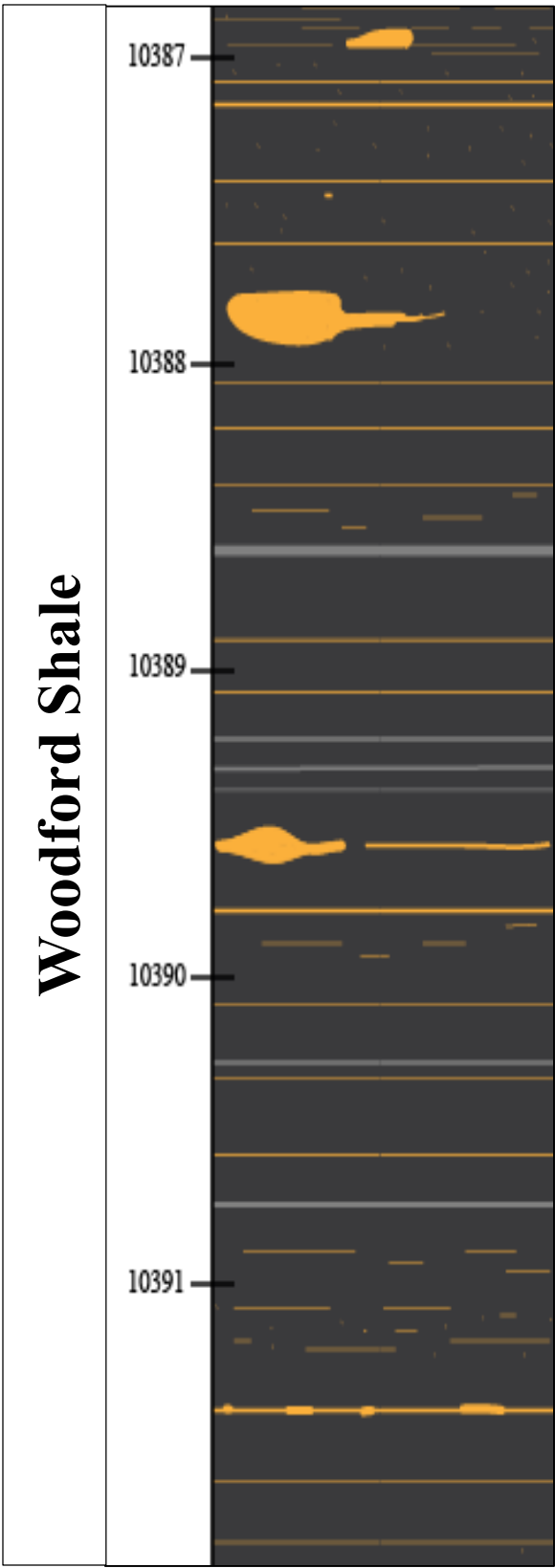


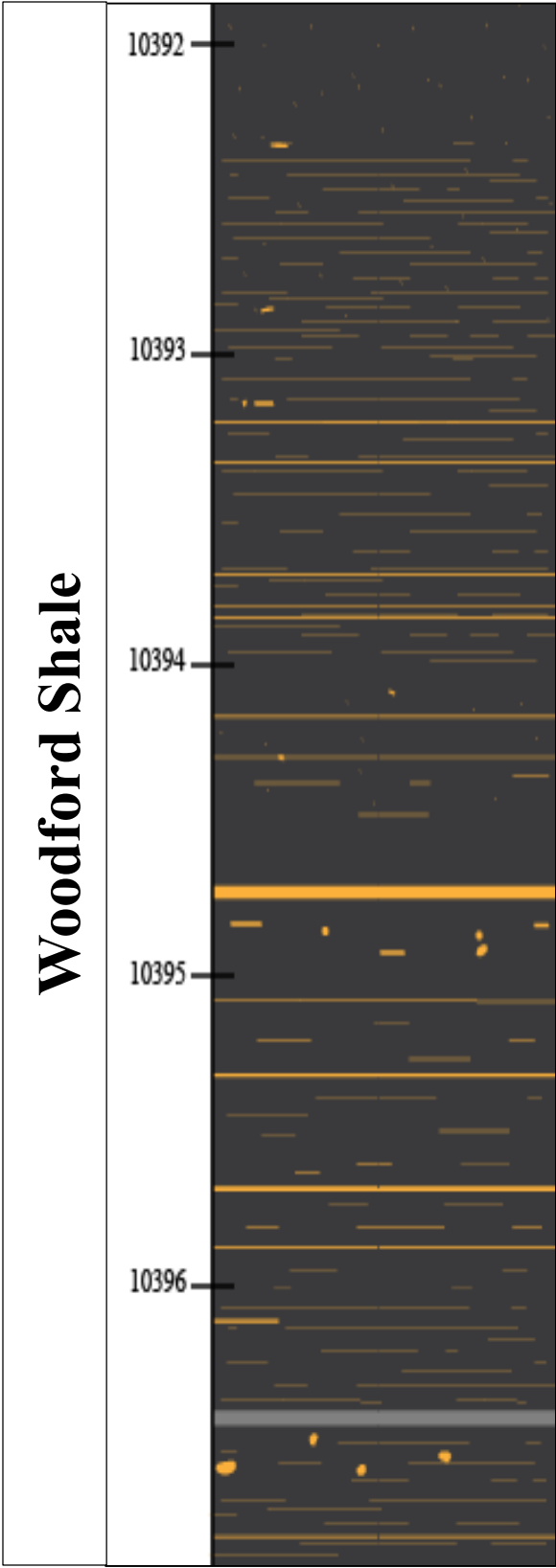


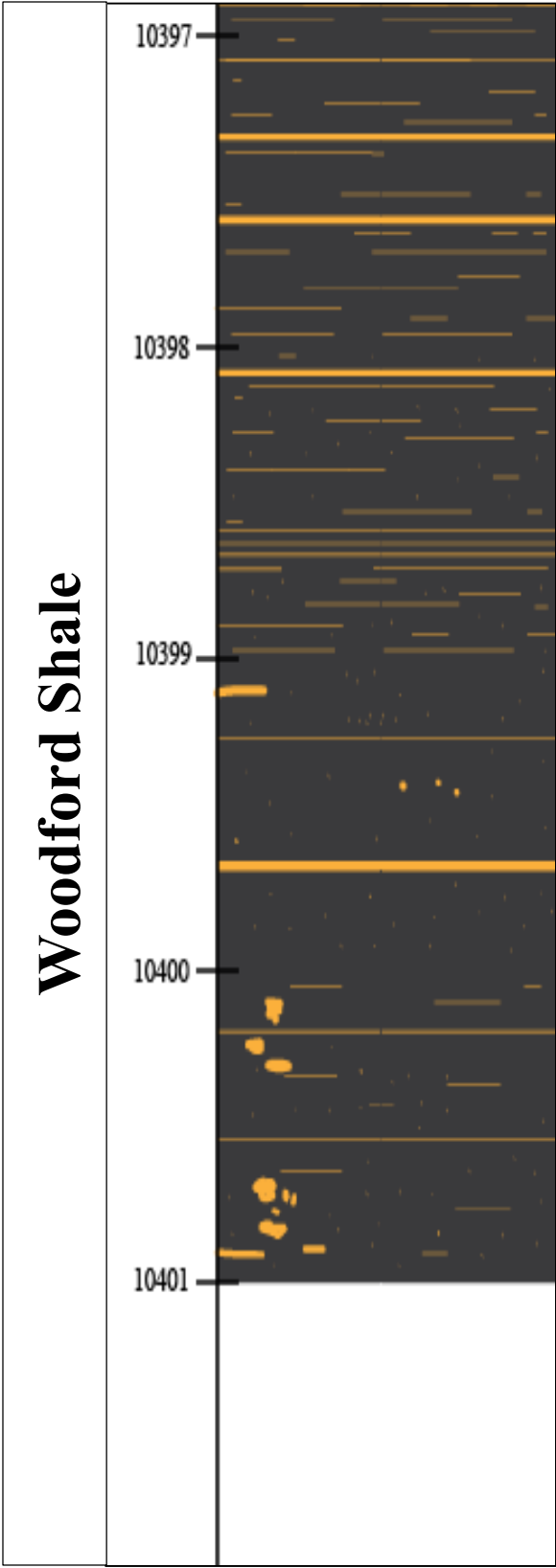


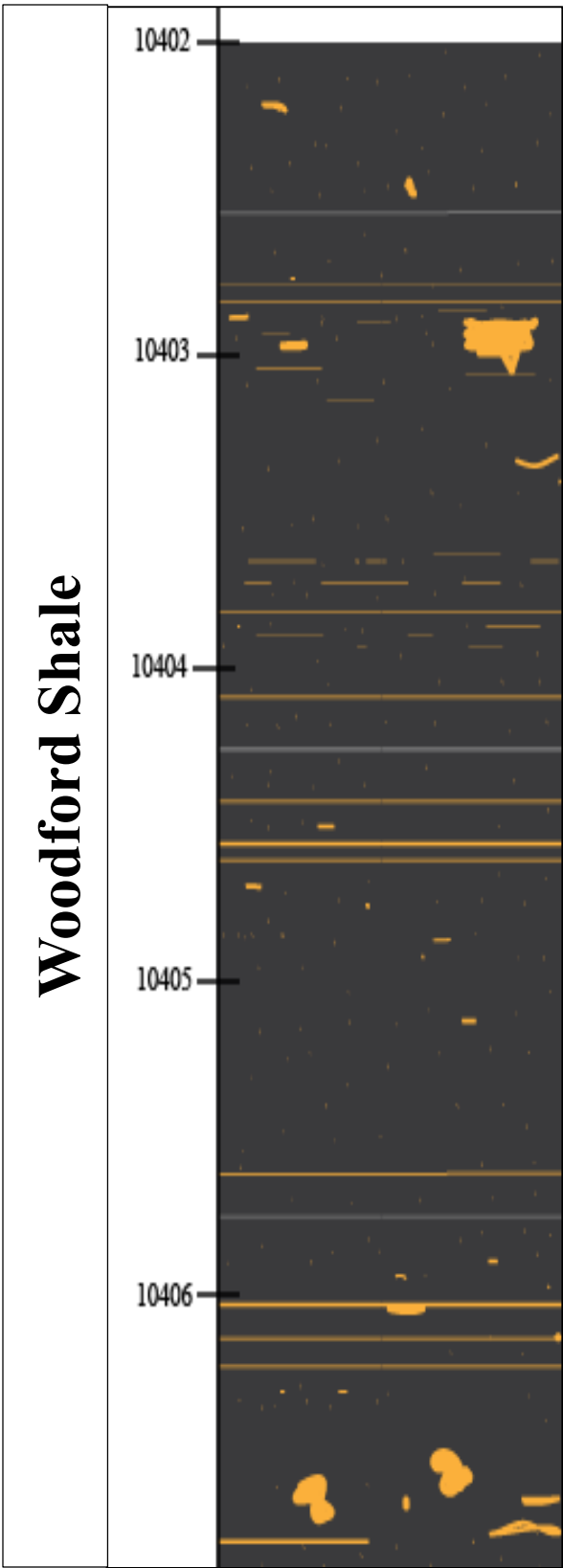


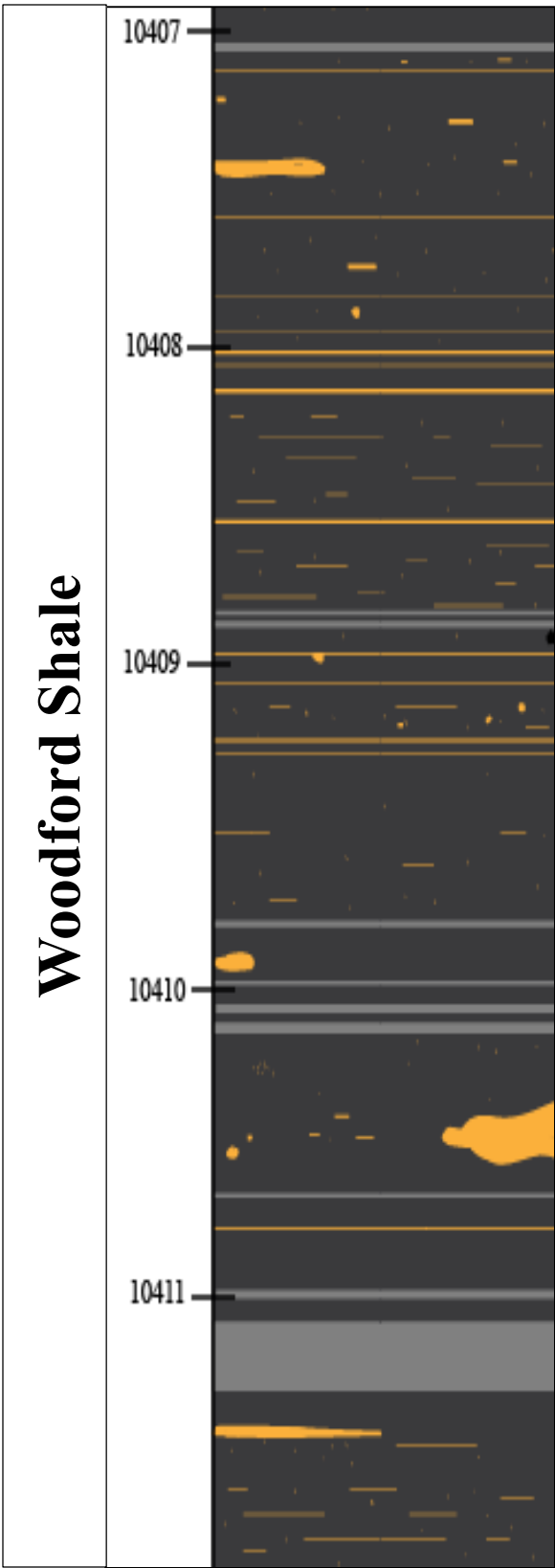




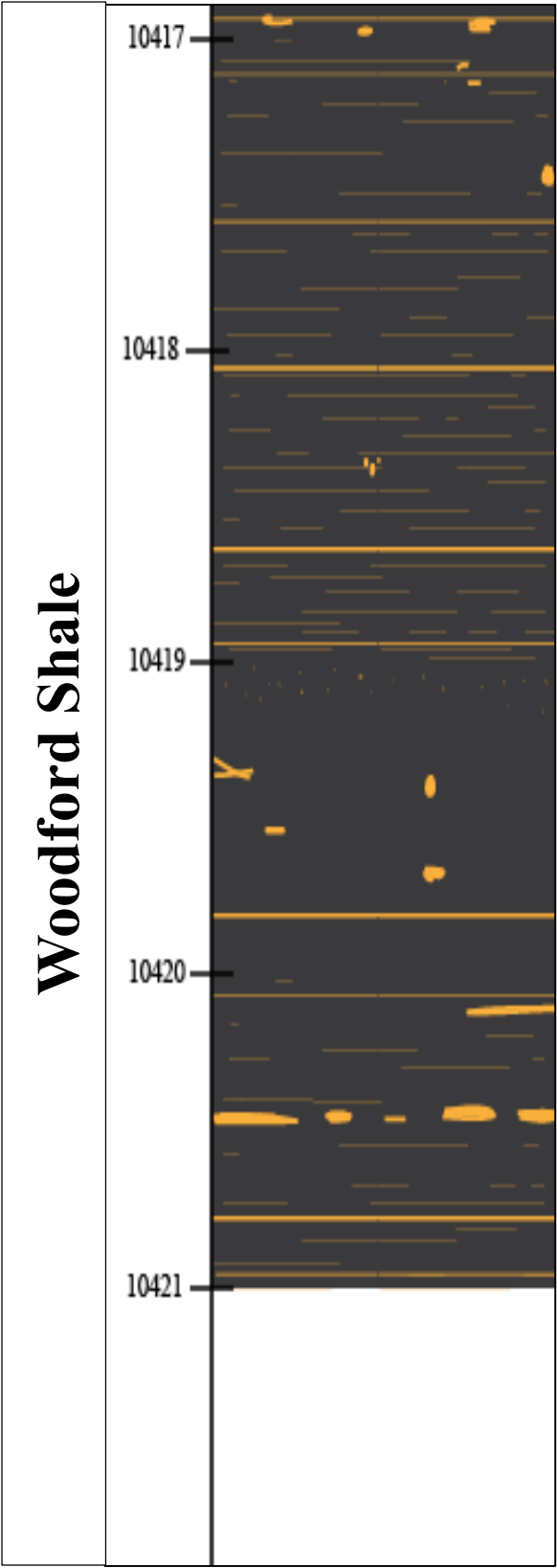


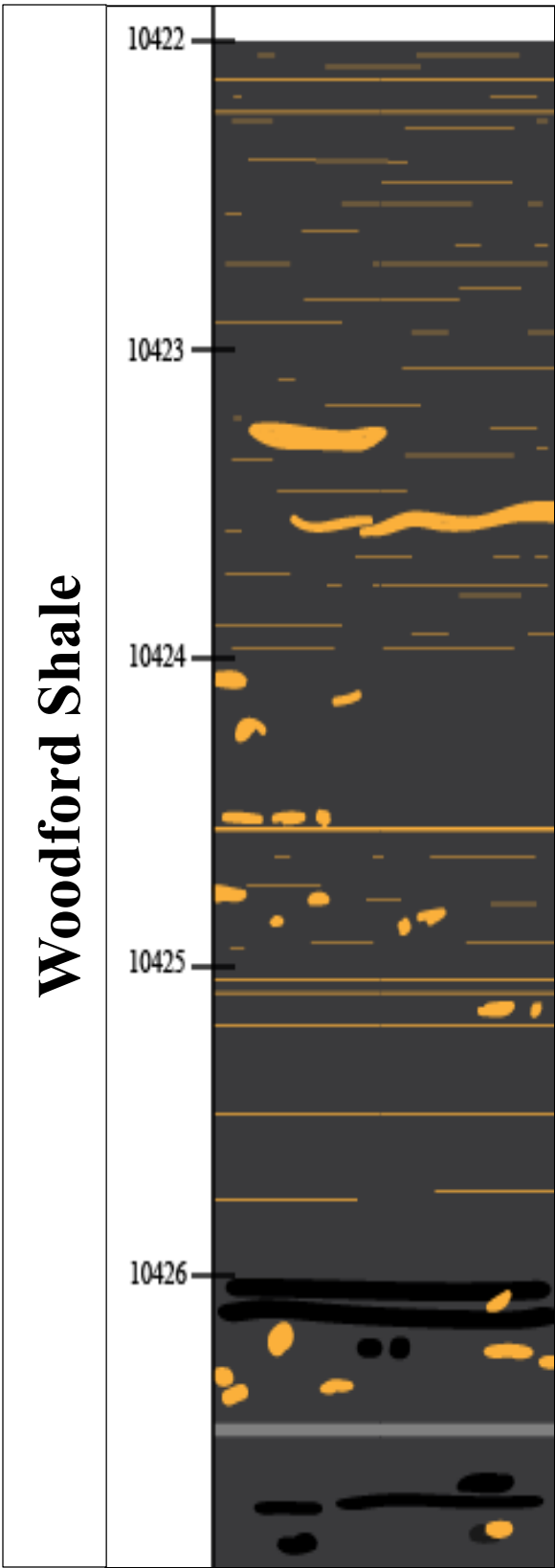


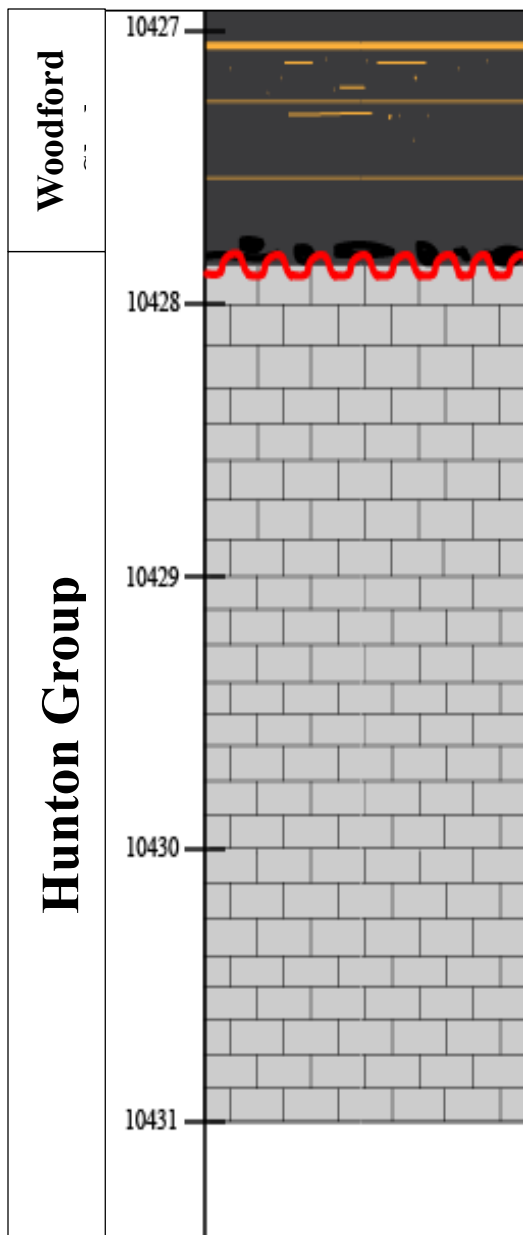




















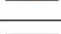



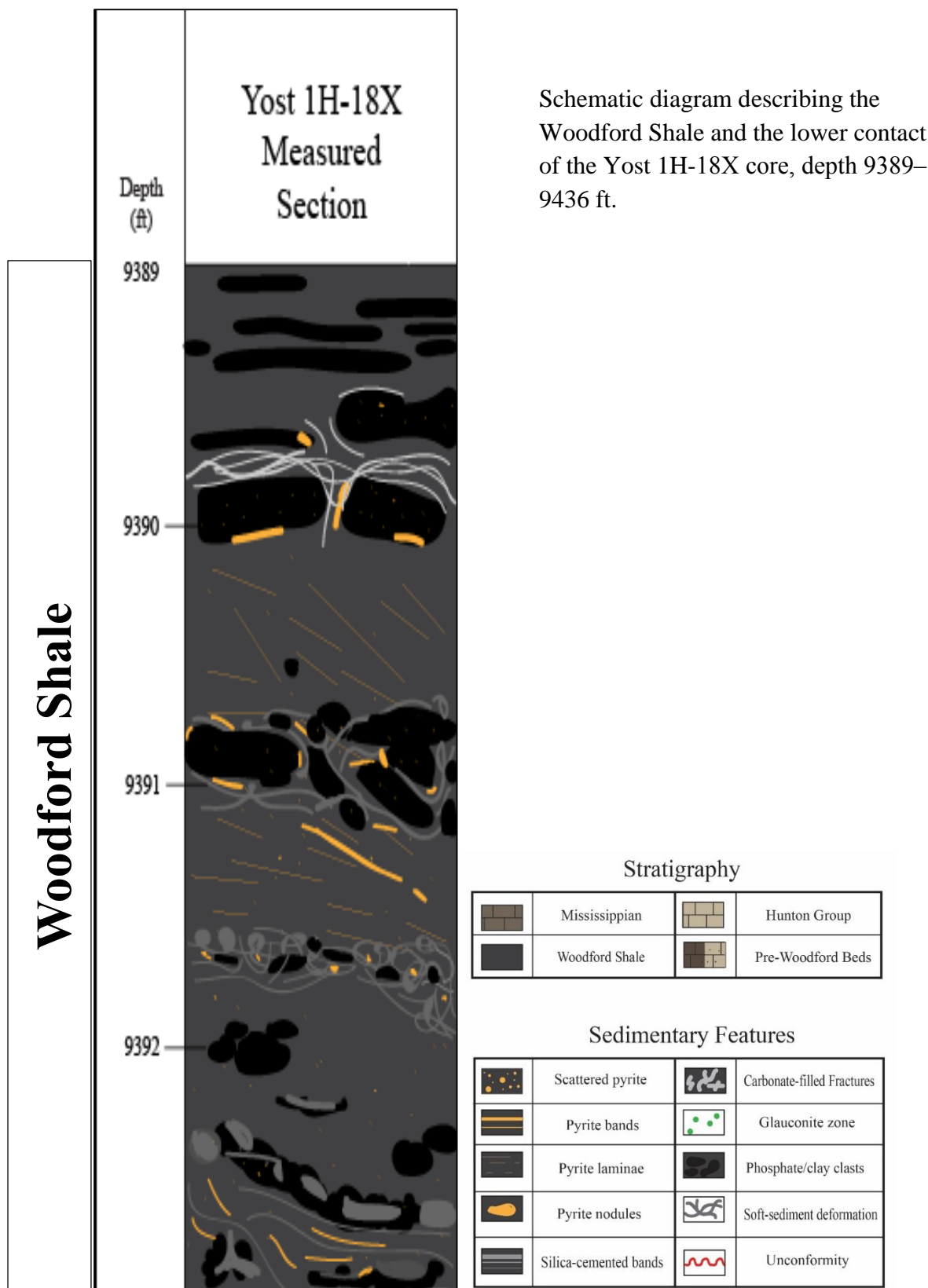


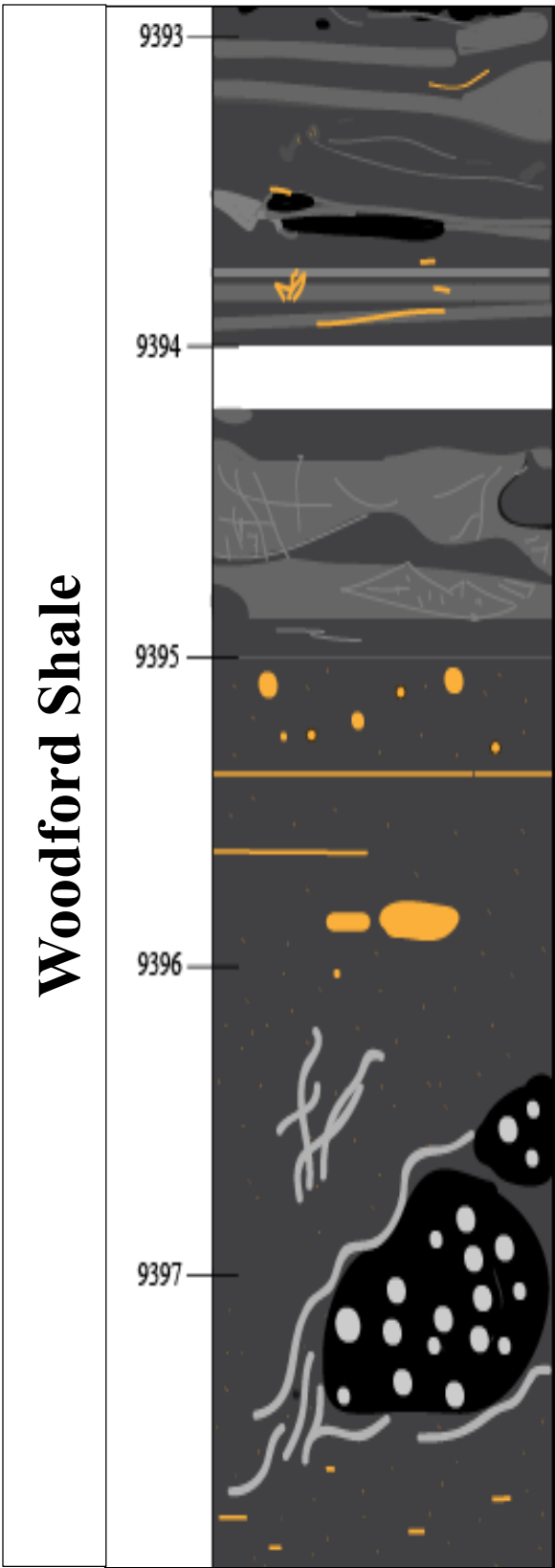
Stratigraphy

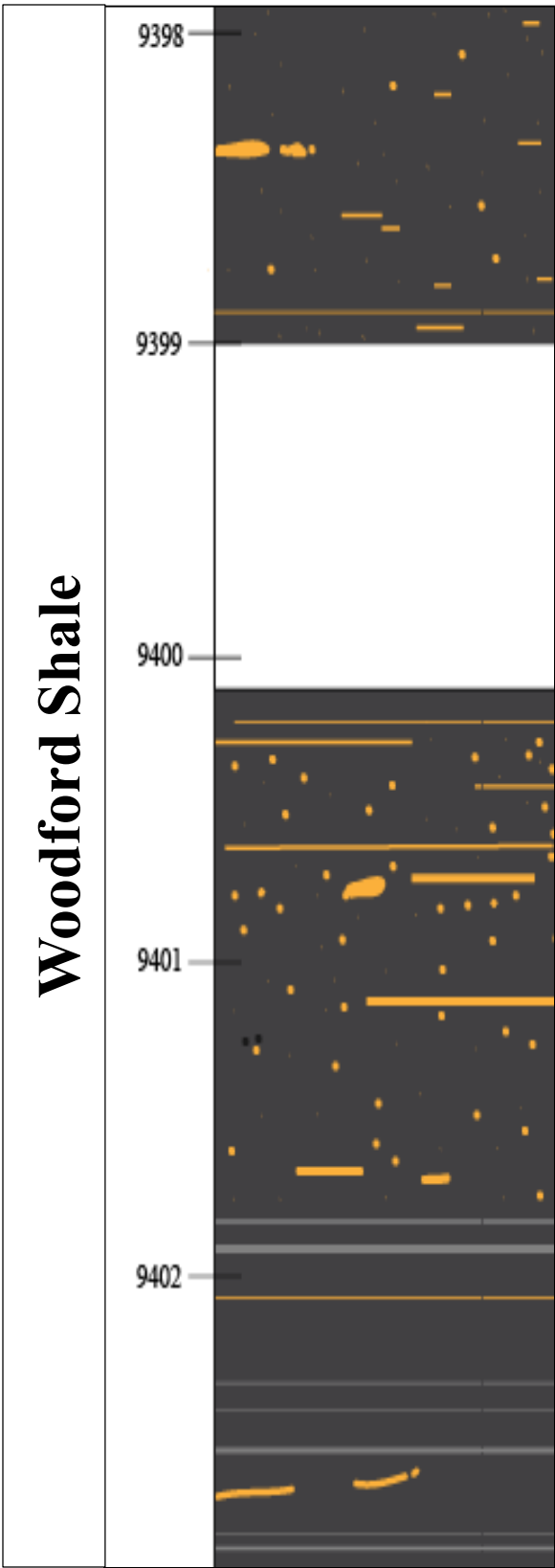
	Mississippian		Hunton Group
	Woodford Shale		Pre-Woodford Beds

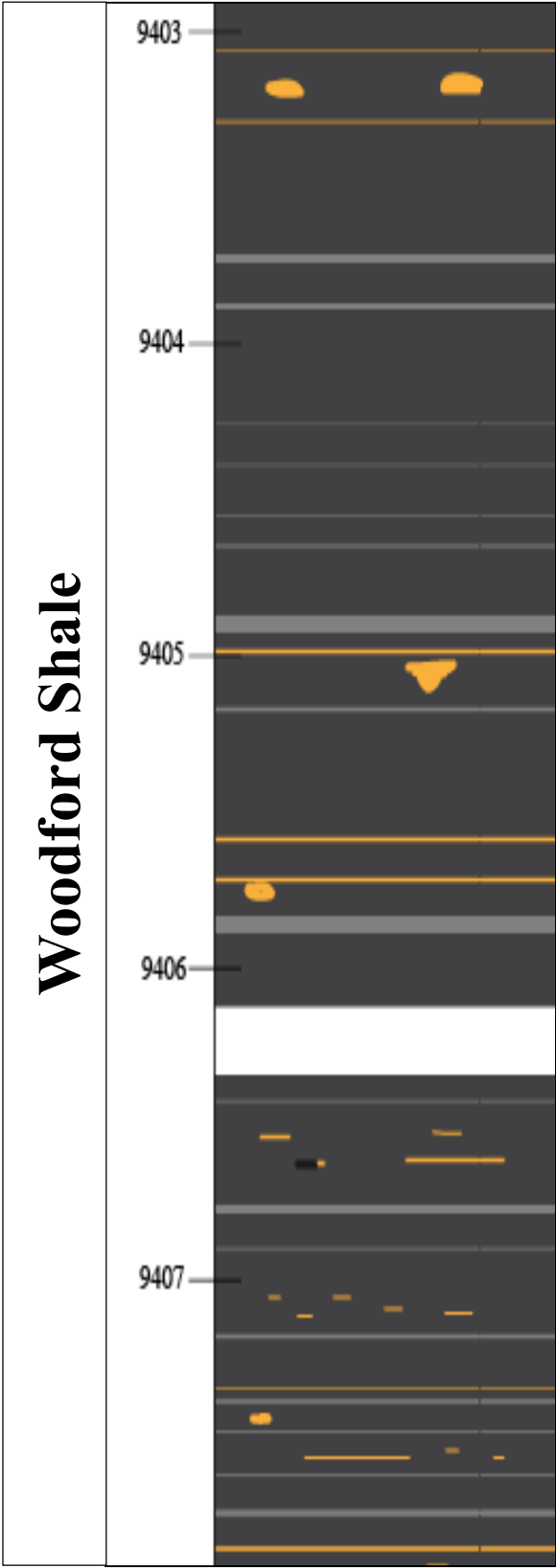
Sedimentary Features

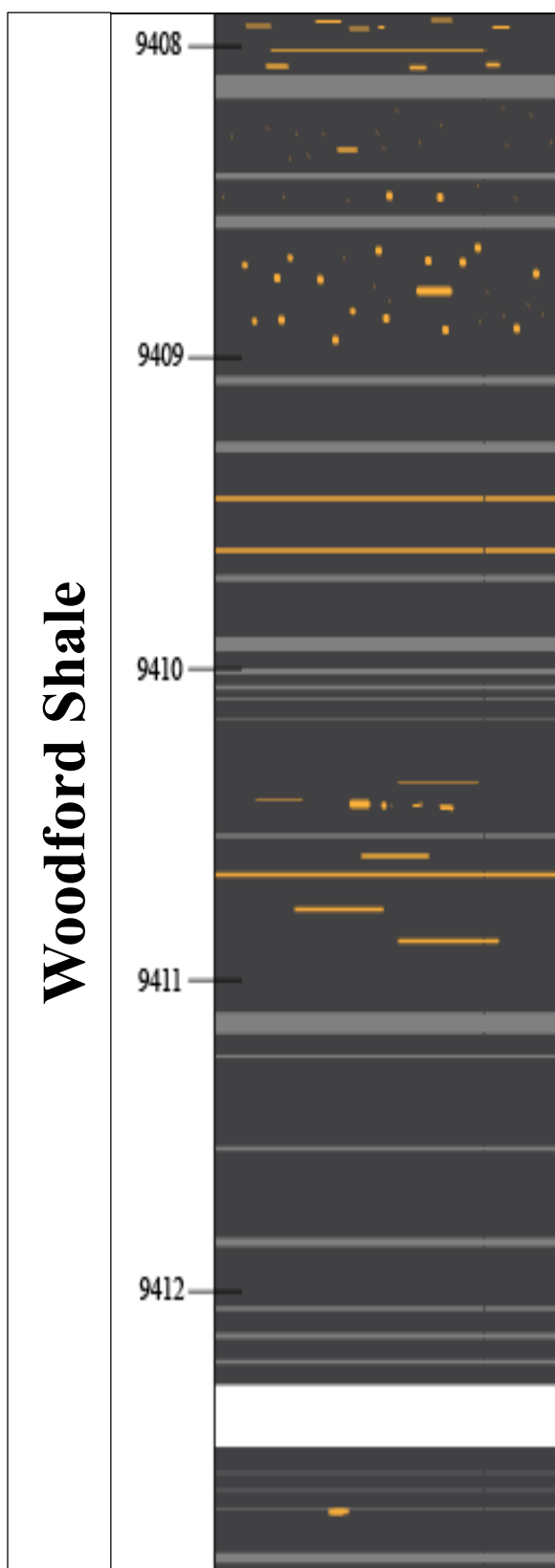
	Scattered pyrite		Carbonate-filled Fractures
	Pyrite bands		Glauconite zone
	Pyrite laminae		Phosphate/clay clasts
	Pyrite nodules		Soft-sediment deformation
	Silica-cemented bands		Unconformity

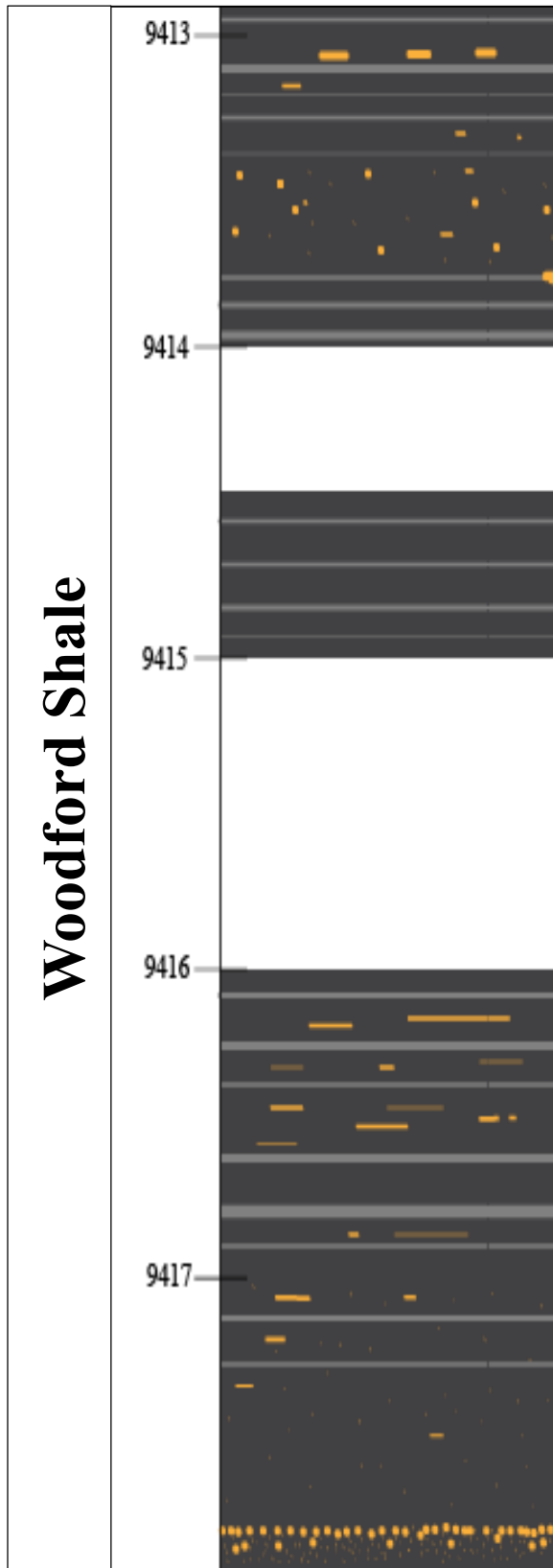


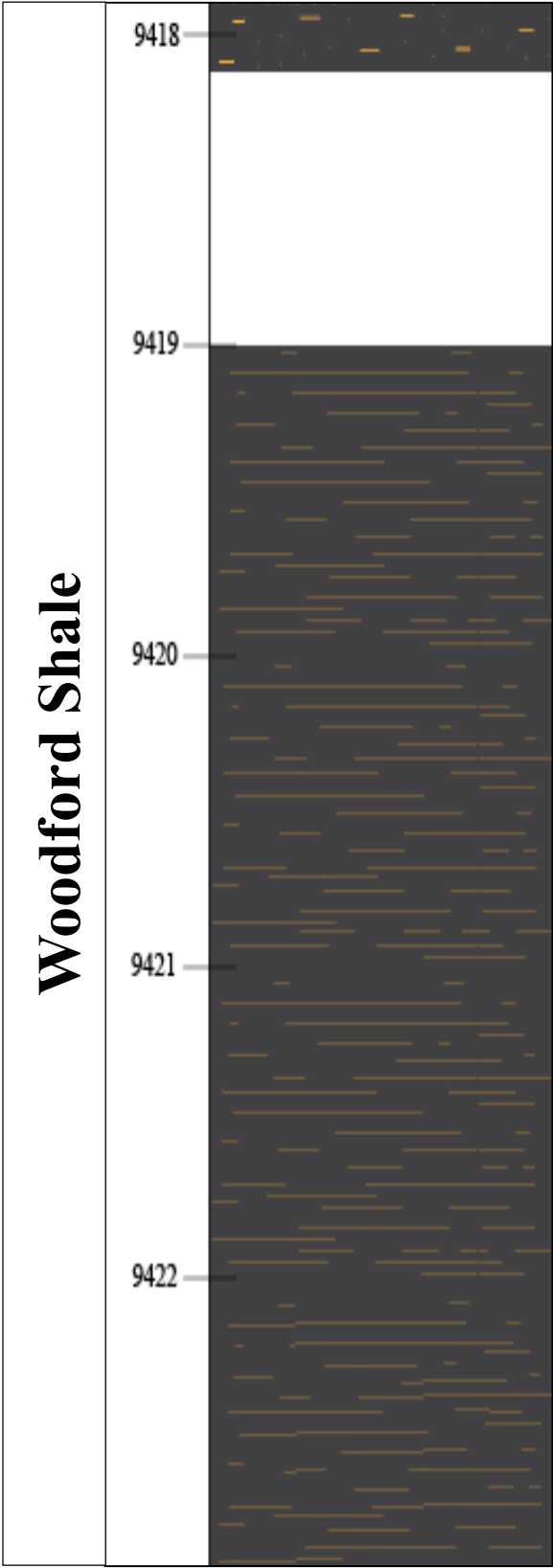


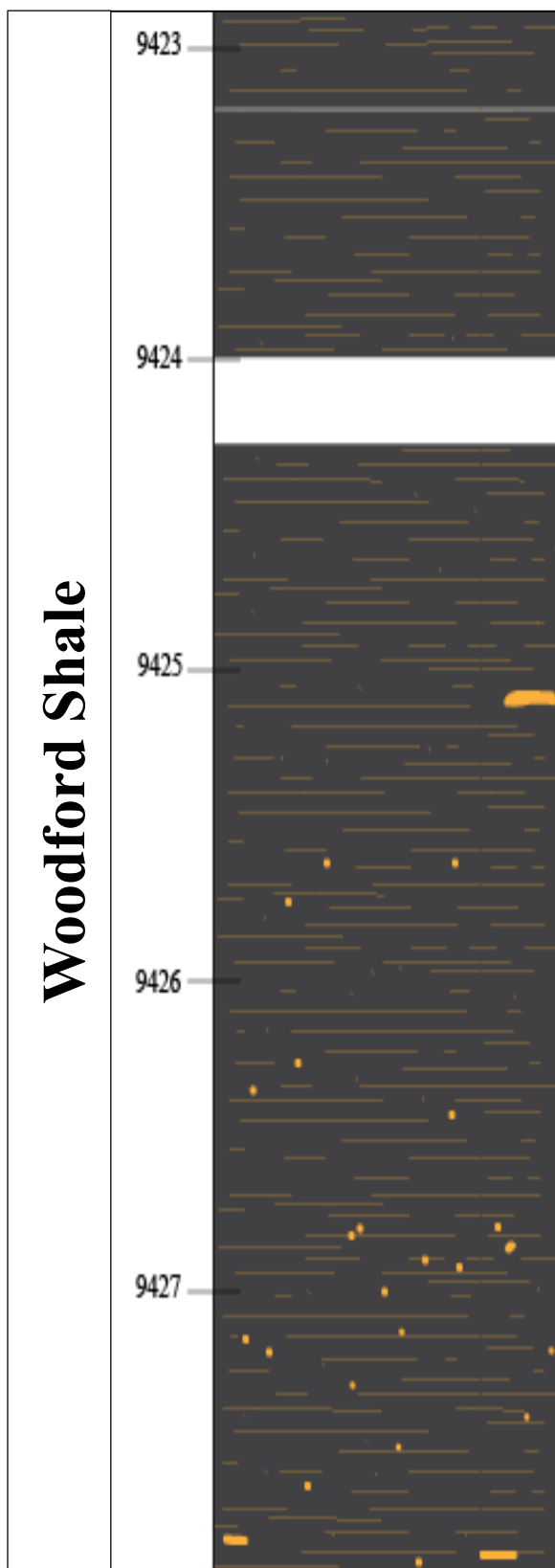


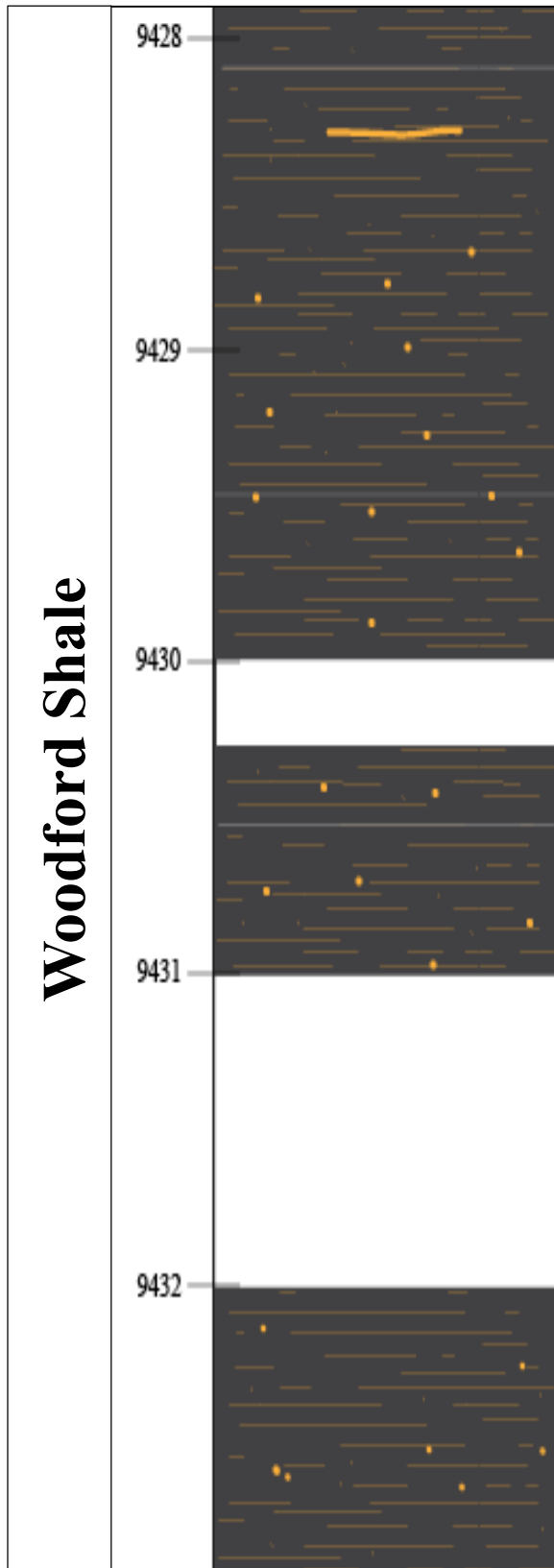


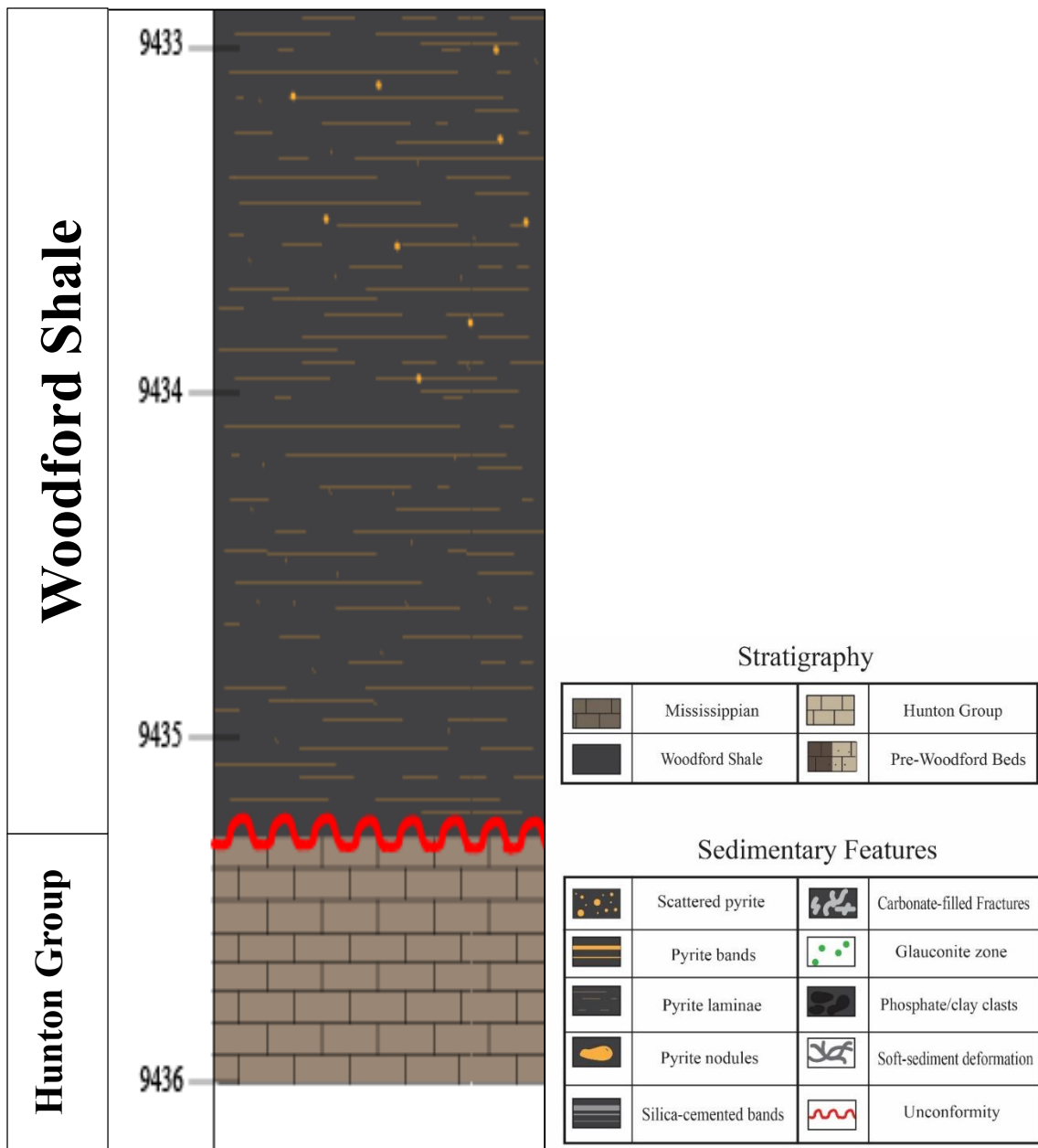


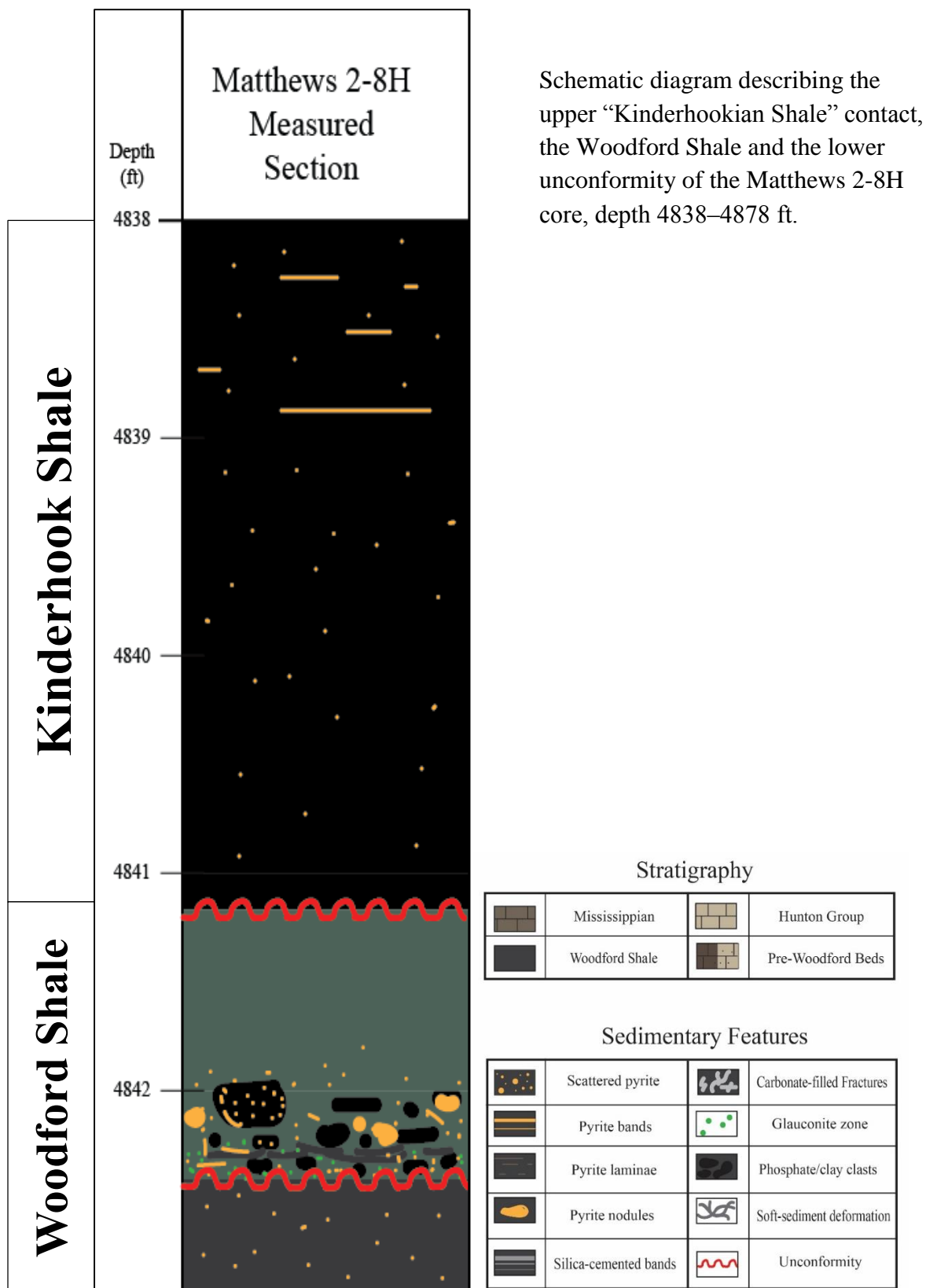




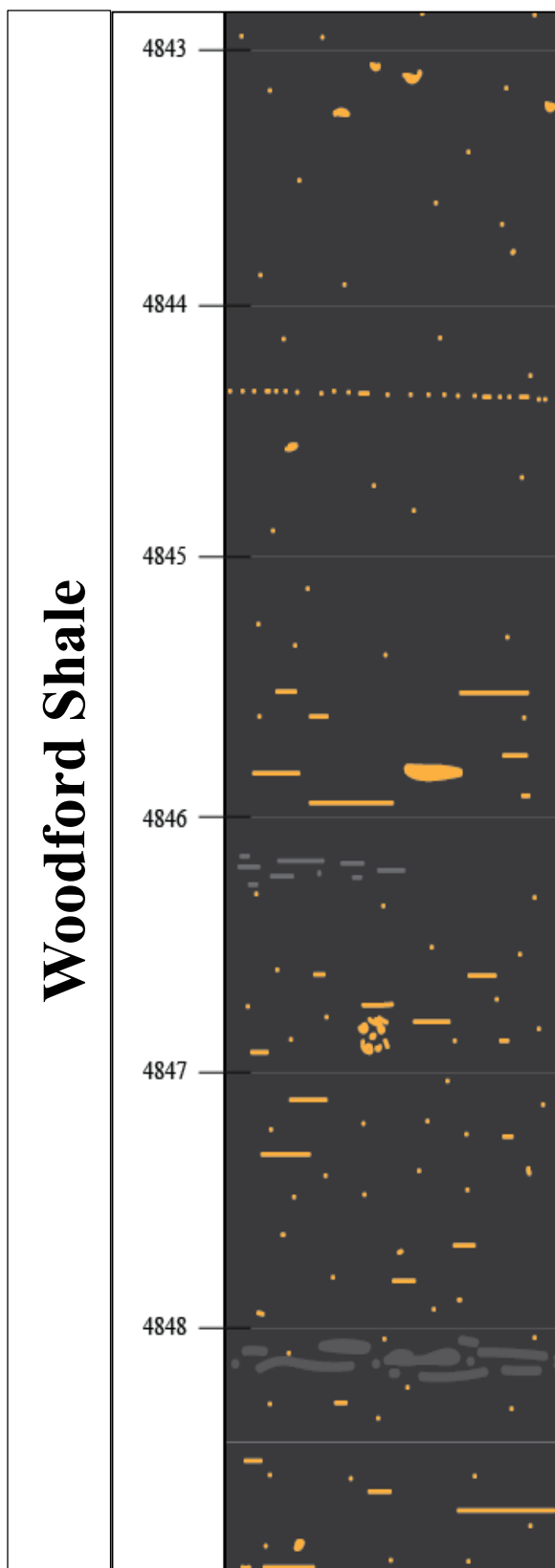


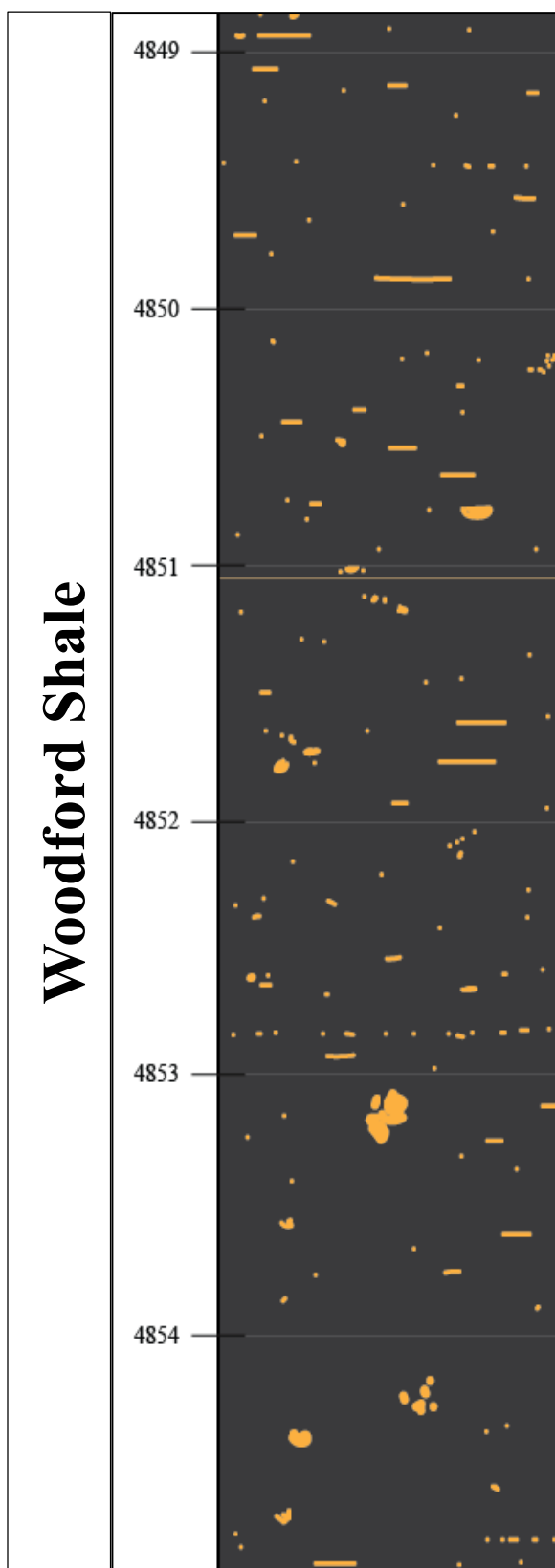


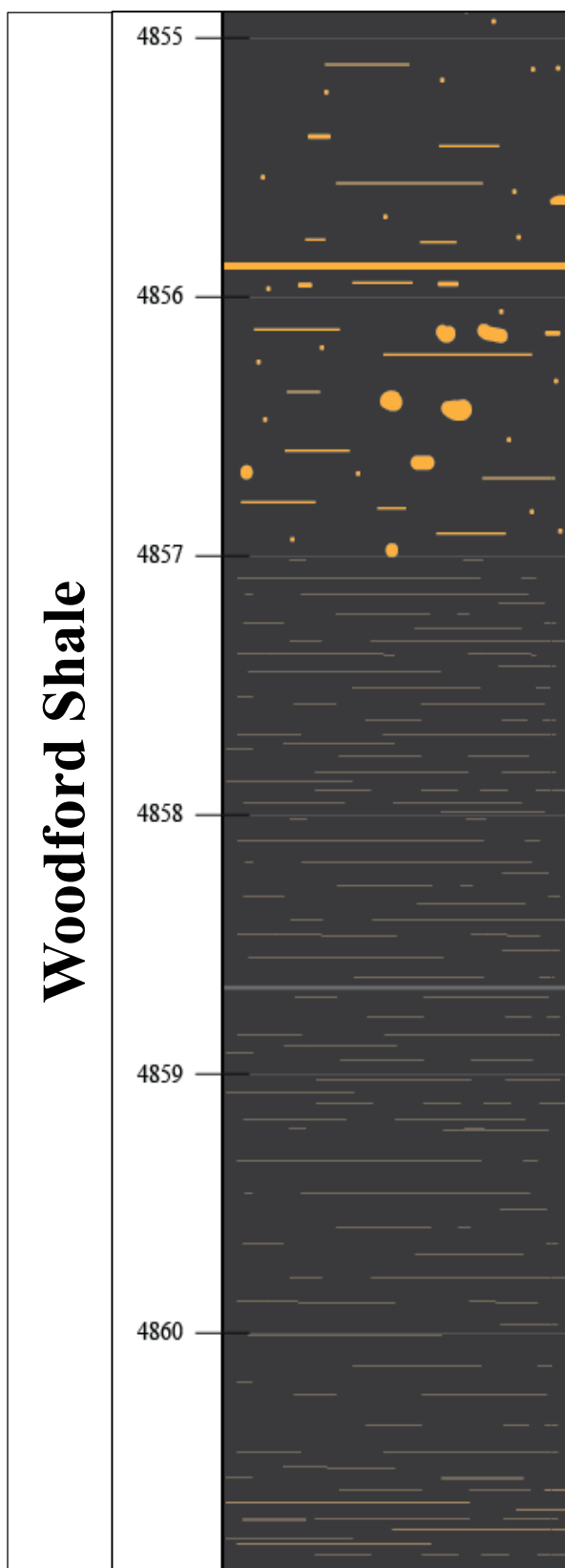


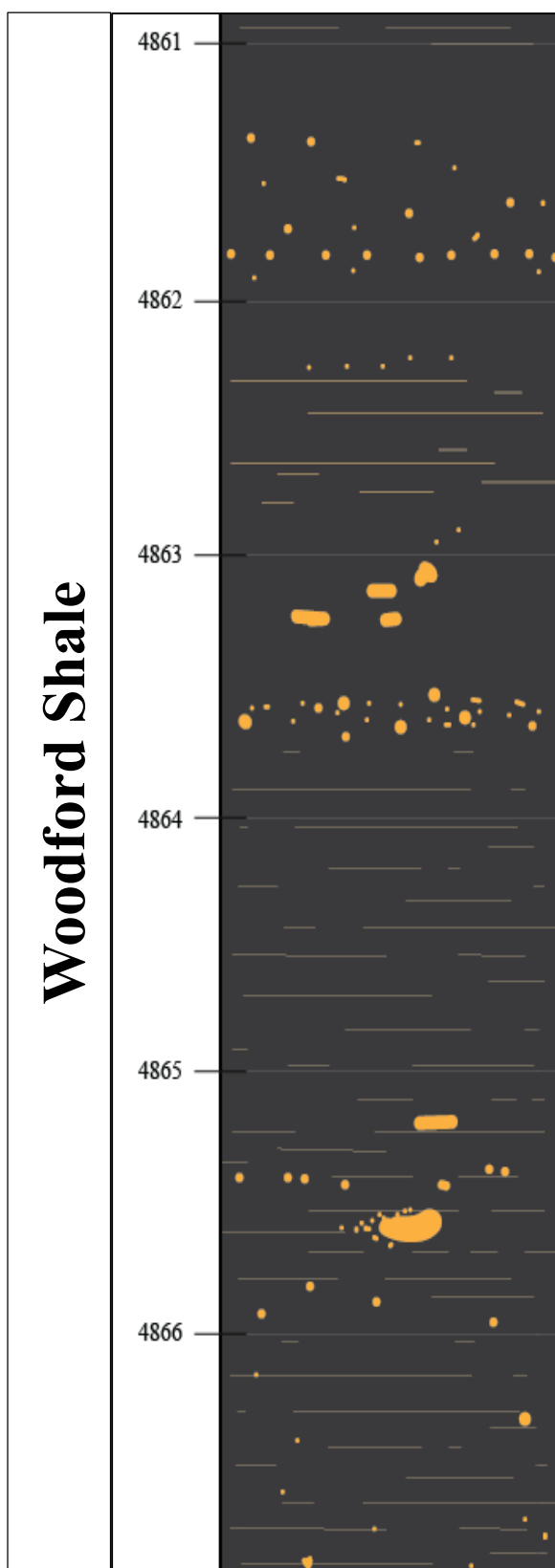


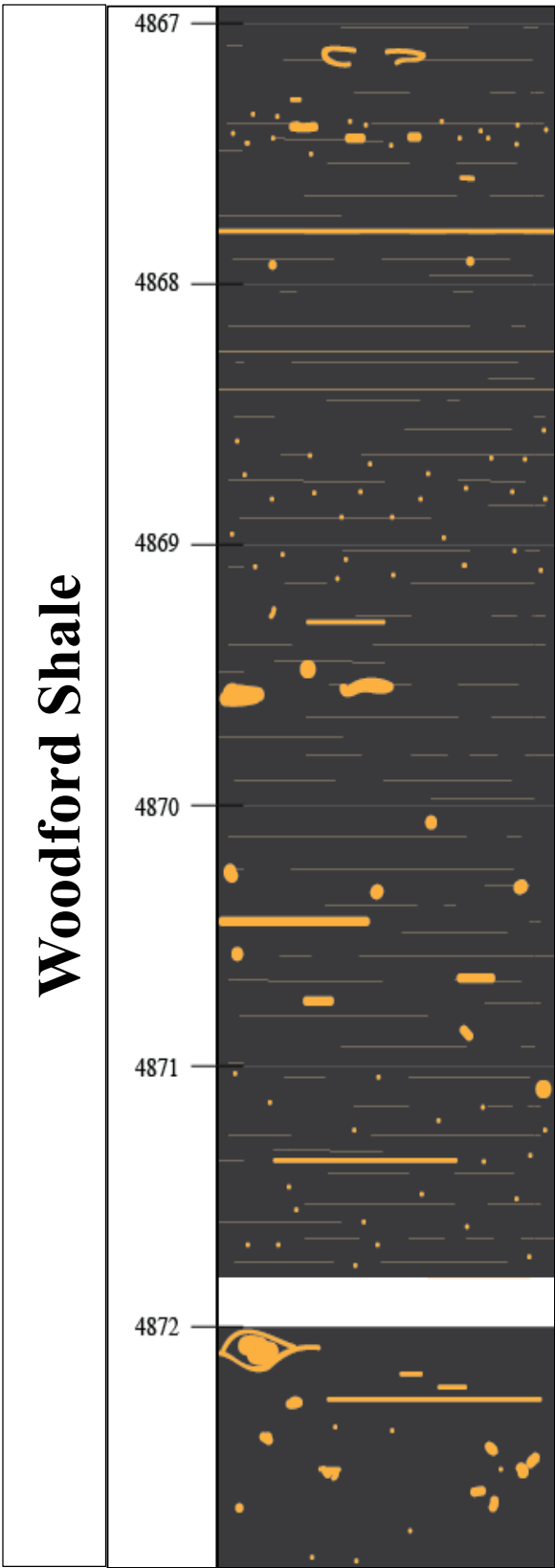
Schematic diagram describing the upper “Kinderhookian Shale” contact, the Woodford Shale and the lower unconformity of the Matthews 2-8H core, depth 4838–4878 ft.

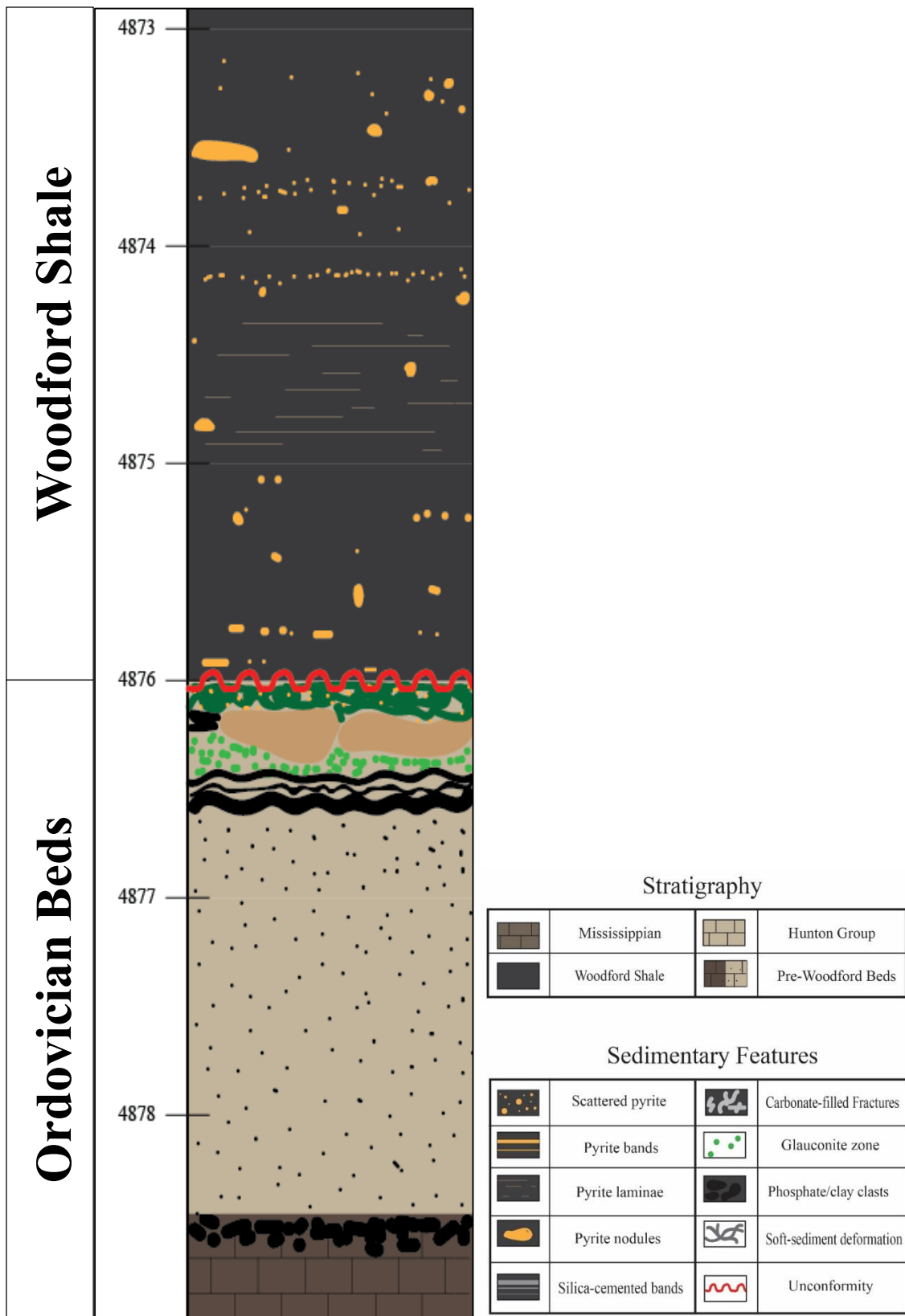












VITA

Kathryne Elizabeth Foltz

Candidate for the Degree of

Master of Science

Thesis: PETROGRAPHIC AND PETROPHYSICAL CHARACTERIZATION OF
THE WOODFORD SHALE, NORTHERN SHELF, ANADARKO BASIN,
OKLAHOMA

Major Field: Geology

Biographical:

Education:

Completed the requirements for the Master of Science in Geology at Oklahoma State University, Stillwater, Oklahoma in July, 2015.

Completed the requirements for the Bachelor of Science in Geology at Wheaton College, Wheaton, IL in 2013.

Completed the requirements for the Bachelor of Arts in History at Wheaton College, Wheaton, IL in 2013.

Experience: Internship at Noble Energy, Summer 2014

Professional Memberships: AAPG